MECHANICAL CHARACTERIZATION AND MODELING OF POROUS POLYMERIC
MATERIALS MANUFACTURED BY SELECTIVE LASER SINTERING

A THESIS SUBMITTED TO
THE GRADUATE SCHOOL OF NATURAL AND APPLIED SCIENCES
OF
MIDDLE EAST TECHNICAL UNIVERSITY

BY

CEVDET MURAT TEKİN

IN PARTIAL FULFILLMENT OF THE REQUIREMENTS
FOR
THE DEGREE OF MASTER OF SCIENCE
IN
MECHANICAL ENGINEERING

DECEMBER 2009

Approval of the thesis:

MECHANICAL CHARACTERIZATION AND MODELING OF POROUS POLYMERIC MATERIALS MANUFACTURED BY SELECTIVE LASER SINTERING

submitted by **CEVDET MURAT TEKİN** in partial fulfillment of the requirements for the degree of
Master of Science in Mechanical Engineering Department, Middle East Technical University by,

Prof. Dr. Canan Özgen
Dean, Graduate School of **Natural and Applied Sciences**   ——————————

Prof. Dr. Süha Oral
Head of Department, **Mechanical Engineering**   ——————————

Assoc. Prof. Dr. Serkan Dağ
Supervisor, **Mechanical Engineering Department, METU**   ——————————

Assist. Prof. Dr. Merve Erdal Erdoğmuş
Co-supervisor, **Mechanical Engineering Department, METU**   ——————————

Examining Committee Members:

Prof. Dr. Bülent Doyum
Mechanical Engineering, METU   ——————————

Assoc. Prof. Dr. Serkan Dağ
Mechanical Engineering, METU   ——————————

Assist. Prof. Dr. Merve Erdal Erdoğmuş
Mechanical Engineering, METU   ——————————

Assist. Prof. Dr. Ender Ciğeroğlu
Mechanical Engineering, METU   ——————————

Assoc. Prof. Dr. Altan Kayran
Aerospace Engineering, METU   ——————————

Date: ——————————

I hereby declare that all information in this document has been obtained and presented in accordance with academic rules and ethical conduct. I also declare that, as required by these rules and conduct, I have fully cited and referenced all material and results that are not original to this work.

Name, Last Name: CEVDET MURAT TEKİN

Signature   :

ABSTRACT

MECHANICAL CHARACTERIZATION AND MODELING OF POROUS POLYMERIC
MATERIALS MANUFACTURED BY SELECTIVE LASER SINTERING

Tekin, Cevdet Murat

M.S., Department of Mechanical Engineering

Supervisor　　　: Assoc. Prof. Dr. Serkan Dağ

Co-Supervisor　: Assist. Prof. Dr. Merve Erdal Erdoğmuş

December 2009, 119 pages

Rapid prototyping methods embrace a family of manufacturing methods that are developed to speed up the prototyping stage of product design. The sole needed input for production being the solid model of the part, mold/tool-free production characteristics and the geometric part complexity that can be achieved due to layer-by-layer production have extended the applicability/research areas of these methods beyond prototyping. Local pore formation in part that occurs as a result of the discrete manufacturing nature of rapid prototyping methods can be viewed as an opportunity for material development. In this thesis, the manufacturing-internal (porous) structure-mechanical property relations of porous materials are investigated. These porous parts are produced via Selective Laser Sintering (SLS) which is a rapid prototyping method. The elastic modulus, tensile strength, rupture strength and Poisson's ratio of uniform porous specimens with known porosities are determined through standardized mechanical tests for polymeric materials. The mechanical property variation profiles in graded materials are determined using the mechanical properties of uniform parts. The mechanical behavior of uniform and graded materials under applied loads are modeled using finite element method and simulation results are compared to the results of mechanical tests performed on graded

materials. In addition, feasibility of producing resin filled composite parts from these uniform and graded porous parts are sought. Porous parts (both uniformly and graded) that are infiltrated with epoxy resin have been characterized mechanically and the results have been compared with the uninfiltrated porous parts.

ÖZ

LAZER SİNTERLEME YÖNTEMİYLE ÜRETİLMİŞ GÖZENEKLİ POLİMERİK MALZEMELERİN MEKANİK KARAKTERİZASYONU VE MODELLEMESİ

Tekin, Cevdet Murat

Yüksek Lisans, Makine Mühendisliğ Bölümü

Tez Yöneticisi　　　　: Doç. Dr. Serkan Dağ

Ortak Tez Yöneticisi　: Yard. Doç. Dr. Merve Erdal Erdoğmuş

Aralık 2009, 119 sayfa

Hızlı prototipleme yöntemleri, ürün tasarım sürecinde prototipleme aşamasının hızlandırılması amacıyla ortaya çıkmış çeşitli üretim yöntemleridir. Üretim için sadece cismin katı modelinin gerekli olması, hızlı prototipleme makinelerinde üretimin kalıp/takımdan bağımsız yapılması, katman-katman üretim doğası nedeniyle çeşitli karmaşıklıkta şekillerin oluşturulabilmesi, bu yöntemlerin uygulama/araştırma alanlarını genişletmiştir. Hızlı prototipleme yöntemlerinin ayrık (discrete) üretim doğası nedeniyle ortaya çıkan ve çoğunlukla hata olarak nitelendirilen, üründe yerel boşluk kalma özelliği, malzeme geliştirilmesi açısından bir fırsat olarak değerlendirilebilir. Bu tezde, lazer sinterleme yöntemi hızlı prototipleme yöntemi ile üretilen gözenekli malzemelerin, üretim - gözenek yapısı (mikroyapı) - mekanik özellik ilişkileri incelenmiştir. Polimerik malzemelerin mekanik özelliklerinin belirlenmesi için geliştirilmiş standart testler kullanılarak, bilinen bir gözenek oranına sahip düzenli gözenekli malzemelerin elastisite modülü (çekme modülü), çekme dayanımı, kopma dayanımı ve Poisson sabitleri ölçülmüştür. Düzenli gözenekli malzemeler için ölçülen mekanik özellikler kullanılarak, derecelendirilmiş gözenekli malzemelerdeki mekanik özellik değişim profilleri bulunmuştur. Sonlu elemanlar yöntemi kullanılarak düzenli ve derecelendirilmiş malzemelerin

uygulanan kuvvetler altında mekanik davranışı modellenmiş, simülasyon sonuçları yapılacak mekanik test sonuçlarıyla karşılaştırıl-mıştır. Ayrıca düzenli ve derecelendirilmiş gözenek-li malzemeler kullanılarak reçine emdirilmiş kompozit malzeme üretimi incelenmiştir. Hem düzenli gözenekli hem de derecelendirilmiş gözenekli parçalara epoksi reçine emdirilerek kompozit malzeme oluşturulmuştur. Bu malzemelere mekanik testler uygulanmış, sonuçlar gözenekli parçaların test sonuçları ile karşılaştırılmıştır.

Anahtar Kelimeler: Lazer Sinterleme, Gözeneklilik, Mekanik Karakterizasyon, Çekme Testi, Sonlu Elemanlar Analizi

To My Father

ACKNOWLEDGMENTS

TABLE OF CONTENTS

LIST OF TABLES

LIST OF FIGURES

FIGURES

NOMENCLATURE

γ_{ij} Shear Strain in the *ij* direction . . . .

ν_{ij} Poisson's Ratio in the *ij* direction . . . .

σ_i Normal Stress in the *i* direction (MPa) . . . .

τ_{ij} Shear Stress in the *ij* direction (MPa) . . . .

θ Angle of Twist (Rad) . . . .

ε_{ij} Strain in the *ij* direction . . . .

a   Determined Fracture Toughness Specimen Crack Length (cm) . . . .

B   Fracture Toughness Specimen Thickness (cm) . . . .

d   Diameter of the Torsion specimen (m) . . . .

$\mathbf{E}_i$ Modulus of Elasticity in the *i* direction (MPa) . . . .

$\mathbf{G}_{ij}$ Shear Modulus in the *ij* direction (MPa) . . . .

$\mathbf{K}_{IC}$ Critical Stress Intensity Factor (MPa $\sqrt{m}$) . . . .

$\mathbf{K}_Q$ Conditional Stress Intensity Factor (MPa $\sqrt{m}$) . . . .

L   Length of the Torsion specimen (m) . . . .

$\mathbf{P}_Q$ Determined Load in Fracture Toughness Test (kN) . . . .

r   Radius of the Torsion specimen (m) . . . .

T   Torque (Nm) . . . .

W   Determined Fracture Toughness Specimen Witdth (cm) . . . .

CHAPTER 1

INTRODUCTION

Rapid prototyping (RP) methods are technologies which are developed and used for determining the possible design and production errors before making an initial investment on tooling during the development process. There are several techniques proposed until the first rapid prototyping idea flashes. Almost all of these techniques are based on adding and bonding of materials especially liquefied polymers or discrete particles. Since the parts are built layer by layer, anything modeled with a CAD software can be produced easily no matter how complex the shape is. Selective laser sintering (SLS) is one of the RP methods in which a wide variety of materials -from polymers to metals- can be used. These materials have to be in powder form which can be joined by laser. Due to the discrete nature of manufacturing some local pores are formed during the building process. Although this property is undesired most of the time, it is necessary for some applications like drug delivery devices or scaffolds for tissue generation. However, increased porosity reduces the strength of the material, one has to select the process parameters by considering both strength and porosity. In this study, mechanical properties of porous polyamide parts that are produced via selective laser sintering are sought. For this reason specimens are produced for various mechanical tests. These specimens are manufactured with an EOSINT P380 laser sintering machine. The basic process parameters of the machine are combined under the term "Energy Density (ED)" whose variation leads to the variation of the porosity. The energy density values must be kept in a range because some problems occur on the produced specimen if the ED is higher or lower than certain limits. Thus, a prestudy is performed and the highest and the lowest limits of the SLS machine are determined experimentally in the produced parts. After the process parameters are determined, uniform porous specimens for tensile, torsion and fracture toughness tests are produced and tested. Since the parts are built layer by layer they don't exhibit same mechanical properties in every direction.

1

Hence transversely isotropic behavior is assumed and tensile specimens for both thickness and length direction are tested. Also shear modulus between planes are determined by the torsion test. Finally fracture toughness tests are performed to determine the K_{IC} value of the material. Later on, functionally graded parts having distinct uniform porous grades are produced and tested. Mechanical behavior of FGM parts which have different number of grades and grades with different mechanical properties are tested and analyzed. Finally a finite element model is created for tensile tests. Results acquired from the model are compared with the experimental results.

1.1 Rapid Prototyping (RP)

Rapid prototyping methods embrace a family of manufacturing methods that are developed to speed up the prototyping stage of product design. It helps manufacturer to process the prototype faster than traditional production methods in order to make optimization and modifications. Because the parts are produced layer by layer and mold/tool free, there is the advantage of producing parts in any complexity without having multiple operations. As a result of this, final product is produced in a shorter time period and relatively cheaper compared to other methods, which reduce the total production cost [1].
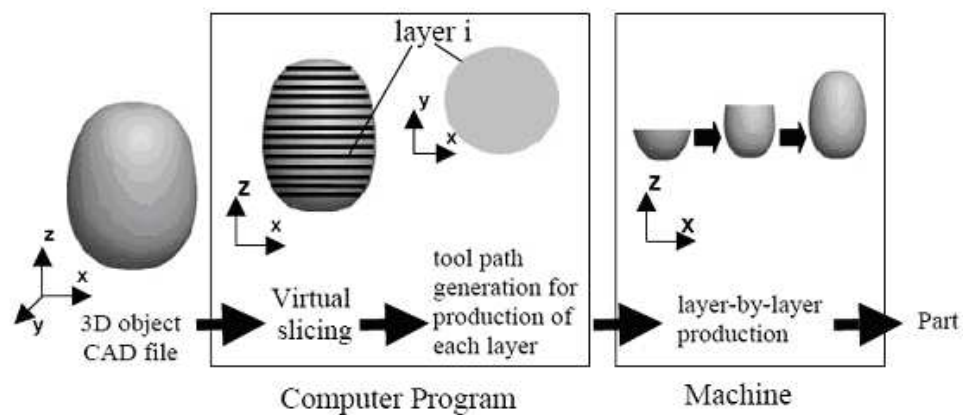
Figure 1.1: Layer by layer manufacturing process [2]

Most of the rapid prototyping methods are based on adding and joining some distinct particles, liquids or solid sheets. But first they all need to be modeled with a CAD program

2

which is needed to have the ability to export the data in STL file format, the current industry standard for facetted models [1]. Once the model is created and exported to the computer program of the RP machine, it is virtually sliced and tool path for each layer is generated. Finally, layers are built according to the relative method until the whole part is manufactured (Figure 1.1). Rapid prototyping methods are popular in biomedical area in which CT and MRI scans are very important for diagnosis. These techniques are used to visualize the human bones and organs with a series of 2D pictures. These pictures are then used to generate the virtual 3D model of the scan [3–5]. Also, a special software allows users to create CAD or STL data from direct CT or MRI scan [5]. This data is then exported to the corresponding RP machine and a physical model is produced. On the other hand, RP methods lead to some porosity during production which reduces the strength of the parts built. Although this situation is undesired most of the time, it can be advantageous in some cases. For example drug delivery systems or scaffolds for tissue generation need porosity on parts [2, 6–9]. There are several techniques used as rapid prototyping methods. Stereolithography (SL), Fused Deposition Modeling (FDM), 3D Printing (3DP) and Selective Laser Sintering (SLS) are the most commonly used techniques. Each of them uses a different way to combine materials [1].

1.1.1 Stereolithography (SLA)

Stereolithography is a process in which liquid photopolymer that is sensitive to ultraviolet light, cured with the help of laser due to the path drawn by the computer program (Figure 1.2). Limited number of materials can be used which are generally expensive and toxic. Although parts built with SLA possess a quality surface finish, they might be brittle and need supports that negatively affect the surface finish [1]. Another advantage of this method is that specific locations of parts can be marked with different colors in order to emphasize something (i.e. tumors in a skull). Also parts built with SLA can be used in operating theatres after sterilizing [4].

1.1.2 Fused Deposition Modeling (FDM)

In fused deposition modeling, parts are built by depositing a molten material through a nozzle onto a substrate (Figure 1.3). A large range of materials (i.e. ABS plastics, waxes etc.) can

Figure 1.2: An engine manifold produced with SLA [10]

be used which are relatively cheaper and non toxic compared to the SLA. However surface finish is not as good as SLA due to the resolution of the process [1].
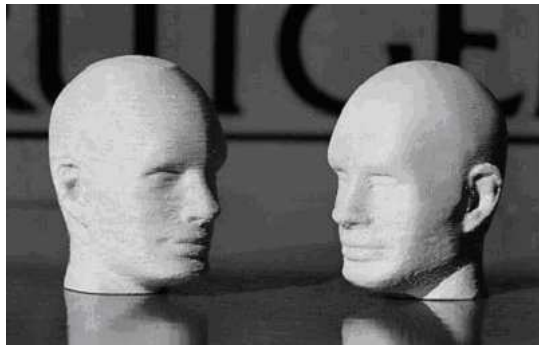
Figure 1.3: Two heads modeled with FDM [11]

1.1.3   3D Printing (3DP)

3DP rapid prototyping technique uses a binder for joining discrete particles. This binder is selectively sprayed on to the particles lying on a substrate through a nozzle (Figure 1.4). After the whole part is built layer by layer it is heated in order to cure the binder. This technique produces parts quicker and cheaper than other RP methods but sometimes needs further surface finishing operations [1].
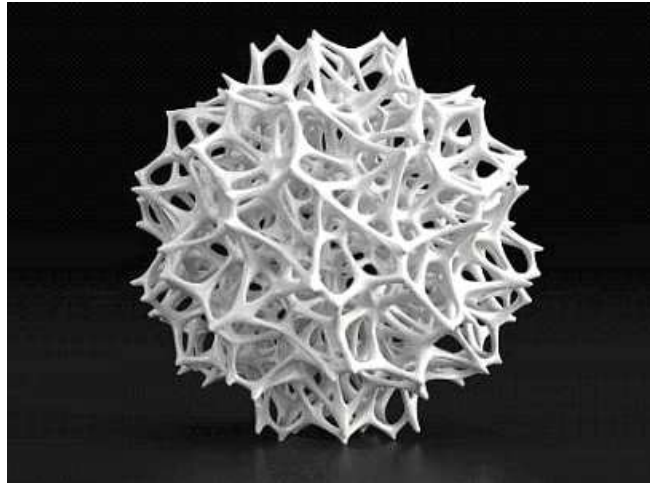
Figure 1.4: A complex shape produced with 3DP [12]

1.1.4 Selective Laser Sintering (SLS)

Selective laser sintering is a process in which discrete powder particles are joined with the help of laser. An advantage of SLS over other RP techniques is that a wide range of materials -from polymers to metals- can be used during manufacturing [13–15].
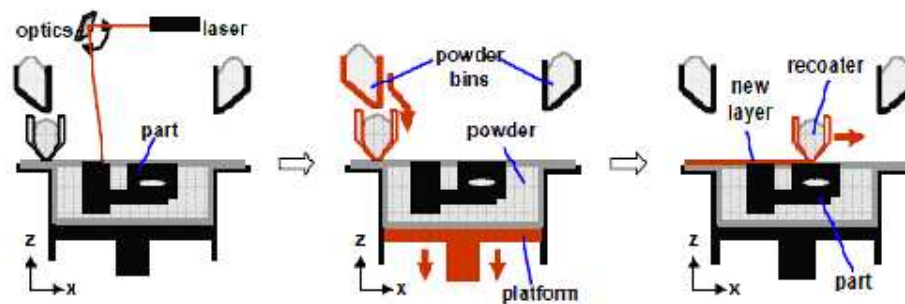
Figure 1.5: SLS production process [2]

As all other RP methods, SLS requires the STL formatted 3D CAD model of the part. This data is virtually sliced by the machine's software and the tool path for each layer is generated. After that, the powder bed is heated just below the melting temperature of the particles in order to avoid thermal distortions and to assure the layer to bond to the next layer. Then the laser

(i.e. CO_2) having a power range of 25-50W is applied to the necessary places on the spread powder and locally melts that region. This process continues until the whole part is produced by lowering the platform and spreading a new layer of particles (Figure 1.5) [2, 5, 15–18].

Selective laser sintering consists of several processing parameters such as, laser power (P), laser scanning speed (LS), hatching distance (HD), laser beam effective diameter and beam offset (Figure 1.6). Each of these parameters has individual effects on the mechanical and physical properties of the parts. These properties can be related with the combination of 3 dominant parameters which are laser power, hatching distance and laser scanning speed. This combination is known as "Energy Density (ED)" which is formulated as follows,

$$ED(J/mm^2) = \frac{P(W)}{LS(mm/s) \times HD(mm)} \qquad (1.1)$$

Energy density values must be varied within a range because each parameter has upper and lower limits themselves in order to get a functional part. Manufacturer of the SLS machine applies default process parameters where the mechanical properties of the materials are in the maximum value referred in the material datasheet. If the energy density value is lower than a certain limit particles may not melt enough to fuse together. Also due to the shear stresses formed between layers, parts curl and become deformed in shape. On the other hand, if the energy density level is too high particles burn and parts degrade [2, 9]. One other problem is shrinkage during cooling which is compensated with a coefficient factor entered to the software before the production begins [19].

Another thing that can be considered as a problem is the scanning strategy of the SLS. In default, laser first scans the circumference of the layer with a constant energy density value generally lower than the usual configuration. This is called "contouring". After contouring the laser scans inside the circumference determined by contouring which is called "hatching". Contouring protects the shape of the part and recovers the errors formed due to orientation. However it strengthens the parts built with low energy densities such that the parts fail even before the contour fails. Therefore no contouring is used for specimens produced in this study.
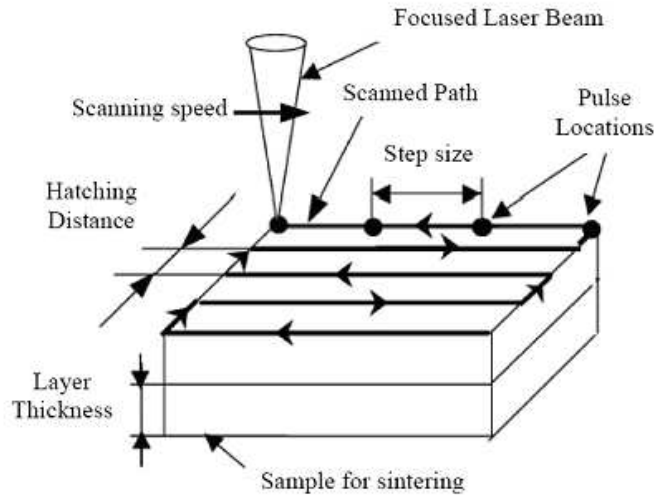
Figure 1.6: Processing parameters of SLS [2]

1.2 Functionally Graded Materials (FGMs)

The first idea of gradually changing a material's property with position [20] was proposed in 1984-1985. A material was desired for a spacecraft which ensures resistance to high temperatures with good mechanical integrity. Researchers decided to grade the composition of two different materials from side to side according to the property desired. It was necessary to use a temperature resistant material at the outer surface while thermally conductive and mechanically strong material at the inner surface. They used ceramic for outer surface which can withstand high temperatures but has weak mechanical properties while a thermally conductive material with strong mechanical properties is used for inner surface. Consequently; studies about functionally graded materials were initiated. Functionally graded materials (FGMs) are defined as composite materials in which the composition or the microstructure is locally varied so that a certain variation of the local material properties are achieved [21]. The difference of FGMs from traditional composite materials is that composite materials are homogenous materials which involve a compromise between the desirable properties of the component materials. In contrast FGMs contain the pure form of each component so that the need for compromise is eliminated. Also the properties of both components can fully be utilized [22]. FGMs are now used in various areas like, aeronautics, machining, electronics, bio engineering etc. The materials can contain either one material or more materials. Multi material FGMs are more commonly used in industry than mono material FGMs. Mono material FGMs can

7

be achieved by varying one of the microstructural properties which is generally the porosity. There are several ways to produce FGMs like, spark plasma sintering, vacuum plasma spraying, electrophoretic deposition, rapid manufacturing etc. In this thesis possibility of producing mono material FGMs via Selective Laser Sintering (SLS) rapid prototyping method is sought. The porosity of the grades is going to be varied by changing the energy density applied.

1.3   Scope of the Study

In this thesis, an experimental study on determining the elastic properties of porous polyamide parts produced via selective laser sintering (SLS) is presented. There are 4 main objectives of this study. First objective is to determine the mechanical properties of uniformly porous polyamide parts produced via SLS. Since the production is carried out layer by layer, parts produced via SLS do not exhibit isotropic behavior. Considering the previous studies transversely isotropic behavior is assumed therefore 5 independent elastic constants are sought. Tensile tests in both thickness and length direction are performed as well as torsion tests for circular parts built in length direction. Compliance matrices are constructed for 9 different sets of parts; and variations of mechanical properties due to the energy density is examined. Also, fracture toughness tests are performed for compact tension specimens built in thickness direction and K_{IC} value is determined.

The second objective of the study is to characterize the graded porous parts with distinct uniform porous grades produced by considering 2 different types. Each type is produced with 3, 5 and 7 grades. Type I contains the weakest grade while type II has the strongest one.

The third objective is to check the feasibility of producing resin filled composite parts from the uniform and graded porous parts are sought.

The forth and the final objective is to create finite element models of the uniformly porous and graded porous tensile test specimens. 3D orthotropic model of tensile test specimens are built and analyzed by using the general purpose finite element analysis program ANSYS. A displacement value in linear elastic region of the material is given as an input and the stress distribution found is compared to the experimental results.

CHAPTER 2

LITERATURE SURVEY

Many studies have been conducted on rapid prototyping, selective laser sintering, mechanical properties of parts produced via selective laser sintering, and production of functionally graded materials with rapid prototyping methods. Most of the studies are in bio engineering area generally investigating the bio compatibility of materials with the production technique.

2.1   Rapid Prototyping and Selective Laser Sintering

Pham et al. [1] have conducted a detailed research on all the rapid prototyping techniques. They grouped them due to the similarities of how the materials added and bonded together. They explained the basic principles and compared them by considering the cost efficiency, materials used, process time and accuracy.

Lohfeld et al. [4] investigated the types of biomodels in macroscale and microscale then focused on virtual and physical biomodels in their study. They emphasize the importance of CT and MRI scans on diagnosis in medical applications. They mentioned the potential of rapid prototyping methods of producing layered parts from direct CT or MRI scans (Figure 2.1).

They reached the conclusion that it becomes easy to visualize macroscale and microscale biomodels with rapid prototyping methods.

A similar study to Lohfeld's is performed by Webb [3]. This paper mentioned the compatibility of CT and MRI scans with some rapid prototyping methods. It is emphasized that Stereolithography (SLA) is the most preferred rapid prototyping method. Also selective laser
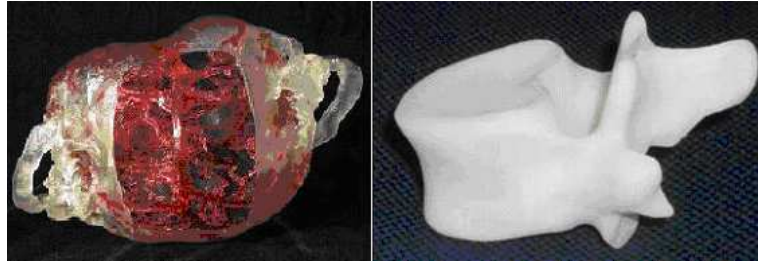
Figure 2.1: Biomodel of conjoint twins, blood vessels colored via SLA (left), vertebral bodies via SLS (right) [4]

sintering (SLS) is suggested due to the durability of parts produced from nylon. Finally, it is pointed out that fused deposition modeling (FDM), can use medical grade ABS which can be used temporarily within the body.

Another similar study is conducted by Berry et al. [23]. They produced 2 human skulls (one is a child's skull other is an adult's) and a femur via SLS directly through their CT scan (Figure 2.2). Both models have very complex shapes but the results showed that they achieved very little dimensional difference with the CT data and the parts produced. They also stated an advantage of SLS over SLA which is the capability of producing parts without any additional supports. According to the desire of supports on SLA, several steps are necessary for production.
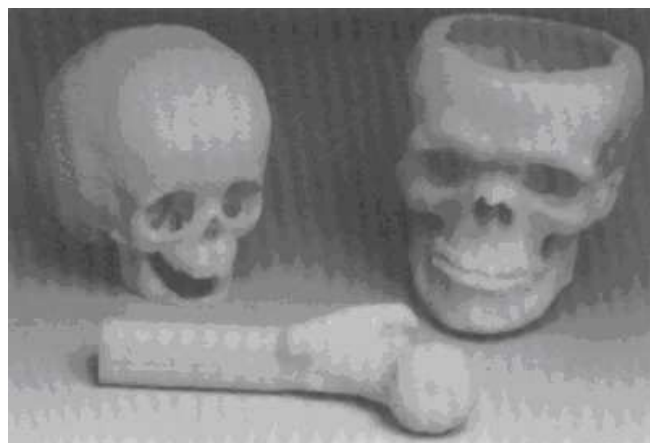
Figure 2.2: 2 human skulls with a femur produced via SLS [23]

Kan et al. [24] sought the possibility of using bio compatible polymers in SLS for building

scaffolds for tissue generation. They tested several biocompatible polymers on SLS and they found that depending on the tissue generated, different biocompatible polymers can be used for tissue generation. They also added that by changing the process parameters of the SLS machine they had the ability to control the porosity of the parts produced.

2.2 Mechanical Properties of Parts Produced via SLS

Williams et al. [25] designed and fabricated polycaprolactone (PCL), which is a biocompatible polymer, scaffolds via selective laser sintering in order to use in bone and cartilage repair. They performed compression tests until the cylindrical porous specimens failed in Z direction. They used image based finite element analysis using the high resolution CT scans and predict the mechanical properties of scaffolds by assuming isotropic behavior. Then they compared the experimental results to predicted values. They found that mechanical properties of PCL scaffolds possess values within the lower range of trabecular bone (Figure 2.3).
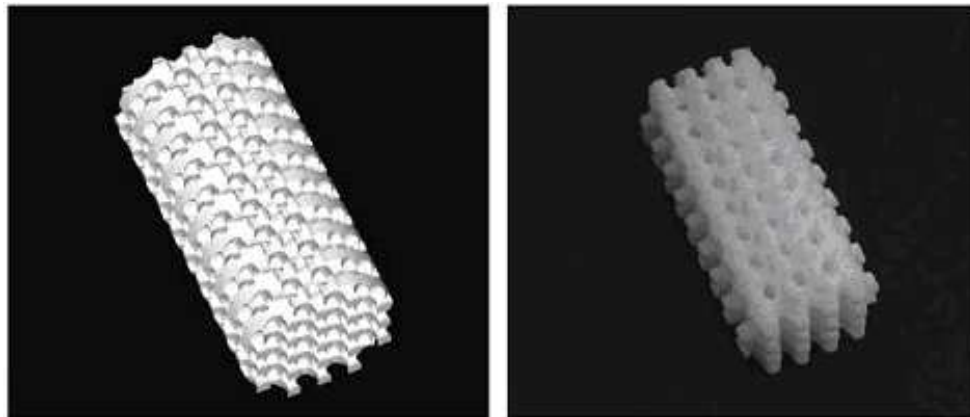
Figure 2.3: CAD drawing of scaffold (left), part built via SLS (right) [25]

Gibson et al. [9] performed a study which considers the relationship between powder properties, fabrication parameters and mechanical properties for parts produced via SLS. They used fine nylon in a Sinterstation 2000 SLS machine and produced tensile test specimens by considering the ASTM D638 standard [26]. They investigated the influence of orientation and position of parts, variation of process parameters and post processing by measuring tensile strength, density and hardness. They showed that mechanical properties vary when different

powders are used if similar process parameters are selected. Also mechanical properties increase when laser power increase and scanning speed and scan spacing decrease. Therefore, porosity decreases and dense parts with good mechanical properties are achieved. Orientation of similar parts on the production chamber has small effect in which only the standard deviation of the test results differ while the average value remains nearly the same (Figure 2.4).
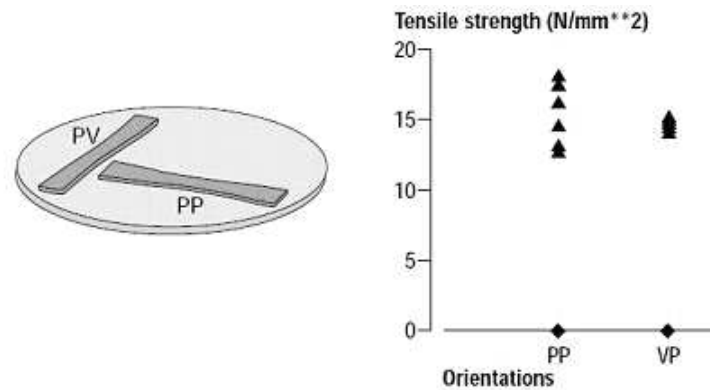
Figure 2.4: Effect of orientation on mechanical properties for SLS parts [9]

Another paper investigating the mechanical properties of parts produced via SLS is written by Caulfield et al. [27]. They investigated the influence of process parameters on physical and mechanical properties of polyamide parts. They performed tensile tests with a video extensometer to determine the mechanical properties according to the standard ASTM D638. They compared all the results for 0 and 90 degrees of orientation of parts (Figure 2.5). They took some SEM pictures to visualize the fracture surfaces. They showed that mechanical properties of parts are highly dependent on process parameters and part orientations.

None of the studies considering the mechanical properties of the plastic parts investigate the Poisson's ratio of the material. Poisson's ratio value can either be found by using a biaxial extensometer or by using strain gages. Both methods have handicaps themselves. Biaxial extensometers are relatively expensive and heavier than a uniaxial extensometer that a plastic part may not carry during tests. Also the adhesives used to install the strain gages locally reinforce the part where applied which may result a deviation on the strength values. Perry [28] made some experiments with orthotropic parts like composites and founded that strain

12
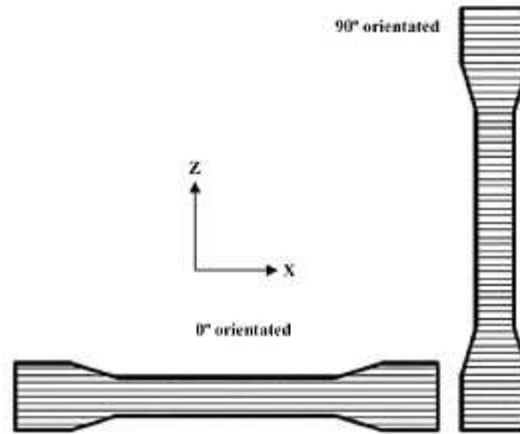
Figure 2.5: 0 and 90 degrees of orientations of tensile test specimens [27]

gages installed along axial and lateral directions, possess same error coefficients as strain gages which are used by assuming that the gages have small transverse sensitivity.

2.3 Functionally Graded Materials

Some plants, tissues, bones and teeth can be considered as perfect examples of FGMs in nature. For instance a tooth requires a high wear resistance outside and a ductile structure inside to overcome the fatigue [29]. According to this similarity FGMs are very popular in bio engineering area. Especially dental implants, artificial bones, drug delivery devices, scaffolds for tissue generation can be built with rapid prototyping.

Watari et al. [30] produced Titanium/Hydroxyapetite FGM dental implants to ensure high biocompatibility at one end and high strength on the other end. They used spark plasma sintering technique during manufacturing. Figure 2.6 shows the comparison of a traditional implant and an FGM implant. They suggest that tissue reaction changes gradiently in response to the composition. Therefore they can control the tissue response by functionally graded structure of biomaterials.

Shishkovski et al. [31] performed a study on combining the computer modeling methods and functionally graded materials, coating methods. He reviewed some existing rapid prototyping techniques which are able to produce FGMs. He stated that FGMs produced via SLS possess
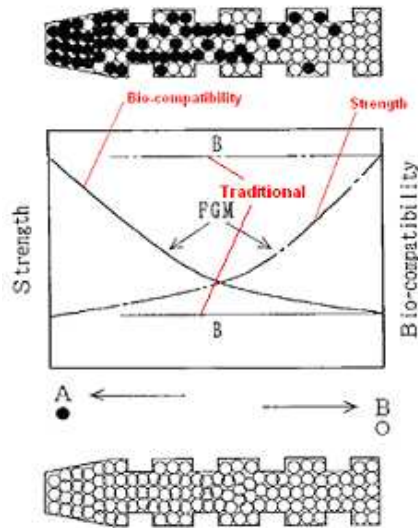
Figure 2.6: An FGM dental implant [30]

a smaller toughness and greater porosity than those produced via volume laser cladding. Parts like gradient filter elements, biocompatible implants, and chemical catalysts can be produced via SLS with the possibility of controlling the porosity and structure.

Leong et al. [32] in their paper, explored the feasibility of using biodegradable polymers as the matrix to build drug delivery devices (DDD) using selective laser sintering (SLS). They studied the process parameters of SLS machine to successfully vary the porosity of the DDDs matrix in order to optimize drug loading and diffusion rate. They achieved more than 50% of porosity which enables the sufficient quantity of drugs to pass through (Figure 2.7).
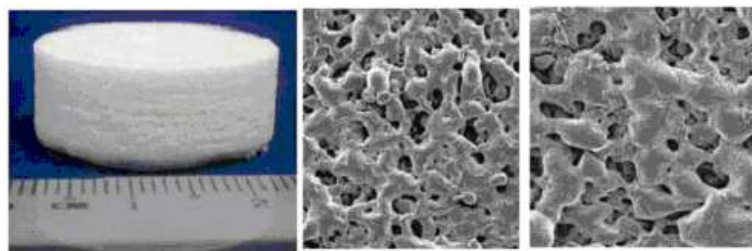
Figure 2.7: A DDD disc (left), SEM picture of inner disc (mid), SEM picture of outer disc (right) [32]

Chung et al. [33, 34] published 2 different papers about glass beads and silica filled Nylon

14

11 FGMs produced via SLS. They first built fully dense particles and performed tensile and compression tests to generate the mechanical behavior of the parts as a function of material composition. Then, they developed optimized compositions with the study on design of experiments (DOE). They fabricate 0-30% volume fractions of glass beads parts and 2-10% volume fractions of silica nanoparticles filled FGMs. They achieved the predicted results for both conditions and successfully produced 1D FGMs without modifying the commercial SLS machine.

CHAPTER 3

PRODUCTION AND CHARACTERIZATION OF UNIFORM POROUS SPECIMENS

As mentioned in the previous chapter, "Energy Density" value which is the combination of laser power (P), laser scanning speed (LS) and hatching distance (HD) can be varied within a range determined by the restrictions of each individual process parameters. Since the parts cannot bond well and curl under low energy density values and, burn - degrade under high energy density values, some tests were performed by İlkgün [2] to determine the maximum and minimum values of these three process parameters. According to the observations given in [2], the laser power could be varied between 36 to 44.5 W, hatching distance could be varied between 0.3 to 0.45 mm, and scanning speed could be varied between 4000 to 5000 mm/s.

Due to formula (1.1), for maximum energy density and the minimum porosity, laser power must be held maximum and hatching distance, scanning speed must be held minimum. According to this information, the combination that avoids burning is found as 44.5 W of power, 0.3 mm of hatching distance and 4000 mm/s of scanning speed (Highest ED = 0.037 J/mm^2).

Similarly for minimum energy density and the maximum porosity, laser power must be held minimum and hatching distance, scanning speed must be held maximum. Therefore, the combination that avoids curling is found as 36 W of power, 0.45 mm of hatching distance and 5000 mm/s of scanning speed (Lowest ED = 0.016 J/mm^2).

In this study uniform porous parts having different energy density values and functionally graded parts with distinct porous grades are produced with an EOSINT P380 (Figure 3.1) laser sintering machine currently set up in Biltir CAD/CAM Center at METU. Production

chamber of the machine have the dimensions of 340 x 340 x 620 mm. The machine can produce layers with a thickness of 0.15 mm ±0.05 mm and a maximum power of 50 W. Nylon 12 based fine polyamide PA 2200 which is a thermoplastic with average particle size of 60 μm is used as the material. Detailed material properties are given in Appendix A.

Figure 3.1: EOSINT P380 Laser sintering machine in Biltir, METU

Referencing the maximum and minimum values found by İlkgün [2], $2^3 = 8$ combinations can be built. By adding the machines default combination which has a laser power of (P) 44.5 W, hatching distance (HD) 0.3 mm, scanning speed of (LS) 4500 mm/s, a total of 9 set of process parameters are chosen for tests. The values can be seen in Table 3.1.

Table 3.1: Predetermined process parameters for SLS parts

Processing Parameter Set	1	2	3	4	5	6	7	8 (*default*)	9
P(%)	66.3	66.3	90	66.3	90	66.3	90	90	90
LS (mm/s)	5000	4000	5000	5000	4000	4000	5000	4500	4000
HD (mm)	0.45	0.45	0.45	0.30	0.45	0.30	0.30	0.30	0.30
ED (J/mm^2)	0.016	0.019	0.020	0.024	0.025	0.029	0.030	0.033	0.037

3.1 Production of Specimens

Selective laser sintering is a layered manufacturing technology. Parts are built layer by layer from the 3D CAD data entered into the machine (Figure 3.2). Producing parts with EOSINT P380 involves several steps mainly categorized as preprocessing and post processing. In pre-processing section the process parameters due to desired mechanical and physical properties are entered.
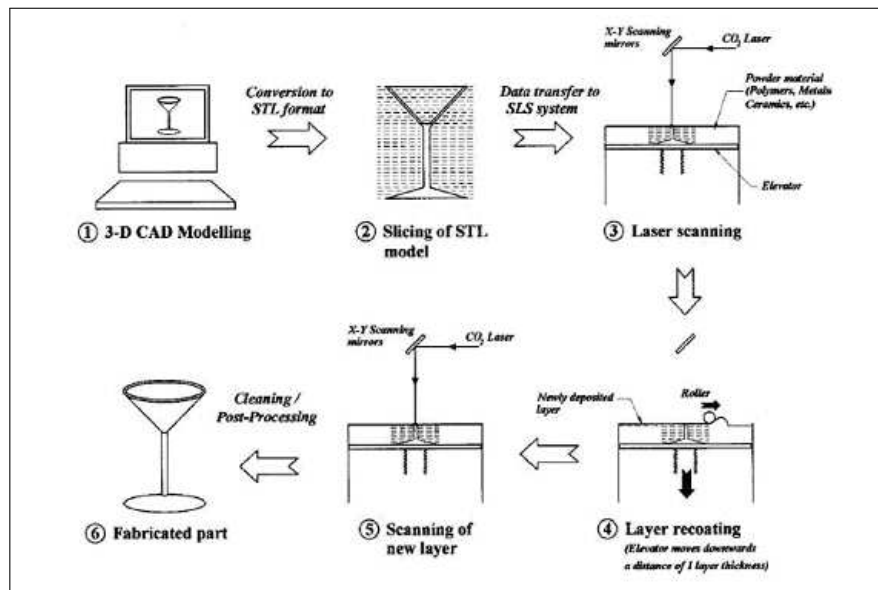
Figure 3.2: SLS process layout [24]

First the 3D model of the part must be created with a CAD program having the ability to export the file in STL format. Each program has different options to export the file. After that the STL file is opened with a software called "Magics" (Figure 3.3). This software is used for rescaling, locating a part on the platform (translation and rotation), checking design errors, and cutting a designed part into different small parts. Scaling factor for any length value in either X or Y direction is constant while in Z-direction scaling factors vary in respect to the height of the part to be manufactured. "Magics" also determines the appearance of the layers on the part to be produced. On the other hand the cost of production depends on part height therefore parts need to be positioned carefully in order to be cost efficient. Another function of "Magics" is to discover design errors which are not generated due to file conversion to STL, but rather inherited from the incorrect solid models.

18
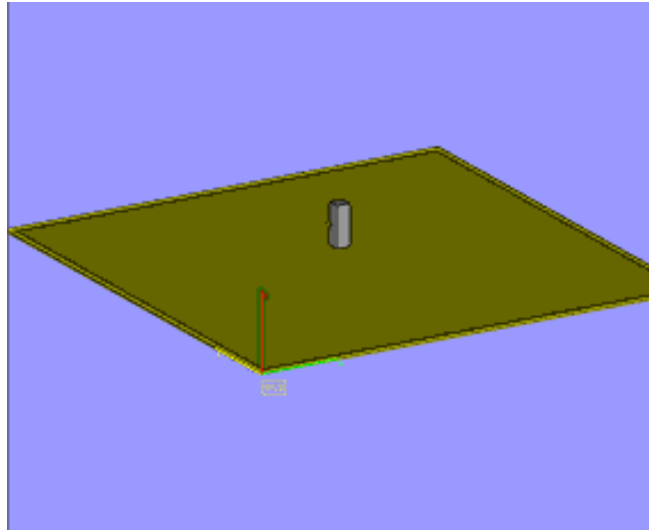
Figure 3.3: A view from "Magics" software

After the properties are set with "Magics", the file is imported into another software called "EOS-RP-Tools" which slices the parts into pieces with desired thickness and creates another file in "SLI" format. One last step before the loading of the parts to the SLS machine is adding the "SLI" file to "PSW P3x0" software. This software is the environment where the process settings are determined for each part. With this program the exposure parameters (power, scanning speed, and hatching distance) are entered for both hatching and contouring as well as some properties for scanning strategy. Finally the saved file with "job" extension is loaded to SLS machine and the preprocessing step is finalized.

After production, there is the post processing step which involves detaching the part from the unsintered powder in the platform, cleaning, and packaging.

Jande [35] was responsible from production of all the parts considered in this study.

3.2 Material Model of Parts Produced via SLS

Materials produced with SLS rapid prototyping technique do not exhibit same mechanical properties in every direction.

Materials having 2 orthogonal planes of symmetry are known as orthotropic materials. This symmetry automatically exists in the 3rd orthogonal plane and requires 9 independent elastic

constants unlike isotropic materials which is represented with 2 independent elastic constants. These constants are, E_x, E_y, E_z, ν_{xy}, ν_{xz}, ν_{yz}, G_{xy}, G_{xz}, and G_{yz} [36, 37].

$$
\begin{bmatrix} \varepsilon_x \\ \varepsilon_y \\ \varepsilon \\ \gamma_{yz} \\ \gamma_{zx} \\ \gamma_{xy} \end{bmatrix}
=
\begin{bmatrix}
\frac{1}{E_x} & -\frac{\nu_{yx}}{E_y} & -\frac{\nu_{zx}}{E_z} & 0 & 0 & 0 \\
-\frac{\nu_{xy}}{E_x} & \frac{1}{E_y} & -\frac{\nu_{zy}}{E_z} & 0 & 0 & 0 \\
-\frac{\nu_{xz}}{E_x} & -\frac{\nu_{yz}}{E_y} & \frac{1}{E_z} & 0 & 0 & 0 \\
0 & 0 & 0 & \frac{1}{G_{yz}} & 0 & 0 \\
0 & 0 & 0 & 0 & \frac{1}{G_{zx}} & 0 \\
0 & 0 & 0 & 0 & 0 & \frac{1}{G_{xy}}
\end{bmatrix}
\cdot
\begin{bmatrix} \sigma_x \\ \sigma_y \\ \sigma_z \\ \tau_{yz} \\ \tau_{zx} \\ \tau_{xy} \end{bmatrix}
\tag{3.1}
$$

Where;

$$
\frac{\nu_{ij}}{E_i} = \frac{\nu_{ji}}{E_j}
\tag{3.2}
$$

However, Gibson and Shi performed some tensile tests for same parts produced via SLS and proposed that parts placed perpendicular on the production platform have similar average tensile strengths but different standard deviations. They explained the difference in the standard deviation like that; if a part has larger cross section on the platform it tends to curl more [9]. But in this study it is assumed that orientation of the part in the production chamber is negligible. Thus no variations in mechanical properties are expected on layers due to orientation for the parts in same energy density. According to this information, whole part becomes transversely isotropic. Transversely isotropic materials are defined as a special case of orthotropic materials. Mechanical properties on a plane are the same in every direction while it changes in the perpendicular direction. Hence 5 independent elastic constants are necessary to define those parts. For example if XY plane is the isotropy plane then (Figure 3.4, Figure 3.5),

$$
E_x = E_y \Rightarrow \frac{\nu_{xy}}{E_x} = \frac{\nu_{yx}}{E_y} \Rightarrow \nu_{xy} = \nu_{yx}
\tag{3.3}
$$

$$
\varepsilon_{x,0} = \varepsilon_{y,90}(\text{for} - \text{perpendicular} - \text{parts}) \Rightarrow \frac{\varepsilon_x}{\varepsilon_z} = \frac{\varepsilon_y}{\varepsilon_z} \Rightarrow \nu_{zx} = \nu_{zy}
\tag{3.4}
$$

20
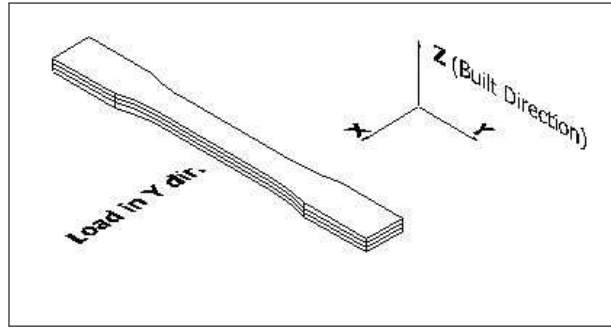
Figure 3.4: Tensile test specimen built in thickness direction lying on XY plane
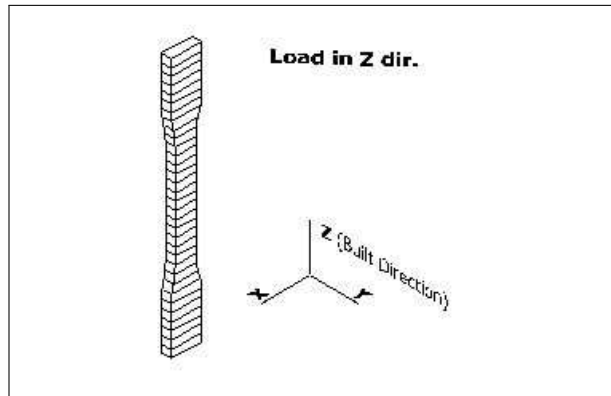
Figure 3.5: Tensile test specimen built in length direction lying on XY plane

$$
\begin{bmatrix}
\varepsilon_x \\
\varepsilon_y \\
\varepsilon_z \\
\gamma_{yz} \\
\gamma_{zx} \\
\gamma_{xy}
\end{bmatrix}
=
\begin{bmatrix}
\frac{1}{E_p} & -\frac{\upsilon_p}{E_p} & -\frac{\upsilon_{zp}}{E_z} & 0 & 0 & 0 \\
-\frac{\upsilon_p}{E_p} & \frac{1}{E_p} & -\frac{\upsilon_{zp}}{E_z} & 0 & 0 & 0 \\
-\frac{\upsilon_{pz}}{E_p} & -\frac{\upsilon_{pz}}{E_p} & \frac{1}{E_z} & 0 & 0 & 0 \\
0 & 0 & 0 & \frac{1}{G_{zp}} & 0 & 0 \\
0 & 0 & 0 & 0 & \frac{1}{G_{zp}} & 0 \\
0 & 0 & 0 & 0 & 0 & \frac{2(1+\upsilon_p)}{E_p}
\end{bmatrix}
\cdot
\begin{bmatrix}
\sigma_x \\
\sigma_y \\
\sigma_z \\
\tau_{yz} \\
\tau_{zx} \\
\tau_{xy}
\end{bmatrix}
\tag{3.5}
$$

Where P designates the isotropy plane (XY) [37].

In order to construct the compliance matrix fully, tensile tests and torsion tests are performed. Specimen in Figure 3.4 is produced to determine the Young's Modulus and the Poisson's ratio of the isotropy plane (E_p, υ_p). On the other specimen in Figure 3.5 is produced to get the Young's Modulus and the Poisson's ratio in the Z direction (E_z, υ_{zp}). Finally torsion test

specimens (Figure 3.6) in which the layers placed in length direction are produced and tested to find the shear modulus (G_{zp}). G_p is calculated due to the Hooke's Law for linear elastic materials.
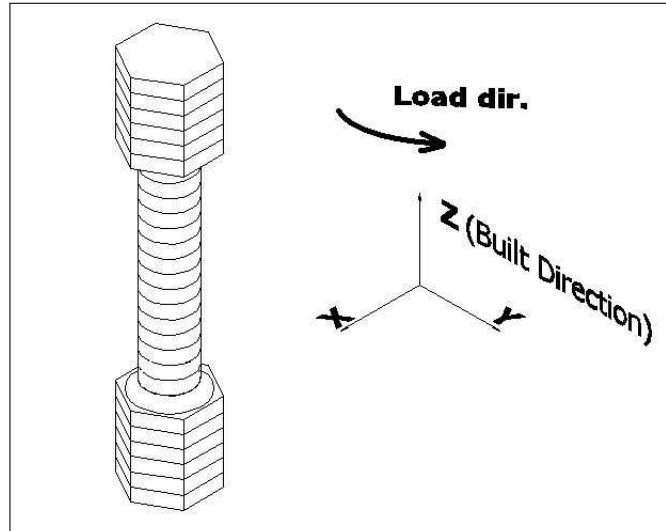
Figure 3.6: Torsion test specimen

3.3 Test Equipment

Several test equipments are used for tensile tests conducted in Materials Testing Lab at the Mechanical Engineering Department at METU. A Zwick tensile test machine and TDG Ai8b data acquisition system with TML strain gages are used during the tests.

3.3.1 Zwick Z020 Tensile Test Machine

Zwick Z020 tensile test machine is set up in materials testing lab in the department of mechanical engineering, METU. This computer controlled system has a maximum load capacity of 20 kN both in tensile and compressive direction (Figure 3.7).

A software called TestXpert drives the whole system. Positioning accuracy of the moving head is maintained within 2μm and there is a height of 1030 mm without crossheads and 440

22

Figure 3.7: Zwick Z020 Tensile test machine, Materials Testing Lab., METU

mm of width for test area. Crosshead speed of the drive system can be varied between 0.0005 mm/min to 1000 mm/min. Crosshead grips for tensile tests have inclined holders supported with springs that are buried in the material during tests (Figure 3.8). Therefore an external force is not necessary for the machine not to slip on the material at the beginning of the test. But generally this property avoids machine to give the exact displacement values of the crosshead. Hence, an extensometer is required to get the strain data. Thus a clip on extensometer is used during the elastic region of the test. After the slope of the load displacement curve starts decreasing, the extensometer is removed in order not to get it damaged.

Figure 3.8: Tensile testing grip of the test machine

3.3.1.1   TestXpert Tensile Test Program

Testxpert program is the software in which it is possible to create test environments and to drive the Zwick Z020 Tensile Test Machine.

Before running the software, the test machine must be turned on and the initialization sound (2 clicks) must be heard. The software will not work properly unless you run it without hearing that voice. One other sign is the arrows on the task bar. If they are green the software is working fine (Figure 3.9).
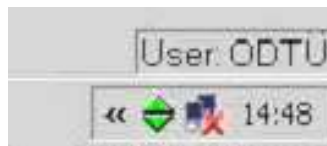
Figure 3.9: TestXpert icon on the taskbar

The first thing on the program is to select a test program in which properties of the desired test is set. Test programs are using "ZPV" extension. Pre performed test series can also be opened in this section with an extension of "ZSE" (Figure 3.10).
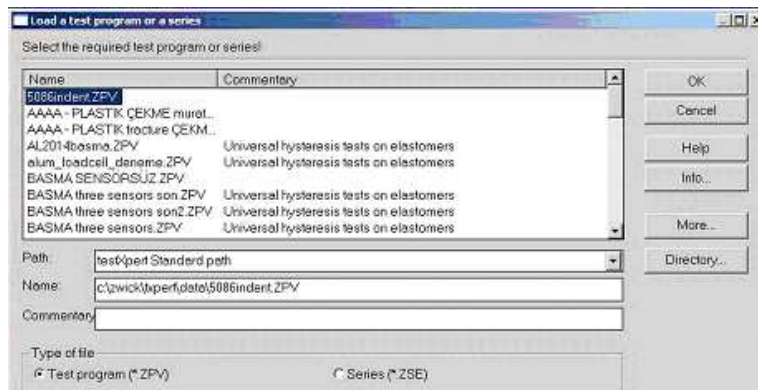
Figure 3.10: Load a test program

After selecting the test program, test machine loads this program and sounds twice as a sign of loading. This time the bar under the screen is red which indicates that the machine is "off". In order to operate the machine using the program, the "on" button on the machine must be

pressed. With this action the red bar turns white and the machine is available for tests (Figure 3.11).

Figure 3.11: Indicator before turning on (up) and after turning on (down) the machine

The TesXpert has a user friendly graphical user interface where the most common functions are added to the top bar as a shortcut (Figure 3.12).
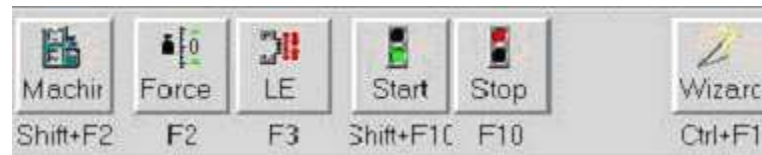
Figure 3.12: Shortcut bar

- "Machine" button is used to adjust options like linking and unlinking the hardware to the software, correcting the crosshead position, or calibrating the machine.

- "Force" is used to zero the initial force on the software.

- "LE" is the distance between the grips. When pressed, the crosshead travels to the initial test position entered to the test program.

- "Start/Stop" button starts and stops the test.

- Through the use of the "Wizard" button, properties of the test can be seen and set. In "Wizard" section there is a list on the left where each property set is grouped. The most important sets in this menu are Verification, Test Definition, Cycles/Steps, Specimen Data, LE Positions and Test Data Memory.

  – In Verification section, type of the set is determined. Either tension or compression can be selected. Also some properties like current LE position, force limits

25
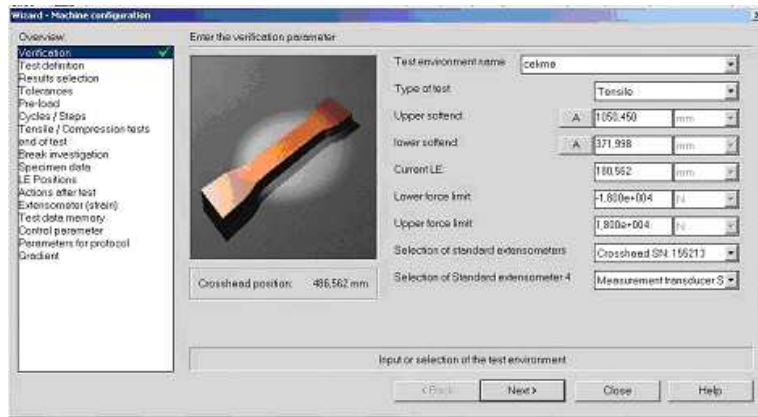
Figure 3.13: Verification set under Wizard section of TestXpert

and hardware selection is done from this screen. For tests performed in this study tensile properties are set (Figure 3.13).

– In Test Definition section, test method is determined. Either constant cycles or stepwise variable cycles can be selected in this screen. For tensile tests and fracture toughness tests constant cycles are selected (Figure 3.14).

Figure 3.14: Test Definition set under Wizard section of TestXpert

– In Cycles/Steps section, number of cycles and cycle speed is determined. Since single cycle tests are performed other properties in this screen like upper and lower reversal points can be neglected. Also the controlling of the speed is set in this section. Either force or position controlling can be selected for tests. For

tensile tests and fracture toughness tests only a single cycle is used with position controlling. Speed of tests is set to 5 mm/min (Figure 3.15).
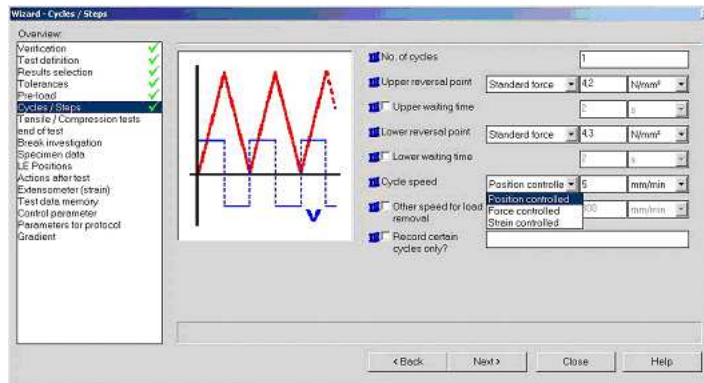
Figure 3.15: Cycles/Steps set under Wizard section of TestXpert

– In Specimen Data section (Figure 3.16), the shape and the dimensions of the specimen is determined. Flat, round or tube specimens can be selected. The dimensions of the specimen can be given in this screen or in the main test screen. Parallel specimen length is a coefficient to approximate the measured displacement and the crosshead movement.It's found by a trial and error method.
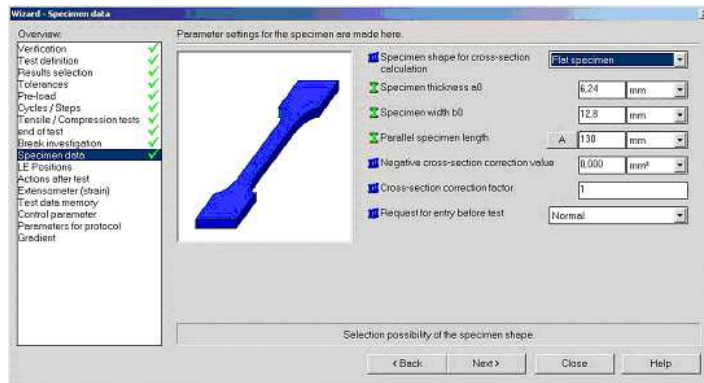
Figure 3.16: Specimen Data set under Wizard section of TestXpert

Since a displacement transducer is used to determine the strain, this value can be neglected. The dimension values entered here are used in the program for calculation of cross section and stress values. Therefore the flat specimen is selected for

the tensile test. Since only load and travel data is necessary for fracture toughness tests this screen is neglected.

– In LE Positions section, initial position of the grips is determined. Grip to grip separation is entered in millimeters by considering the specimen length. Also crosshead travel speed when "LE" button pressed is determined here. If you tick the "LE Accept" box, the program doesn't ask to travel to the LE position entered. It accepts the current position and starts the test (Figure 3.17).
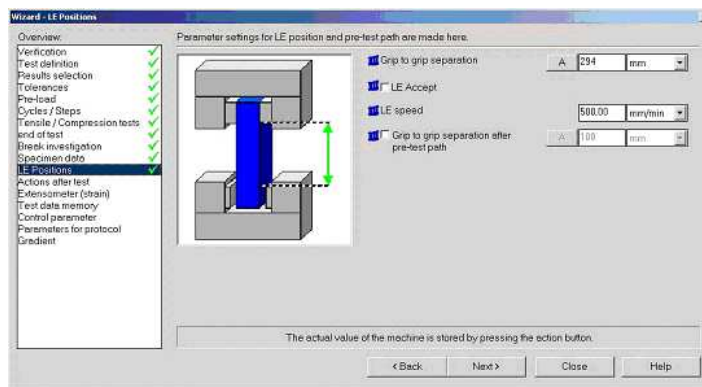
Figure 3.17: LE Positions set under Wizard section of TestXpert

– In Test Data Memory, you can determine the interval to collect one data. Position, force or time intervals can be used to get the data (Figure 3.18).
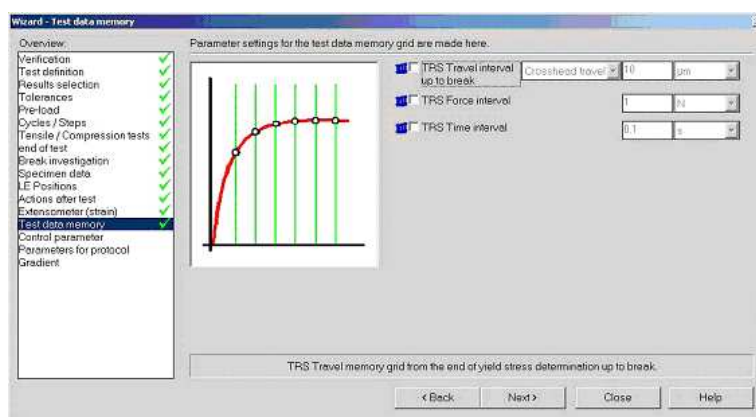
Figure 3.18: Test Data Memory set under Wizard section of TestXpert

Other properties not mentioned in this section can be used in default mode such as the load and displacement restrictions, determination of result screens etc.

One advantage of this program is that it calculates all the results even if they are not selected in properties. After the test, all results can be examined. After the test program is set up, the machine is ready for the test. First, grips must be positioned for the test by clicking "LE" button and force must be zeroed by clicking "Force" button. Then the specimen can be installed. A pre stress in compressive direction occurs when the clamps are released. This force is not zeroed in tests but it can be compensated by giving a pre load to the specimen. Finally the test can be started. It determines the fracture automatically and stops the test. If a clip on extensometer is used, it has to be removed at the end of the linear portion (Figure 3.19).
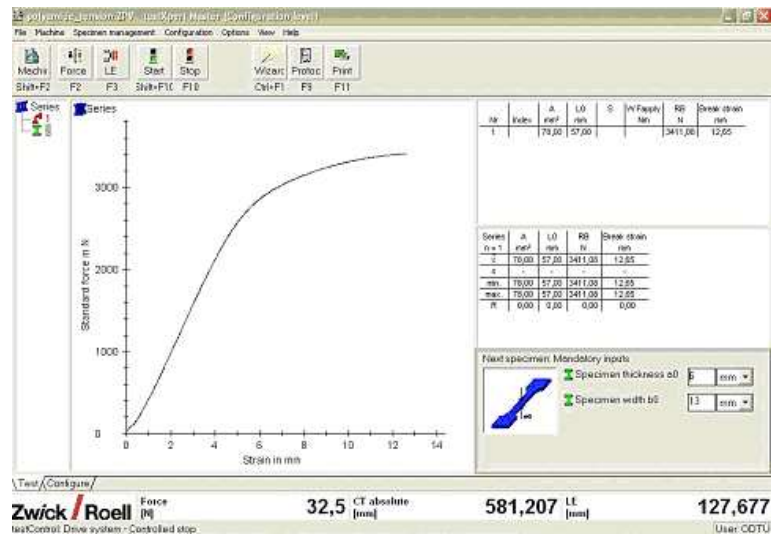
Figure 3.19: Screenshot after test

Some basic results can be read from the main test screen. Also the raw data can be exported to Microsoft Excel and can be evaluated. First we select the data series to be exported on the left hand side of the main screen. Then using file menu and export interfaces is selected. The "TRA" file and the "ZSE" file are exported. TRA file is the raw data of the test. The user determines which data groups are to be exported. Standard Travel, Standard Force and Sensor 1 (extensometer) are sufficient for evaluation. This file can be opened by Excel. Using the "text to column" option on data menu, each data can be set into one cell. ZSE file contains

all the information about that test process. Later on the ZSE file can be opened and different data groups belong to the test can be seen.

3.3.2   TDG Ai8b Data Acquisition System and TML Strain Gages

This system is used to determine the Poisson's ratio of the materials. An axial and a transverse strain gage are installed on the specimen and the data is obtained from the machine's software which is called TDG CODA. Test environment is created by using the software. All the necessary information such as gage factor, calibration coefficient, channel gain is entered to this program and the strain data is read directly from the software. A special cable is used to construct a Wheatstone Bridge. 8 cables can be connected at the same time where all channels have individual signal processing units. It takes maximum 8 samples per second with 16 bits of resolution. Each channel has 8 different gain settings within a ±10 V range. When the gain is increased the sensitivity of the measurement increases and more smooth curves achieved but the values reach out of range quicker. Also +5V or +10 volts of excitement can be applied to gages [38] (Figure 3.20). A gateway device is used as a converter for serial to USB. With this device DAQ can be connected to any computer having a USB port without the desire to a specific card.
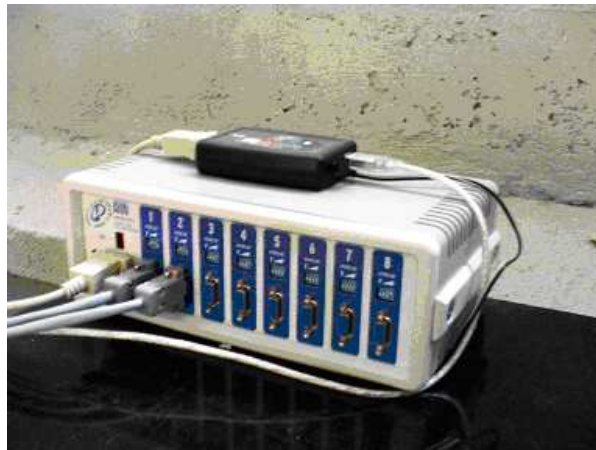
Figure 3.20: TDG Ai8b DAQ system, Materials Testing Lab., METU

The hardware has to be turned on approximately 15 minutes before test in order to reach the optimum working conditions.

Unlike metallic materials, polymeric materials are not stiff enough and reinforcement due to the adhesives can not be neglected. Parts built with SLS are also affected from the adhesives. Due to the porous structure of the material, installing gages take longer time than metallic materials. Also, axial strain data is get approximately one third of thethat of data taken by extensometer. C.C. Perry who has made several experiments with low modulus and orthotropic materials indicates the true strain with some strain transformation coefficients. He suggests those coefficients to be characterized by the same function in axial and transverse direction. Also Ajovalasit et al, suggests that no calibration process is required for Poisson's ratio if up to date commercial gages are used which have low transverse sensitivities [28, 39]. This means when the strain data is measured with same strain gages both in axial and transverse direction under same conditions; they exhibit the same error due to the adhesives. The ratio of both values cancels the errors and the apparent Poisson's ratio is found. Therefore it is decided to use these strain gages only in the determination of the Poisson's ratio.

TML GFLA-3-50 strain gages which have a 2.09 ±1% gage factor are used for the tests. These gages are produced especially for plastic materials and work within a temperature range of -20 to 80 $^o C$. The gages have 3 mm of gage length with a 120 ±0.3Ω of gage resistance. Gage material is Cu-Ni alloy and it has the strain limit of 3%. Cyanoacrylate based CN adhesive is used to install the gages [40].
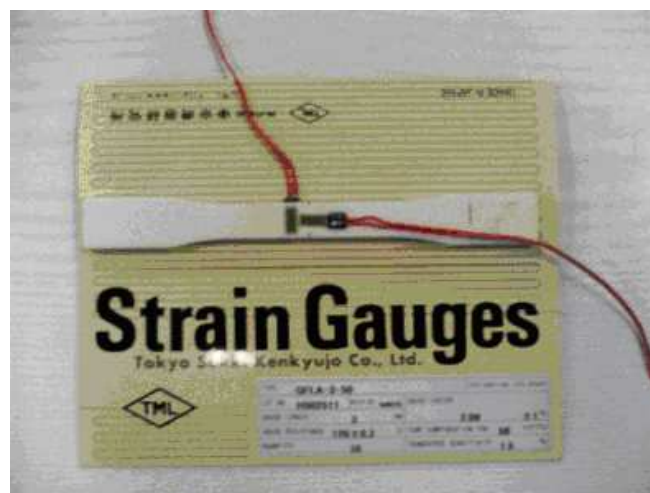
Figure 3.21: TML GFLA-3-50 Strain gauges installed on a polyamide specimen

3.3.2.1 TDG Coda Software

This software consists of several sub programs in which 3 of them are used mainly (Test Editor, Logger Express, Locomotive) and 3 of them are used for setting up the options (Language Selector, Device Manager, Calibrator).

- Language Selector and Device Manager are used just once when the system is connected to the computer for the first time. Either English or Turkish can be selected as languages for user interface. In Device Manager Program, one initializes the Gateway and establishes a connection between the computer and the Ai8b hardware via the gateway. No other property change is necessary on this program (Figure 3.22).
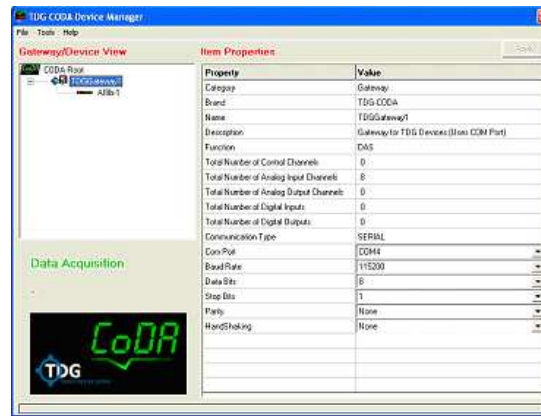
Figure 3.22: TDG CODA Device Manager

- Calibrator program is used for calibration. Since the hardware is calibrated before it is purchased, this program is not used at all.

- Test Editor is used to create test environments such as channels and graphics. It makes a compromise between the direct channels in which voltage output is read directly and channels used for desired output. Constants used to convert the voltage to strain according to the gage properties are entered in this program. Virtual channels like can be created with this program. Also properties of the graphics on the test screen are set in this screen. If a routine test is performed then it is not necessary to run this program after creating a working test environment (Figure 3.23).

32
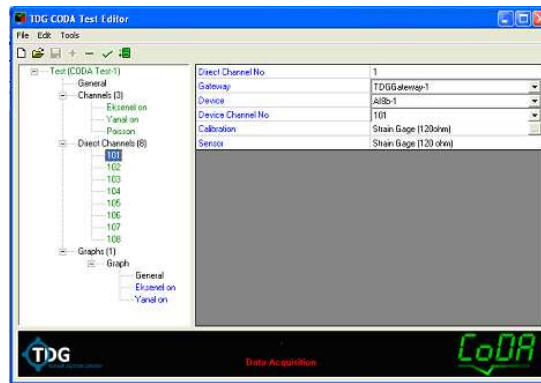
Figure 3.23: TDG CODA Test Editor

- Open or create a test environment from the file menu. First add all the device channels as direct channels by right clicking the "Direct Channels" section. There are 8 direct channels named from 101 to 108. The gateway and device is selected automatically as it is initialized in device manager program. Only sensor type is selected from the pre defined sensors.

- Then channels in which data is acquired must be added to "Channels" section by right clicking on. One can give names to selected channels, enter the coefficients to convert voltage to strain or create a virtual channel in this screen.

- Finally one can add graphics by right clicking on the "Graphs" section. The grid properties and axis properties can be adjusted by using this screen.

- After the setup is completed, "Thick" icon on top is clicked to confirm that if the setup is done correctly. Then one saves the environment and exits the program.

• Logger Express program is the basic way of visualizing the strain in terms of voltage for each channel. Test environments are not loaded for this program. Also, zero calibration of the individual channels are carried out.

- First, one needs to connect the device to the test program. Control menu is used and start connection button is clicked. When connection is established the program is ready to acquire data. Zero calibration of the channel is done by turning the little knob on the bridge cables where the strain gages are connected (Figure 3.24).

33

Figure 3.24: TDG CODA Logger Express

- Locomotive is the main test program (Figure 3.25). First, one needs to load test environment from file menu by clicking open test. Then the test environment is selected with test editor. It establishes the connection to the hardware automatically. Then use zero window in the tools menu to zero the channel on software. After this, the program is ready for tests. One can start and stop the test in test menu. Finally one exports the data by using export wizard on the tools menu. The program creates a file in "CSV" format which Excel recognizes.

Figure 3.25: TDG CODA Locomotive

3.4 Mechanical Tests

In order to determine the mechanical properties of plastic polyamide materials produced via SLS, tensile tests and torsion tests are performed. Also fracture toughness tests are conducted to determine the K_{IC} value of the material.

3.4.1 Tensile Test

Tensile test is one of the most important tests in mechanical engineering in which the reaction of material to tension can be examined. These tests generally not expensive and fully standardized [41]. ASTM E8 standard is used to determine the mechanical properties of metallic materials while ASTM D638 is used for plastics [26]. Either flat or circular specimens can be used then subjected to tension until the material breaks according to the corresponding standard.

Tensile test specimens are produced according to the standard of ASTM D638. Considering the chamber size of the SLS machine and the production costs, Type I specimen is chosen which suggests the use of specimens having thickness between 4 to 7 mm. 5 specimens for each energy density value are tested to check repeatability (Figure 3.26). During the tests, machine is set to move at a speed of 5 mm/min.
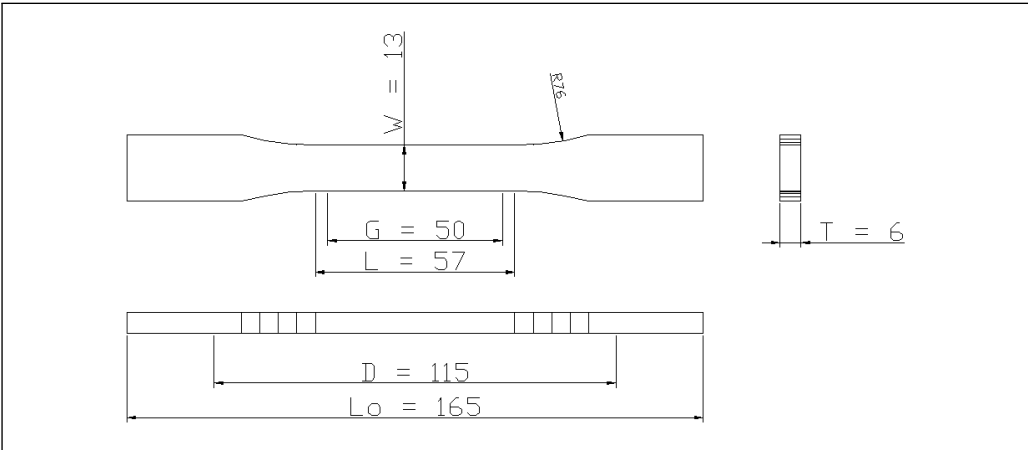
Figure 3.26: Geometry of the produced specimens

Load - displacement data is acquired from the test machine. By dividing the load data to

initial cross section of the specimen, engineering stress values are found. If an extensometer is used during the test, elongation of the gage length is divided by the initial gage length and the strain data is achieved. Although load displacement data differs from specimen to specimen, stress strain data is a material property and does not show significant differences for different specimens. Several material properties are determined from a stress strain curve some of which are ultimate tensile strength (UTS), rupture strength, modulus of elasticity and Poisson's ratio.

3.4.1.1   Ultimate Tensile Strength (UTS)

Ultimate tensile strength is the maximum stress that a material can withstand under tensile load. It is the maximum point on the stress strain curve and the unit is N/mm^2 (MPa). It is determined from the load data given by the test machine and is not related to the strain (Figure 3.27).
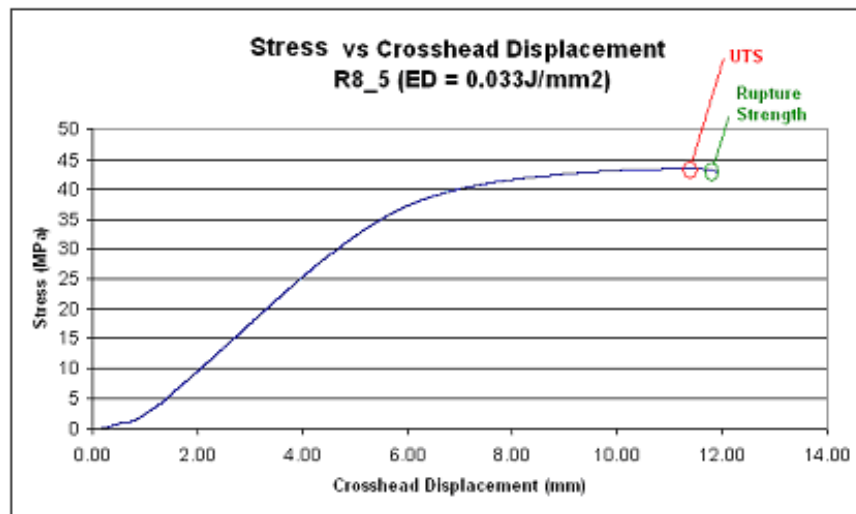
Figure 3.27: Stress vs. Crosshead displacement diagram of a default specimen

3.4.1.2   Rupture Strength

Rupture strength is the stress at the point where material fails. It is the final load data taken from a tensile test. Unit is same as that of UTS which is N/mm^2 (MPa). This property also is

not related to the strain (Figure 3.27).

3.4.1.3 Modulus of Elasticity

Modulus of elasticity is the resistance of material to elastic deformation. It is the slope of the stress strain curve on the linear portion. An extensometer is required to get the strain data at least during the elastic region. Data interval of linear portion is separated from the whole data and the scattered graph is plotted by Excel. Almost linear graph is fitted with a straight trendline and the equation of the line is found. Coefficient of the X value on the equation corresponds to the slope of the line consequently the modulus of elasticity of the material. The unit is N/mm^2 (MPa) (Figure 3.28).
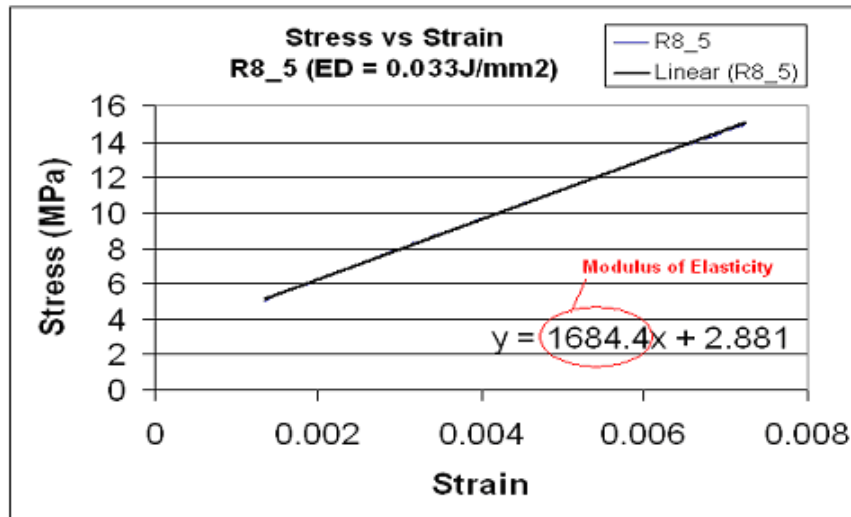
Figure 3.28: Stress vs. Strain diagram of a default specimen

3.4.1.4 Poisson's Ratio

Poisson's ratio is the negative sign of proportion of the transverse strain to the axial strain on the material. For isotropic materials this ratio varies between 0 - 0.5 where approximately 0.3 is used for many engineering metals. But, for orthotropic materials this range is not a restriction. However due to the symmetry on the compliance matrix, equation (3.2) is valid and equations below must be satisfied [36];

$$\nu_{ij}.\nu_{ji} < 1 \qquad\qquad (3.6)$$

$$\sqrt{\frac{E_i}{E_j}} > |\upsilon_{ij}| \qquad\qquad (3.7)$$

Poisson's ratios of the materials are determined from the data acquired from the DAQ via strain gages.

3.4.2 Torsion Test

Torsion tests are performed in order to get the shear modulus which is the resistance to torsional deformation of the material. ASTM E 142-2 is used as the standard [42].

Tests are performed in Gazi University Department of Mechanical Engineering Mechanics and Strength Lab with a SM21 Torsion Test Machine. SM21 machine has 200 Nm of maximum torque capacity which is measured by a digital measurement system (Figure 3.29). It supports specimens up to 300 mm with hexagonal ends. Produced specimen's dimensions can be seen in Figure 3.30. Torque reaction is applied with a pendulum. Since the digital measurement system doesn't have any computer connections, revolution number and torque is read every 5 seconds manually.

Figure 3.29: SM21 Torsion test machine, Mechanics and Strength Lab, Gazi Uni.
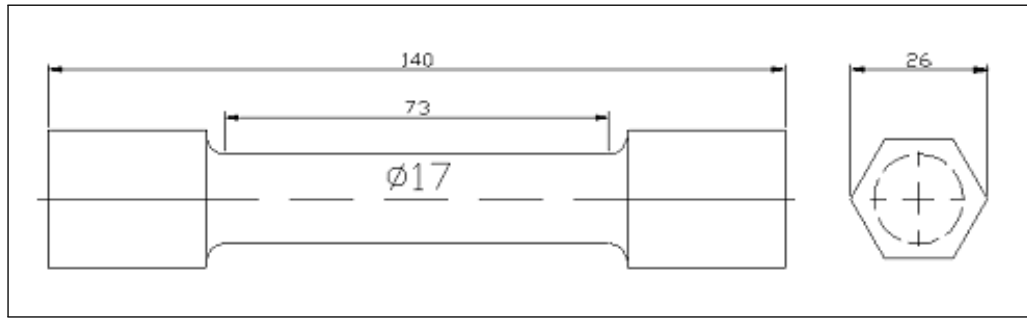
Figure 3.30: Torsion test specimen

Revolution of the machine is determined with a counter in which an increment corresponds to 0.3 degrees. Also torque is measured with a digital torque meter. By using the formulas below, shear stress and shear strain values are found and the graph is plotted. Slope of the trendline fitted through the linear portion gives the shear modulus of the material (Figure 3.31).

$$\tau = 16.T/\left(\pi.d^3\right) \tag{3.8}$$

$$\gamma = r.\theta/L \tag{3.9}$$

3.4.3 Fracture Toughness Test

Fracture toughness is the resistance of material to cracks. There are 3 modes of fracture. Mode I is known as the opening mode in which tensile stress is applied normal to the crack plane. Mode II is known as sliding mode in which shear stress acts parallel to the plane of the crack and perpendicular to the crack front. Finally, Mode III is known as the tearing mode in which shear stress acting parallel to the plane of the crack and parallel to the crack front. ASTM E399 standard is used to determine the Mode I fracture toughness K_{IC} for metallic materials while ASTM D5045 is used for plastics [43]. Compact tension test specimens are manufactured for tests (Figure 3.32). In order to clamp the specimens on the tensile test machine a clevis is built after making several iterations on specimens which ensure the plane
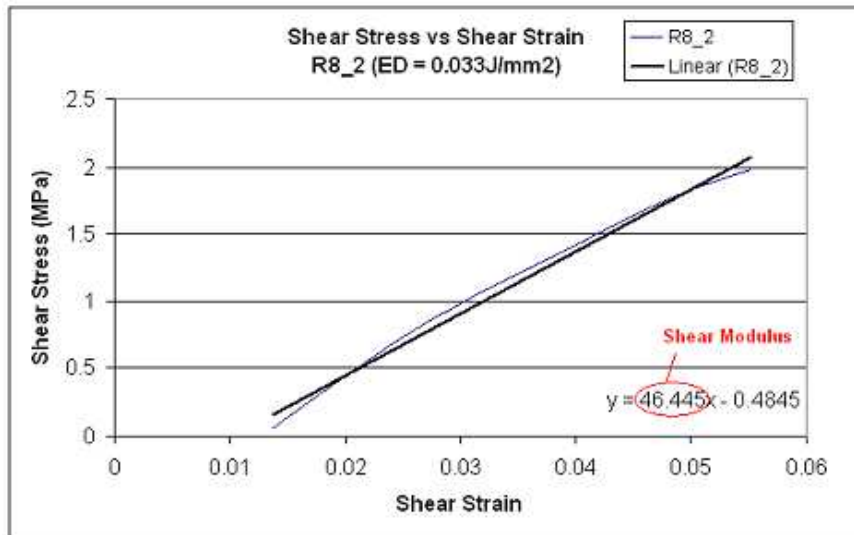
Figure 3.31: Shear Stress vs. Shear Strain diagram of a default specimen

strain condition. The specimens must be thick enough for not to be effected from the strains in Z direction.
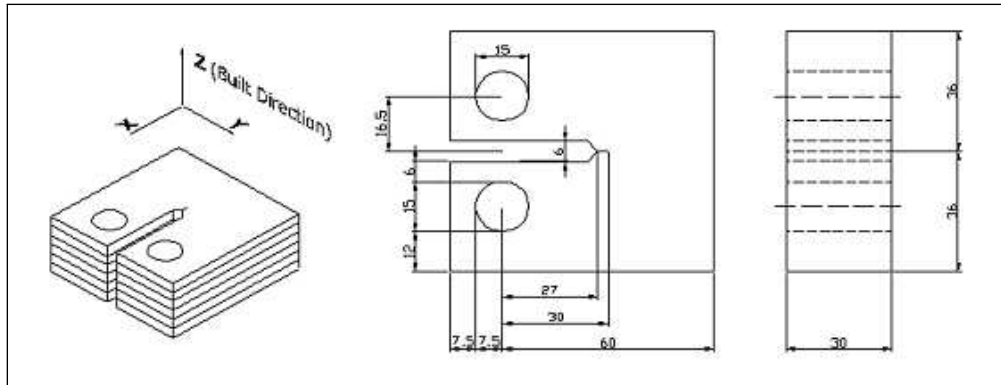
Figure 3.32: Building direction and dimensions of compact tension specimen

First, a straight line (B curve) is fitted on the linear part of the load - crack opening displacement curve and the angle between B curve and Y axis is found (θ). 1.05θ gives the angle between Y axis and the B' Curve. The intersection of B' curve and the load curve gives the P_Q. The ratio of P_Q to the maximum load P_{max} has to be greater than 1.1 otherwise the test is invalid (Figure 3.33).

40
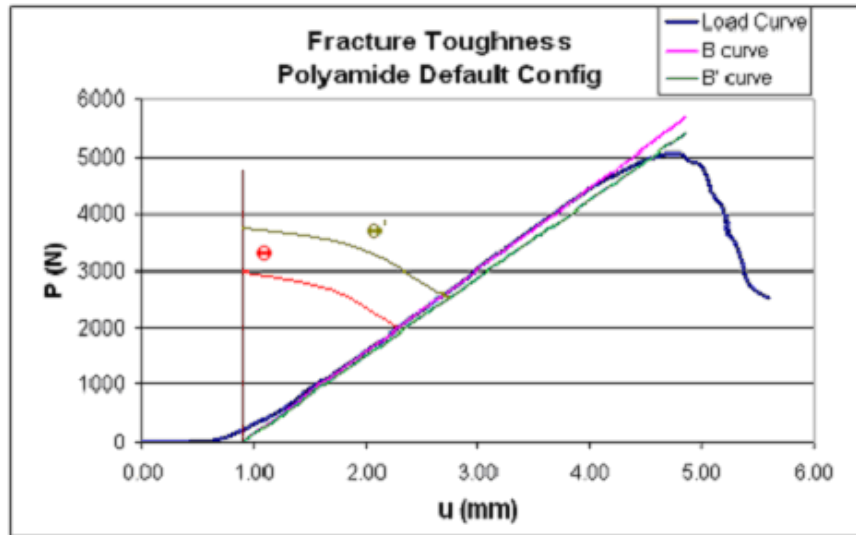
Figure 3.33: Fracture toughness test result for a default specimen

Then K_Q is calculated with the following formula;

$$K_Q = \frac{P_Q}{B\sqrt{W}} f(x) \tag{3.10}$$

where,

$$f(x) = \frac{(2+x)(0.886 + 4.64x - 13.32x^2 + 14.72x^3 - 5.6x^4)}{(1-x)^{1.5}} \Rightarrow x = \frac{a}{W} \tag{3.11}$$

If the thickness is large enough to ensure the plain strain condition in equation 3.11 then K_Q is taken as the K_{IC}. Otherwise the test is invalid and it has to be repeated with specimens having at least 1.5 times the original dimensions.

$$B, a > 2.5\left(K_Q/\sigma_y^*\right)^2 \tag{3.12}$$

3.5 Evaluation of Test Results

In order to check the repeatability and the consistency of the results several tests are performed in experimental studies. Some results generated may not seem valid and have to be rejected.

41

A criterion called "Chauvenet's Criterion" is used to eliminate the irrelevant data from the results [44–46]. According to this criterion, "a reading may be rejected if the probability of obtaining the particular deviation from the mean is less than 1/2n" where n is the number of data points read [45]. First, mean value and the standard deviation (σ) of the data points are found. Then absolute difference of each individual data point from the mean value is calculated (d_i). When d_i is divided by the standard deviation (σ) of the whole data points, the number found can not exceed the maximum value calculated according to the number of data points given in Table 3.2.

Table 3.2: Number of experiments (n) and maximum value to reject a data (dmax/σ)

n	d_{max}/σ	n	d_{max}/σ
3	1.38	25	2.33
4	1.54	50	2.57
5	1.65	100	2.81
6	1.73	300	3.14
7	1.80	500	3.29
10	1.96	1000	3.48
15	2.13		

For example if 5 data points are acquired from a test, the absolute difference from the mean for each data point divided by the standard deviation has to be smaller than 1.65. If this value is exceeded then the data can be cancelled. After the irrelevant data is rejected the mean value and the standard deviation is recalculated. Although this criterion can be applied more than once, only the first application can be used.

3.6   Results of Mechanical Tests for Uniform Porous Specimens

Since the objects are built layer by layer with this production method, they exhibit linear orthotropic behaviour. As a result, tensile specimens produced in thickness and length directions have to be tested. As mentioned in the previous chapters, we assume that the global behaviour of the material as transversely isotropic. Thus only circular specimens in length direction are

produced and torsion tests are performed. Information achieved from tensile tests and torsion tests allow us to generate the complete compliance matrix of the material for different energy density values.

3.6.1 Results of tensile tests for uniform porous structures

In tensile tests, several properties of the material such as ultimate tensile strength, rupture strength, modulus of elasticity and Poisson's ratio are determined. 5 specimens without contours for each energy density value are produced and tested as suggested in the ASTM D638 standard. The results are averaged and standard deviations are calculated. Although small values of standard deviations are found for results, higher values are faced for Poisson's ratio which may result from the errors in installation. For parts built in thickness direction (layers are parallel to the load direction) it is expected to get higher results compared to the parts built in length direction (layers are perpendicular to the load direction). Also, an increase in trend up to a certain value then a decrease due to degradation is expected over the whole energy density range. Actually this property is expected for all mechanical tests because excessive energy applied distorts the material significantly. The results for tensile test specimens built in thickness direction are given in Figures 3.34 to 3.37 and Table D.1.

From Figure 3.34 to Figure 3.37 square data sets (purple) corresponds to mid configurations which have different energy density values determined by İlkgün [2]. These set of specimens are built to check whether the mechanical properties fit on the actual trend. Numerical results of mid configurations can be seen in Table 3.5.
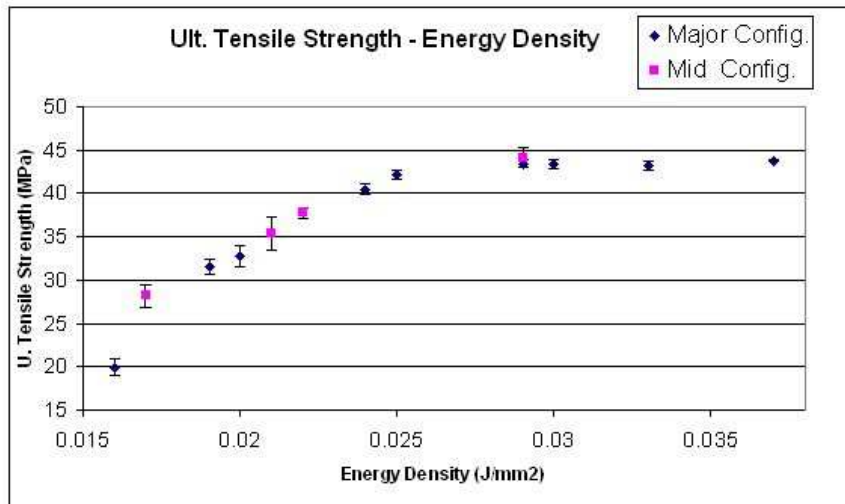
Figure 3.34: Ultimate tensile strength vs. Energy density for parts built in thickness.
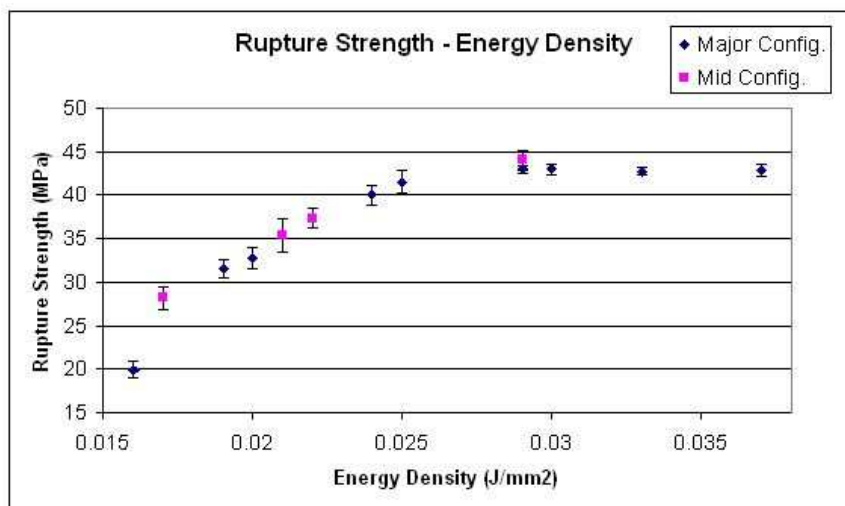
Figure 3.35: Rupture strength vs. Energy density for parts built in thickness direction.
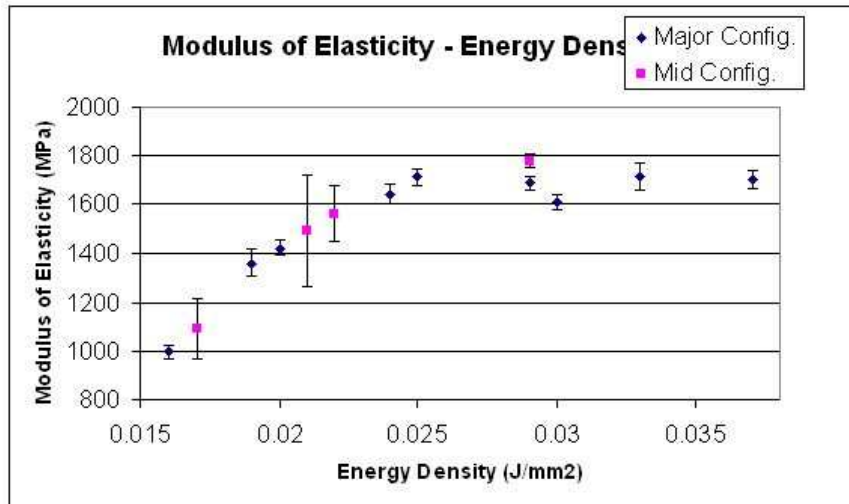
Figure 3.36: Modulus of elasticity vs. Energy density for parts built in thickness direction.
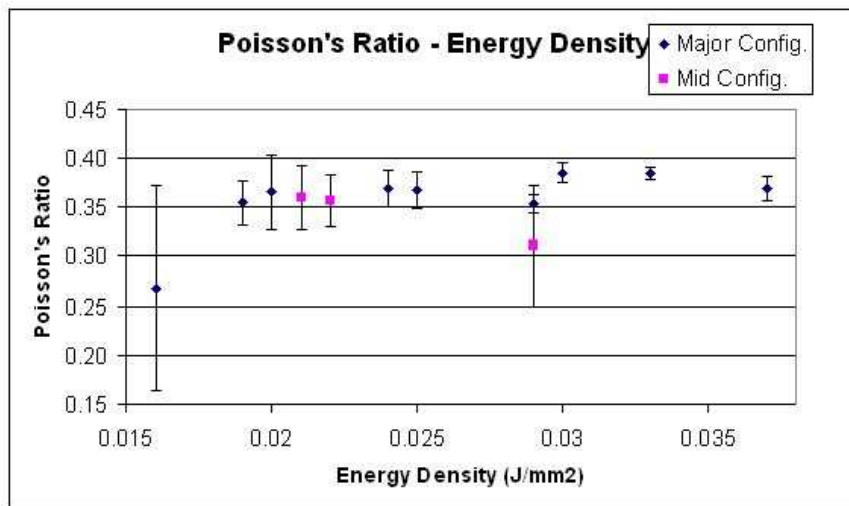
Figure 3.37: Poisson's ratio vs. Energy density for parts built in thickness direction.

45

Table 3.3: Numerical Results for tensile test specimens built in thickness direction

	ED (J/mm^2)	Modulus (MPa)	Std. Dev.	Poisson's Ratio	Std. Dev.	UTS (MPa)	Std. Dev.	Rupture (MPa)	Std. Dev.
R1	0.016	997.725	28.808	0.268	0.104	19.980	0.912	19.978	0.913
R2	0.019	1362.250	52.548	0.355	0.023	31.620	0.911	31.554	0.972
R3	0.020	1421.350	30.567	0.365	0.038	32.822	1.157	32.804	1.153
R4	0.024	1641.840	41.649	0.370	0.019	40.422	0.595	39.994	1.134
R5	0.025	1712.817	34.741	0.368	0.019	42.126	0.510	41.458	1.289
R6	0.029	1686.950	28.279	0.353	0.009	43.397	0.417	42.932	0.469
R7	0.030	1608.100	31.569	0.385	0.010	43.378	0.515	42.937	0.628
R8	0.033	1714.480	57.923	0.384	0.006	43.174	0.497	42.732	0.516
R9	0.037	1701.860	37.458	0.369	0.013	43.736	0.103	42.880	0.729

Table 3.4: Numerical Results for tensile test specimens built in thickness direction (mid configurations), (Poisson's ratio for part having 0.017 J/mm2 can not be achieved due to experimental errors)

ED (J/mm^2)	Modulus (MPa)	Std. Dev.	Poisson's Ratio	Std. Dev.	UTS (MPa)	Std. Dev.	Rupture (MPa)	Std. Dev.
0.017	1093.530	125.600	-	-	28.250	1.310	28.220	1.320
0.021	1491.670	228.360	0.360	0.030	35.350	1.930	35.340	1.930
0.022	1559.800	114.120	0.360	0.030	37.740	0.610	37.290	1.150
0.029	1778.430	27.120	0.310	0.060	44.070	1.150	44.030	1.160

From Figure 3.38 to Figure 3.41 tensile test results for specimens built in length direction can be seen. Since the layers placed perpendicular to the load direction parts are weaker than other tensile test specimens built in thickness direction. Besides, no results can be achieved for parts having energy densities lower than 0.025 J/mm^2. They are broken even before they are placed on the test machine. Numerical results are given in table 3.5.
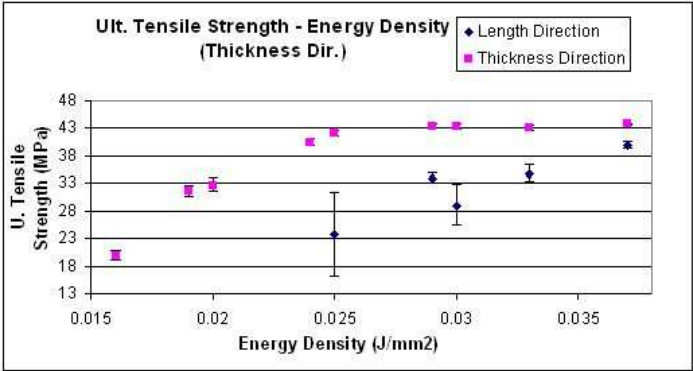
Figure 3.38: Ultimate tensile strength vs. Energy density for parts built in length direction.
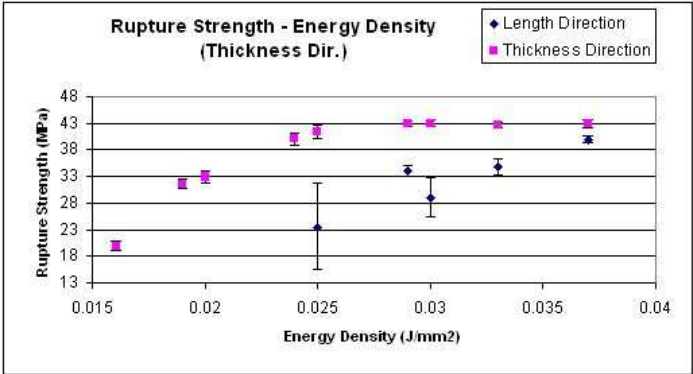
Figure 3.39: Rupture strength vs. Energy density for parts built in length direction.
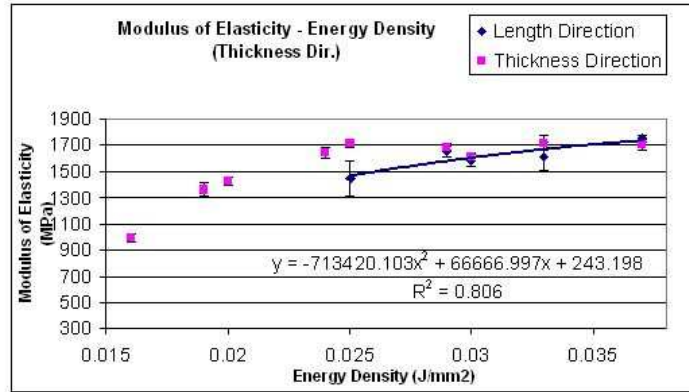
Figure 3.40: Modulus of Elasticity vs. Energy density for parts built in length direction.
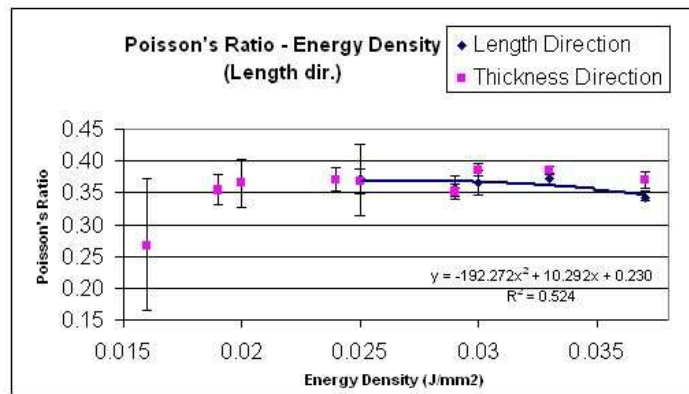
Figure 3.41: Poisson's Ratio vs. Energy density for parts built in length direction.

Table 3.5: Numerical Results for tensile test specimens built in length direction

	ED (J/mm^2)	Modulus (MPa)	Std. Dev.	Poisson's Ratio	Std. Dev.	UTS (MPa)	Std. Dev.	Rupture (MPa)	Std. Dev.
R5	0.025	1443.300	138.689	0.371	0.055	23.853	7.635	23.600	8.042
R6	0.029	1653.000	40.438	0.357	0.018	33.880	0.987	33.873	0.997
R7	0.030	1579.200	47.800	0.365	0.020	29.127	3.485	29.127	3.485
R8	0.033	1613.833	105.371	0.372	0.009	34.797	1.524	34.787	1.511
R9	0.037	1751.833	26.822	0.344	0.008	39.940	0.583	39.907	0.563

3.6.2 Results of torsion tests for uniform porous structures

In torsion tests, shear modulus of the circular parts built in length direction are found. The torque is applied on the periphery of the layer therefore very small values are expected during tests. Similar to tensile test specimens built in length direction no results can be achieved for parts having energy densities lower than 0.025 J/mm^2. They are broken just after the test begins therefore no valid data is read from the torque meter. In Figure 3.42 shear modulus vs. energy density graph is given. Numerical results are given in Table 3.6.
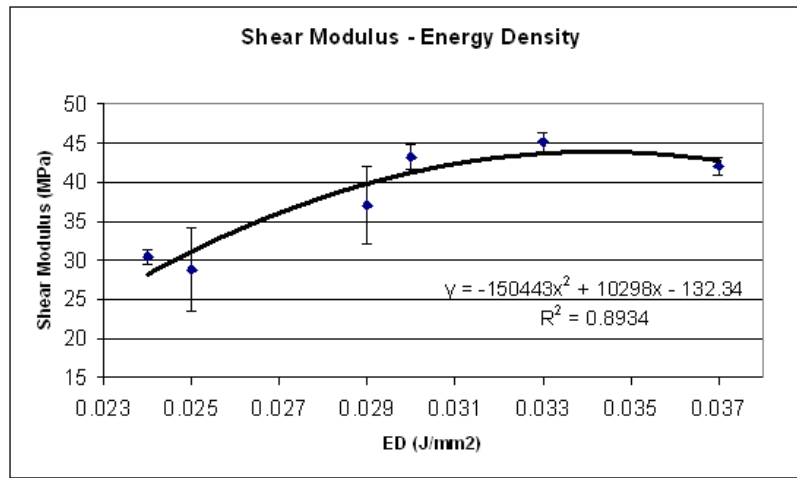
Figure 3.42: Shear modulus vs. Energy density for circular parts built in length direction.

Table 3.6: Numerical results for circular torsion test specimens built in length direction.

	ED (J/mm^2)	Shear Modulus (MPa)	St. Dev.
R4	0.024	30.456	0.935
R5	0.025	28.798	5.324
R6	0.029	36.987	4.971
R7	0.030	43.249	1.615
R8	0.033	45.187	1.202
R9	0.037	42.017	1.151

3.6.3 Results of fracture toughness tests for uniform porous structures

In fracture toughness tests, K_{IC} value for compact tension specimens built in thickness direction are found. 3 specimens for each configuration are produced and tested as suggested in ASTM 5045-99. Results can be seen in Figure 3.43 and Table 3.7.
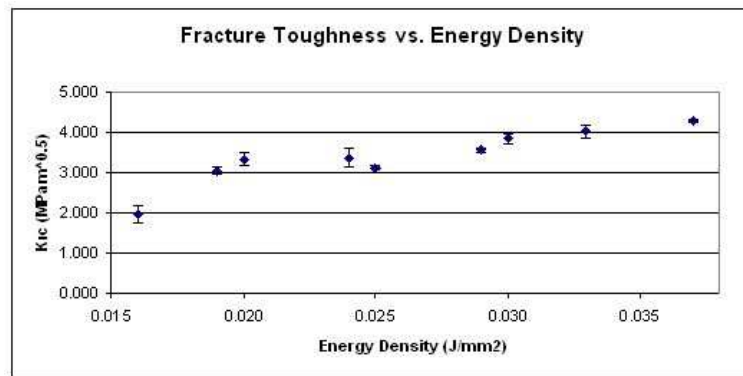
Figure 3.43: K_{IC} vs. Energy density for compact tension fracture toughness specimens.

Table 3.7: Numerical K_{IC} values for compact tension fracture toughness specimens.

	ED (J/mm^2)	K_{IC} (MPa $\sqrt{m}$)	ST Dev
R1	0.016	1.980	0.209
R2	0.019	3.035	0.097
R3	0.020	3.325	0.152
R4	0.024	3.362	0.228
R5	0.025	3.080	0.080
R6	0.029	3.545	0.060
R7	0.030	3.840	0.131
R8	0.033	4.012	0.155
R9	0.037	4.284	0.029

CHAPTER 4

PRODUCTION AND CHARACTERIZATION OF FUNCTIONALLY GRADED SPECIMENS

4.1   Production of Graded Porous Specimens (Grades in Thickness Direction)

Functionally graded specimens are designed in two types in which there are 3, 5 and 7 grades individually. Tensile test specimens are similar to the uniform porous specimens described in ASTM D 638 standard. Grades are given in thickness direction as shown in Figure 4.1. Each grade is uniformly porous itself.
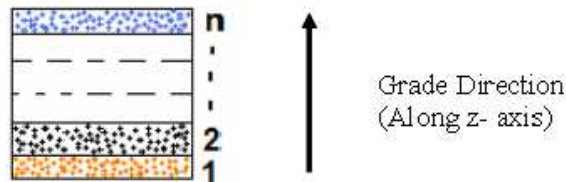
Figure 4.1: Layout of Distinct Grades for Graded Porous Specimens

For Type I, grades are given in a range of 0.016 J/mm^2 and 0.030 J/mm^2 of energy density while in Type II grades are given in a range of 0.019 J/mm^2 and 0.033 J/mm^2 of energy density. In other words, Type I contains the weakest energy density value and Type II contains the strongest energy density value. For each specimen, grade thicknesses are kept equal in order to satisfy the 6 mm of total thickness. 3 specimens are tested to check repeatability. Energy density values for each type are given in Table 4.1.

51

Table 4.1: Energy Density values of grades for Type I and Type II Specimens

	ED (J/mm²)													
	Type I							Type II						
3-grades	0.016			0.024			0.03	0.019			0.025			0.033
5-grades	0.016		0.02	0.025	0.029		0.03	0.019	0.024		0.025		0.03	0.033
7-grades	0.016	0.019	0.02	0.024	0.025	0.029	0.03	0.019	0.02	0.024	0.025	0.029	0.03	0.033

4.2 Test Results

In tensile tests of graded porous specimens, effect of number of grades within the same energy density range is sought. Also parts having same number of grades with different energy density values are compared. The results are given below both graphically and numerically in Tables 4.2 and 4.3 and Figures 4.2 and 4.3.
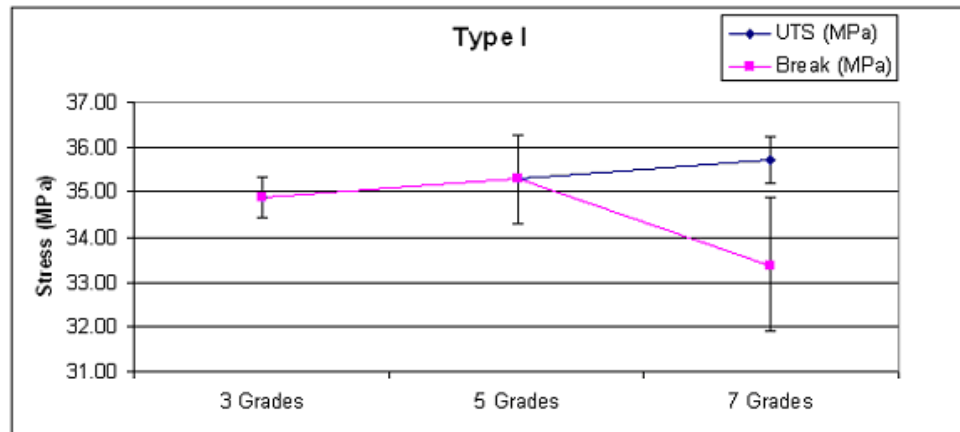
Figure 4.2: Test results for Type I Specimens

Table 4.2: Comparison of UTS (MPa) and Rupture Strength (MPa) of Type I specimens

	Type I					
	3 Grades		5 Grades		7 Grades	
	UTS	Rupture	UTS	Rupture	UTS	Rupture
S1	35.38	35.36	36.27	36.27	35.11	35.11
S2	34.75	34.74	34.31	34.31	36.09	32.44
S3	34.49	34.49	35.32	35.32	35.95	32.61
Avg.	**34.87**	**34.86**	**35.30**	**35.30**	**35.72**	**33.39**
St. Dev.	**0.458**	**0.448**	**0.980**	**0.980**	**0.530**	**1.495**
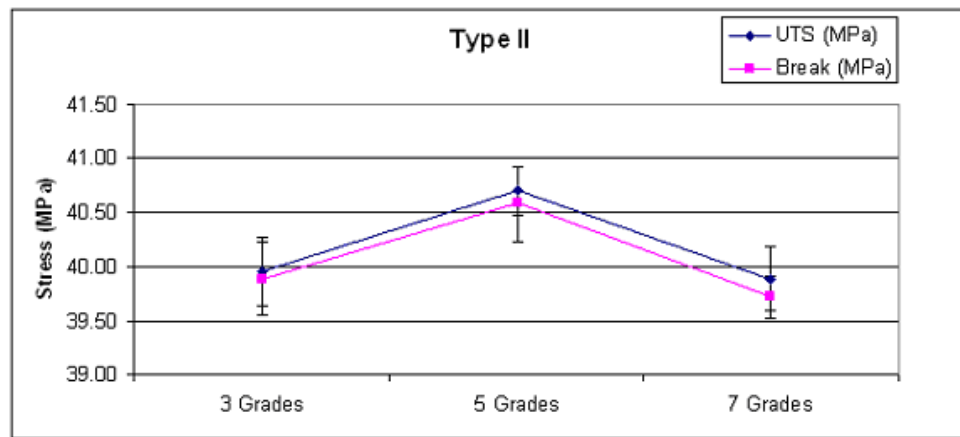
Figure 4.3: Test results for Type II Specimens

Results for both types differ within a range of 1 MPa. Type I specimens which include the weakest grade (0.016 J/mm^2), have a decreasing trend on rupture with 7 graded parts compared to other parts. That is because 2 of 3 specimens have the failure on the weakest grade before the rupture. Although the uniform porous parts produced with 0.016 J/mm^2 of energy density can only stand for 20 MPa of tensile strength, it is increased up to 35 MPa by introducing gradation into the parts.

Table 4.3: Comparison of UTS (MPa) and Rupture Strength (MPa) of Type II specimens

	Type II					
	3 Grades		5 Grades		7 Grades	
	UTS	Rupture	UTS	Rupture	UTS	Rupture
S1	40.08	40.06	40.94	40.93	40.23	39.95
S2	40.19	40.11	40.48	40.25	39.75	39.60
S3	39.59	39.50	40.66	40.56	39.70	39.61
Avg.	**39.95**	**39.89**	**40.69**	**40.58**	**39.89**	**39.72**
St. Dev.	**0.319**	**0.339**	**0.232**	**0.340**	**0.293**	**0.199**

On the other hand, parts containing the weakest grade (Type I) have the tensile strength of 35 MPa while parts having the strongest grade have the tensile strength of 40 MPa. This shows that parts without the weakest grade are 14 % stronger than the other parts.

4.3 Additional Tests for Graded Porous Specimens

After tensile tests are performed for graded porous specimens, similar specimens are produced and tested by using an extensometer for both sides of the parts. These experiments are conducted in order to see the effect of different grades on the surface and to generate comparable information with the finite element model of the graded porous specimens.

For tensile tests, 4 specimens are produced for each type and grade combination. 2 of the specimens are tested by mounting the extensometer on the weak surface while the other 2 is tested by mounting the extensometer on the strong side. According to the test results, stress at 0.4 mm of elongation and 0.5 mm of elongation is compared with the uniform porous specimens and the gain of the grades are calculated. Calculated gain values for 0.4 mm of elongation and 0.5 mm of elongation are then averaged.

Table 4.4: Weak and Strong side comparisons of TI 3Grades Parts

| | TI3G | | | | | |
	Weak Side (MPa)	Uniform (R1) (MPa)	Gain (W) (%)	Strong Side (MPa)	Uniform (R7) (MPa)	Gain (S) (%)
0.4 mm	11.238	**8.700**	29.2	16.036	**13.906**	15.3
0.5 mm	14.426	**10.481**	37.6	19.027	**17.047**	11.6
Av. Gain (%)			33.4			13.5

Table 4.5: Weak and Strong side comparisons of TI 5Grades Parts

| | TI5G | | | | | |
	Weak Side (MPa)	Uniform (R1) (MPa)	Gain (W) (%)	Strong Side (MPa)	Uniform (R7) (MPa)	Gain (S) (%)
0.4 mm	16.940	**8.700**	94.7	15.947	**13.906**	14.7
0.5 mm	20.050	**10.481**	91.3	19.071	**17.047**	11.9
Av. Gain (%)			93.0			13.3

Table 4.6: Weak and Strong side comparisons of TI 7Grades Parts

| | TI7G | | | | | |
	Weak Side (MPa)	Uniform (R1) (MPa)	Gain (W) (%)	Strong Side (MPa)	Uniform (R7) (MPa)	Gain (S) (%)
0.4 mm	16.505	**8.700**	89.7	15.090	**13.906**	8.5
0.5 mm	19.445	**10.481**	85.5	17.945	**17.047**	5.3
Av. Gain (%)			87.6			6.9

Table 4.7: Weak and Strong side comparisons of TII 3Grades Parts

| | TII3G | | | | | |
	Weak Side (MPa)	Uniform (R2) (MPa)	Gain (W) (%)	Strong Side (MPa)	Uniform (R8) (MPa)	Gain (S) (%)
0.4 mm	16.105	**11.585**	39.0	15.664	**14.213**	10.2
0.5 mm	19.107	**14.133**	35.2	18.786	**17.323**	8.4
Av. Gain (%)			37.1			9.3

Table 4.8: Weak and Strong side comparisons of TII 5Grades Parts

	TII5G					
	Weak Side (MPa)	Uniform (R2) (MPa)	Gain (W) (%)	Strong Side (MPa)	Uniform (R8) (MPa)	Gain (S) (%)
0.4 mm	16.407	**11.585**	41.6	15.408	**14.213**	8.4
0.5 mm	19.434	**14.133**	37.5	18.648	**17.323**	7.6
Av. Gain (%)			39.6			8.0

Table 4.9: Weak and Strong side comparisons of TII 7Grades Parts

	TII7G					
	Weak Side (MPa)	Uniform (R2) (MPa)	Gain (W) (%)	Strong Side (MPa)	Uniform (R8) (MPa)	Gain (S) (%)
0.4 mm	15.140	**11.585**	30.7	14.517	**14.213**	2.1
0.5 mm	18.210	**14.133**	28.8	17.640	**17.323**	1.8
Av. Gain (%)			29.8			2.0

According to the results, weak sides of the graded specimens gain around 35 % of strength compared to the uniform porous specimens. Unlikely, for Type I 5 grades and Type I 7 grades specimens gained around 90 % of strength on the weak sides. On the other hand, strong sides of the graded specimens gain around 10 % of strength. However, Type II 7 grades specimen gains 2 % of strength. Furthermore, except Type I 3grades specimens weak sides of all the specimens have higher strength values compared to their strong sides.

CHAPTER 5

PRODUCTION AND CHARACTERIZATION OF RESIN FILLED COMPOSITE SPECIMENS

In this chapter, we consider resin filled composites built by using uniform porous and type I graded tensile test specimen. Tensile tests are performed and mechanical properties are sought. The aim is to check if the pores are filled with resin and to see the effect of resin on the mechanical properties of the polyamide parts.

5.1 Production of resin filled composite specimens

Huntsman LY564 resin is mixed with XB3486 hardener according to the instructions supplied from the manufacturer. During experiments, parts are placed in a container (Figure 5.1) where they can float freely inside the resin without touching each other. The container is then put in a desiccator which is vacuumed with a vacuum pump (Figure 5.2). Proper parts of the desiccator are sealed in order to prevent leakage of air. One entrance of the desiccator is used for vacuuming while the other one used to intake the resin.

Desiccator is vacuumed up to -600mmHg of pressure. After that, valve on the vacuum line is closed and the valve on the intake line is opened until the container is filled with resin. Eventually the intake valve is closed and vacuum valve is opened again. Parts floated in the resin for about 4 hours. Then the intake valve is opened to let the air in and the parts are exposed to atmospheric pressure for about 1 hour.

After this process, parts are cleaned and placed on to a plate in order to cure the resin in an

Figure 5.1: Specimens in container

oven. Before the plate is put in the oven, Renlease QV5110 mold release is applied on the plate to avoid sticking of the parts onto the plate. Parts are left in the oven about 15 hours as instructed in the resin's datasheet.

Resin infiltration process for both unifom and graded specimens is performed by Jande [35].

Figure 5.2: Dessicator - Vacuum Pump - Oven - Specimens on Plate

5.2 Mechanical Tests

Tensile tests performed are similar to those performed for the uniform porous and the graded parts. Strain gages and extensometer are used for uniform parts to find the modulus of elasticity and Poisson's ratio. Only UTS and rupture strength is sought for graded parts; therefore no additional equipment is used.

Since the porosity is decreased with the increasing energy density, more infiltration is expected for higher porosity parts. Hence, high strength gain on weak parts and low strength gain on strong parts are expected.

5.2.1 Test Results

During the preparation of the specimens, adhesive is not absorbed by the pores therefore strain gages are installed easier. The specimens are cleaner and dust free which shows that the surface is filled with resin.

Three sets of uniform porous specimens which have the lowest energy density values (R1, R2, R3) are not cleaned well before the curing process. Thus, an approximately 0.5 mm thick and hard resin layer is formed on the parts which probably increased the strength beyond the expected value.

Almost all specimens have flat fracture surfaces. Parts become more brittle as a result they break just after the end of the elastic region. Hence, UTS and rupture strength of most of the parts are the same.

From Figures 5.3 to 5.6 and Tables 5.1 to 5.4, results for uniform porous specimens are given while results of graded parts are given in Figures 5.7 and Table 5.5

-
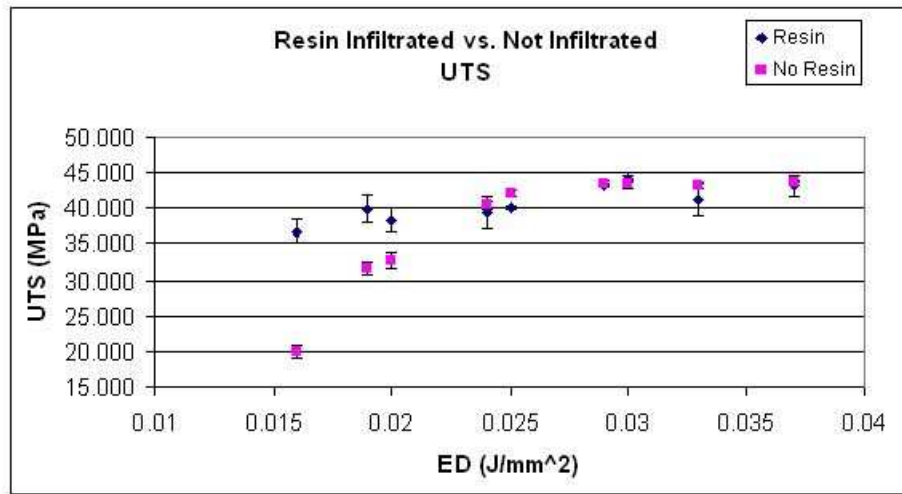
Figure 5.3: Comparison of resin filled parts - UTS (Parts produced in thickness direction)
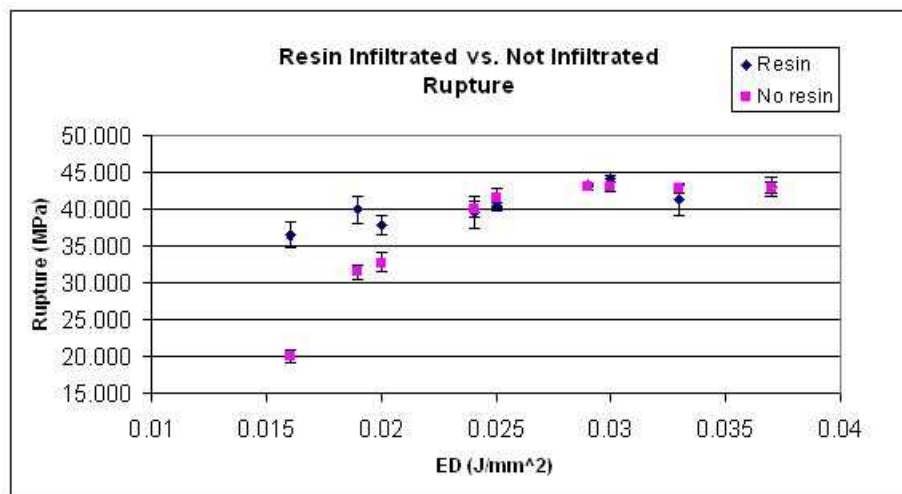
Figure 5.4: Comparison of resin filled parts - Rupture Strength (Parts produced in thickness direction)
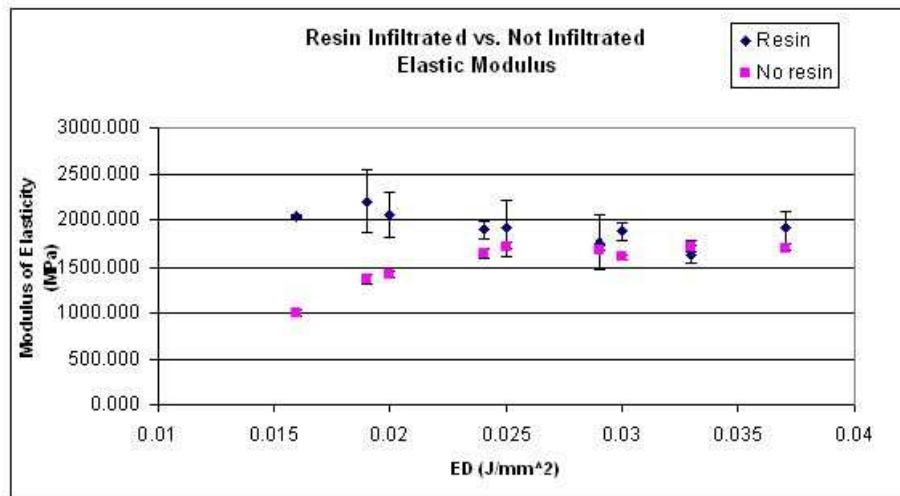
Figure 5.5: Comparison of resin filled parts - Modulus of Elasticity (E_x or E_y) (Parts produced in thickness direction)
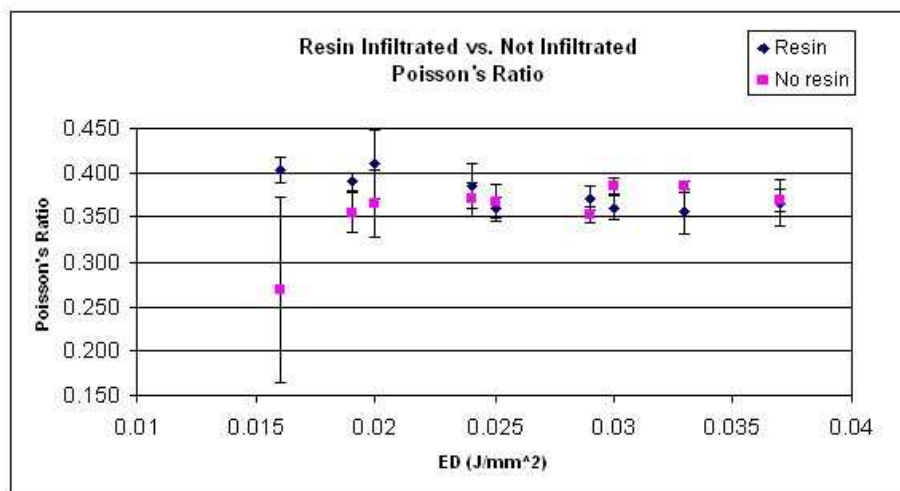
Figure 5.6: Comparison of resin filled parts - Poisson's Ratio (ν_{xy}) (Parts produced in thickness direction)

Table 5.1: Comparison of resin filled parts numerical results - UTS (Parts produced in thickness direction)

| | ED | UTS (MPa) | | | |
| | | Resin | | No Resin | |
	J/mm^2	Avg.	St. Dev	Avg.	St. Dev.
R1	**0.016**	36.790	1.631	19.980	0.912
R2	**0.019**	39.873	1.897	31.620	0.911
R3	**0.020**	38.370	1.758	32.822	1.157
R4	**0.024**	39.437	2.199	40.422	0.595
R5	**0.025**	40.060	0.325	42.126	0.510
R6	**0.029**	43.200	0.238	43.397	0.417
R7	**0.030**	44.130	0.439	43.378	0.515
R8	**0.033**	41.233	2.235	43.174	0.497
R9	**0.037**	43.157	1.455	43.736	0.103

Table 5.2: Comparison of resin filled parts numerical results - Rupture Strength (Parts produced in thickness direction)

| | ED | Rupture Strength (MPa) | | | |
| | | Resin | | No Resin | |
	J/mm^2	Avg.	St. Dev	Avg.	St. Dev.
R1	**0.016**	36.390	1.745	19.978	0.913
R2	**0.019**	39.870	1.903	31.554	0.972
R3	**0.020**	37.750	1.274	32.804	1.153
R4	**0.024**	39.437	2.199	39.994	1.134
R5	**0.025**	40.330	0.521	41.458	1.289
R6	**0.029**	43.153	0.235	42.932	0.469
R7	**0.030**	44.060	0.420	42.937	0.628
R8	**0.033**	41.177	2.153	42.732	0.516
R9	**0.037**	43.067	1.315	42.880	0.729

Table 5.3: Comparison of resin filled parts numerical results - Modulus of Elasticity (Parts produced in thickness direction)

		Modulus of Elasticity (MPa)			
	ED	Resin		No Resin	
	J/mm^2	Avg.	St. Dev	Avg.	St. Dev.
R1	0.016	2035.100	24.814	997.725	28.808
R2	0.019	2200.167	340.511	1362.250	52.548
R3	0.020	2052.700	251.173	1421.350	30.567
R4	0.024	1892.467	98.558	1641.840	41.649
R5	0.025	1913.833	304.248	1712.817	34.741
R6	0.029	1759.700	286.537	1686.950	28.279
R7	0.030	1870.233	100.014	1608.100	31.569
R8	0.033	1628.233	90.719	1714.480	57.923
R9	0.037	1914.367	177.341	1701.860	37.458

Table 5.4: Comparison of resin filled parts numerical results - Poisson's Ratio (Parts produced in thickness direction)

		Poisson's Ratio			
	ED	Resin		No Resin	
	J/mm^2	Avg.	St. Dev	Avg.	St. Dev.
R1	0.016	0.402	0.015	0.268	0.104
R2	0.019	0.390	0.010	0.355	0.023
R3	0.020	0.410	0.039	0.365	0.038
R4	0.024	0.385	0.026	0.370	0.019
R5	0.025	0.360	0.013	0.368	0.019
R6	0.029	0.371	0.013	0.353	0.009
R7	0.030	0.360	0.013	0.385	0.010
R8	0.033	0.356	0.025	0.384	0.006
R9	0.037	0.366	0.026	0.369	0.013
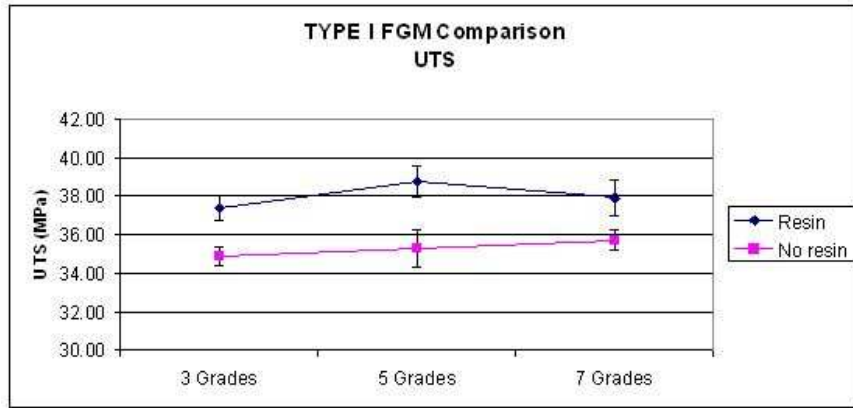
Figure 5.7: Comparison of resin filled parts - TYPE I

Table 5.5: Comparison of resin filled parts numerical results - TYPE I (Parts produced in thickness direction)

		Type I (MPa)		
		3 Grades	5 Grades	7 Grades
		UTS	UTS	UTS
Resin	Avg.	37.370	38.780	37.910
	St. Dev.	0.624	0.801	0.911
No resin	Avg.	34.873	35.300	35.717
	St. Dev.	0.458	0.980	0.530

According to the results, more porous parts gained more strength while less porous parts remained around the same strength as expected. Some part of the gain on more porous parts is probably derived because of the undesired coating. On the other hand graded parts gained around 10 % strength.

CHAPTER 6

FINITE ELEMENT ANALYSIS OF THE TENSILE TEST

In this chapter finite element analysis of the tensile tests will be described. Finite element analyses are used in two ways. Firstly, the analyses are used to check the elastic properties found by mechanical tests and validate the model created by the finite element program. Furthermore the models are used to predict the undetermined elastic properties which can not be found by tests. ANSYS 11 finite element program is employed for analyses and tensile test specimens built in thickness direction are modeled. Fully characterized sets are analyzed first by giving a displacement in linear elastic region and the stress found from the real test is compared to the stress distribution found by finite element analysis. Then several runs are conducted in similar way to obtain a valid interval for undetermined mechanical properties.

6.1 Modeling of the Tensile Specimen

For finite element analysis "1:1" model of tensile test specimen is created by ANSYS 11. In this part 3D modeling of the part will be described.

ANSYS 11 has a user friendly graphical user interface where all commands can be easily found from the tree view main menu and the pull down menus. It also has a very useful help section where each command is explained in detail. First lines are created using keypoints then an area is formed using these lines. After the fillets are generated, the area is extruded to the desired thickness. An important thing is that ANSYS doesn't have the "undo" command therefore one has to save the job after all the commands. Before starting use "Change Job Name" command on the "File" menu and give a name to the job; then save the job. Another thing is that units entered to program have to be consistent with each other because ANSYS

doesn't ask for units. We used "mm" for dimensions and "MPa" for material properties.

Modeling section is located under the "preprocessor" section (Figure 6.1). First select create keypoints under the heading of "modeling".

- Preprocessor -> Modeling -> Create -> Keypoints -> In active CS
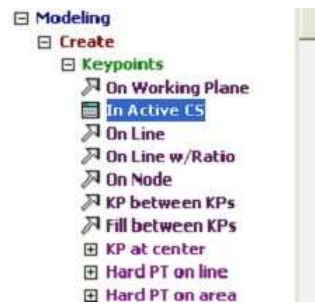
Figure 6.1: Create Keypoints from the main menu

Use "In active CS" command to generate keypoints by entering the coordinates on the work plane.
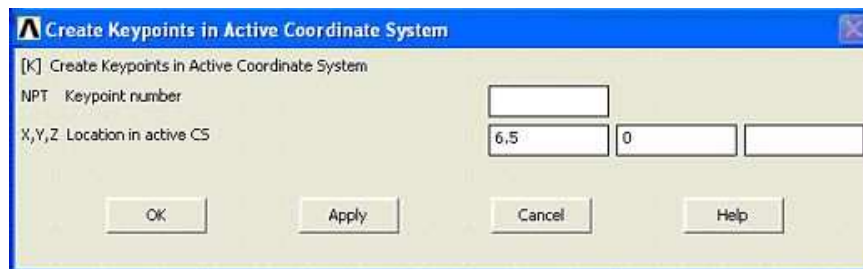
Figure 6.2: Create Keypoints in Active CS

Enter the keypoint coordinates to the box that appears (Figure 6.2). Keypoint numbering is automatically done by the program therefore one doesn't need to number the keypoints. Entered points are given in Table 6.1.

After all keypoints are created select "create lines" to join the keypoints (Figure 6.3).

Table 6.1: Keypoint coordinates for the tensile test specimen

pt	x	y	pt	x	y
1	6.5	0	12	-6.5	0
2	6.5	25	13	-6.5	-25
3	6.5	28.5	14	-6.5	-28.5
4	9.5	28.5	15	-9.5	-28.5
5	9.5	57.5	16	-9.5	-57.5
6	9.5	82.5	17	-9.5	-82.5
7	-9.5	82.5	18	9.5	-82.5
8	-9.5	57.5	19	9.5	-57.5
9	-9.5	28.5	20	9.5	-28.5
10	-6.5	28.5	21	6.5	-28.5
11	-6.5	25	22	6.5	-25

- Preprocessor -> Modeling -> Create -> Lines -> Lines -> Straight Line

Figure 6.3: Lines through Keypoints

Then select "create areas by lines" and generate the base area (Figure 6.4).

- Preprocessor -> Modeling -> Create -> Areas -> Arbitrary -> By Lines

In order to form the radius fillets, create circles on the corners. End point for the circle is given in Table 6.2.
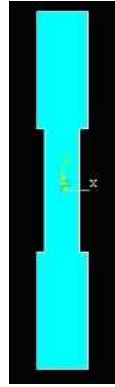
Figure 6.4: Base area

- Preprocessor -> Modeling -> Create -> Areas -> Circles -> By End Points

Table 6.2: End points for the circle

XE1	6.5
YE1	28.5
XE2	158.5
YE2	28.5

Then reflect the circle with respect to Y-Z plane and reflect both circles with respect to X-Z plane (Figure 6.5).

- Preprocessor -> Modeling -> Reflect -> Areas
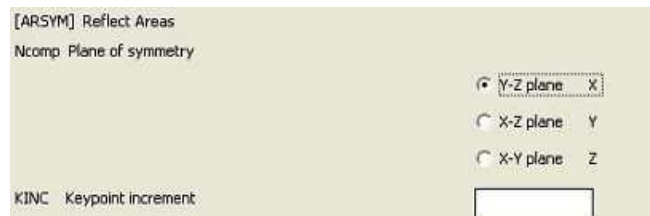
Figure 6.5: Reflect Areas

Then subtract the circles from the base area to achieve the desired shape. First choose the base area; click ok and choose the 4 circles and click ok (Figure 6.6).

- Preprocessor -> Modeling -> Operate -> Booleans -> Subtract -> Areas
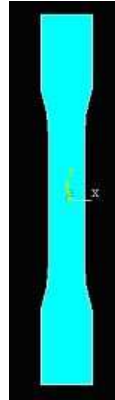
Figure 6.6: Base area on test specimen shape

After completing the first area we can extrude it due to desired thickness which is 6 mm for the tensile test specimen (Figure 6.7).

- Preprocessor -> Modeling -> Operate -> Extrude -> Areas -> Along Normal
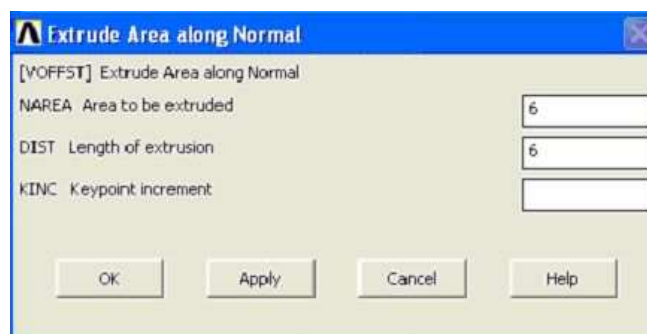
Figure 6.7: Extrude area along normal

Modeling is almost completed but we need to divide the areas onto which we will apply the loads from the volume. Therefore, first we need to create areas which are in contact with the

testing machine. We have created keypoints at the beginning. Use the keypoints which has the Y coordinate of 57.5 or -57.5 and create 4 areas with corner points (Figure 6.8).

- Preprocessor -> Modeling -> Create -> Areas -> Arbitrary -> Through KPs
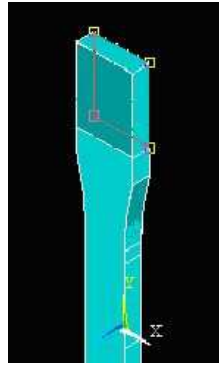
Figure 6.8: Create areas on volume

Finally divide the volume by areas using the last 4 areas created and the 3D model is ready. First pick the volume and click ok then select the 4 areas and click ok. By doing this we obtain areas on the volume where we can apply loads (Figure 6.9).

- Preprocessor -> Modeling -> Operate -> Booleans -> Divide -> Volume By Area
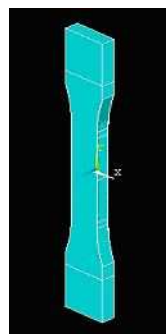
Figure 6.9: 3D Model of tensile test specimen

6.2 Analyses of Uniform Porous Structures

After modeling of specimens is completed, other preprocessing options such as entering material model, specifying material properties, meshing, application of loads are needed to be completed.

First element type is selected (Figure 6.10).

- Preprocessor -> Element Type -> Add/Edit/Delete -> Add -> Solid -> Brick 20 Node 186
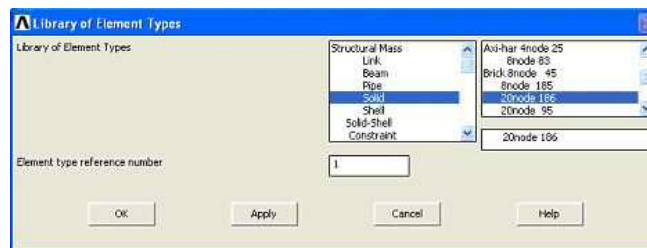
Figure 6.10: Add element type

Solid brick 20 Node element which is known as SOLID186 is selected for analyses. It is a higher order 3-D solid element that exhibits quadratic displacement behavior. The element is defined by 20 nodes having three degrees of freedom per node: translations in the nodal x, y, and z directions. The element supports plasticity, hyperelasticity, creep, stress stiffening, large deflection, and large strain capabilities. It also has mixed formulation capability for simulating deformations of nearly incompressible elastoplastic materials, and fully incompressible hyperelastic materials [47].

Then material model is defined with the elastic properties determined in mechanical tests. As mentioned in previous chapters, parts produced via SLS possess different mechanical properties in different directions. Therefore, transversely isotropic behavior is assumed during studies. It is a special case of orthoropic materials. Thus linear elastic orthotropic model is chosen (Figure 6.11).

- Preprocessor -> Material Props -> Material Models / Material Models Available ->

Structural / Linear / Elastic / Orthotropic
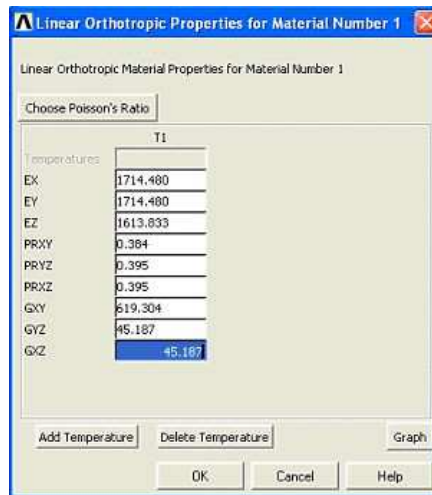
Figure 6.11: Entering material properties

ANSYS demands following elastic properties for linear elastic orthotropic materials,

- E_x, E_y, E_z

- ν_{xy}, ν_{yz}, ν_{xz}

- G_{xy}, G_{yz}, G_{xz}

Following properties are found through mechanical tests,

- E_x, E_z

- ν_{xy}, ν_{zx}

- G_{xz}

As the material is assumed transversely isotropic, formulas in 3.3, 3.4 and 3.5 are valid. Then following equalities are valid,

- $E_x = E_y$

- $v_{xy} = v_{yx}$

- $G_{xy} = \frac{2(1+v_p)}{E_p}$, p = isotropy plane (XY)

Also by using the following equation which is valid for othotropic materials,

-

$$\frac{v_{ij}}{E_i} = \frac{v_{ji}}{E_j} \qquad (6.1)$$

all the elastic properties are found for parts produced via SLS.

Using the mesh tool, global size of the meshes are set to 2 for finer meshing (Figure 6.12).

- Preprocessor -> Meshing -> Size Controls / Global / Set -> SIZE
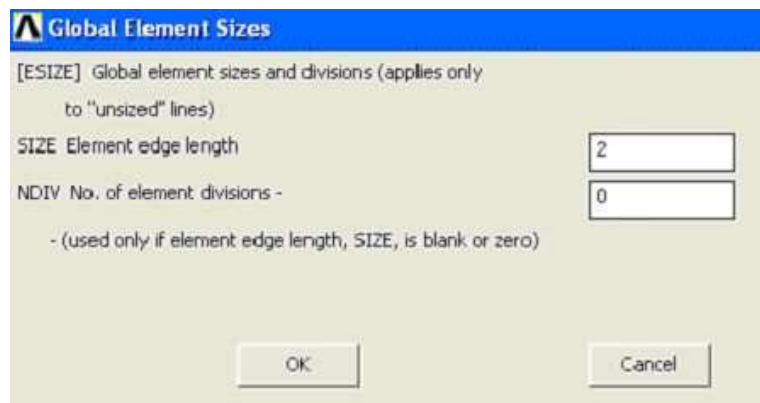
Figure 6.12: Entering global element size

Then "Hex/Wedge" is selected in the shape portion of the mesh tool screen, and click sweep to create the mesh (Figure 6.13).

One last step before solving the problem is the definition of the loads. In this step apply displacement to the areas created in modeling. As described in previous chapters, upper cross head of the tensile test machine moves while the lower end is stationary. Therefore, zero displacement for the lower end is entered. For the upper end, the value entered must
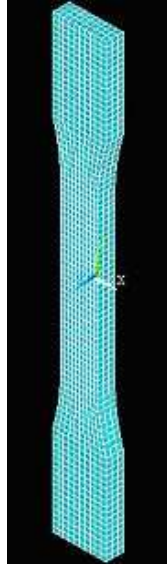
Figure 6.13: A fine meshed tensile test specimen

be multiplied with a coefficient which is because the stress value that will be compared is measured within the gage length of 50 mm. But the displacement between grips is 115 mm. In order to simulate the tension in 50 mm, 115/50 = 2.3 times more displacement has to be entered. This can be proved with Hooke's Law for linear elastic materials.

$$\sigma = E.\varepsilon \Rightarrow \varepsilon = \frac{\Delta l}{l} \Rightarrow \sigma = \frac{E\Delta l}{l} \tag{6.2}$$

Therefore "$\Delta l / l$" is directly proportional for same materials for same stress values.

$$\sigma_1 = \sigma_2 \Rightarrow \frac{E\Delta l_1}{l_1} = \frac{E\Delta l_2}{l_2} \Rightarrow \frac{\Delta l_1}{l_1} = \frac{\Delta l_2}{l_2} \Rightarrow \Delta l_2 = \frac{\Delta l_1.l_2}{l_1} \Rightarrow \Delta l_2 = \left(\frac{115}{50}\right)\Delta l_1 \tag{6.3}$$

$$\Delta l_2 = 2.3\Delta l_1 \tag{6.4}$$

Since the parts are brittle and do not elongate much, 0.4 and 0.5 mm of displacement in the gage length is simulated for which the values are within the elastic regions of all the sets. 0.92 for 0.4 mm and 1.15 for 0.5 mm is entered in only Y direction (Figure 6.14).

- Preprocessor -> Loads -> Define Loads -> Apply -> Structural -> Displacement -> On

Areas
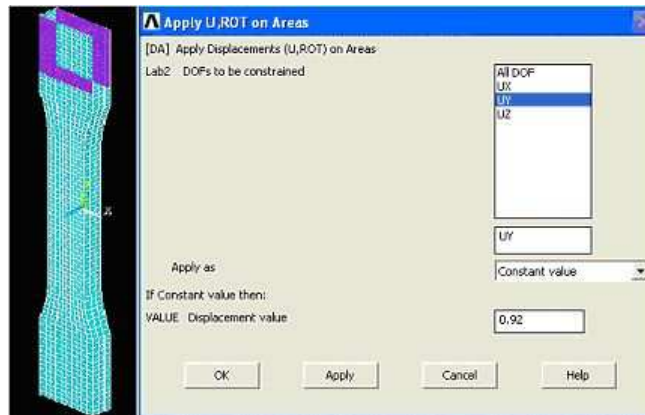
Figure 6.14: Defining loads

After preprocessing is completed, problem is ready to be solved.

- Solution -> Solve -> Current LS

Results are read from the General Postproc section.

- General Postproc -> Plot Results -> Contour Plot -> Nodal Solu -> Stress -> Y-Component of stress

This procedure is repeated for each set and stress distributions are found. Then real stress values obtained from tensile tests are compared with the simulation. If the real value is within the stress interval found by simulation then the analyses are considered to be valid.

As explained in previous chapters some mechanical properties of parts having low energy density values could not be found (R1 to R4) therefore first analyses for fully characterized sets (R5 to R9) are performed to check whether the model is working. After the model is confirmed as working, a study to predict the undetermined parameters is conducted.

6.3 Results Obtained by FEA of Uniform Porous Structures

The elastic properties of parts are determined with tensile and torsion tests. Tensile specimens produced in length direction and torsion specimens are weaker then others therefore properties for parts having energy density values lower than 0.025 J/mm^2 could not be found. Elastic properties of fully characterized parts are given in Table 6.3.

Table 6.3: Fully characterized polyamide parts produced via SLS

	R5	R6	R7	R8	R9
Energy Density (J/mm^2)	0.025	0.029	0.030	0.033	0.037
E_x (MPa)	1712.817	1686.950	1608.100	1714.480	1701.860
E_y (MPa)	1712.817	1686.950	1608.100	1714.480	1701.860
E_z (MPa)	1443.300	1653.000	1579.200	1613.833	1751.833
ν_{xy}	0.368	0.353	0.385	0.384	0.369
ν_{yz}	0.440	0.364	0.372	0.395	0.335
ν_{xz}	0.440	0.364	0.372	0.395	0.335
G_{xy} (MPa)	626.213	623.334	580.437	619.304	621.661
G_{yz} (MPa)	28.798	36.987	43.249	45.187	42.017
G_{xz} (MPa)	28.798	36.987	43.249	45.187	42.017

These properties are entered to ANSYS as the material model of linear elastic orthotropic parts. Parts are subjected to 0.3 and 0.4 mm of displacement in Y direction and results are compared to those obtained from the real tests. The expected stress and computed stress intervals are given in Table 6.4.

"Found Stress intervals" shown in the following tables are the stress intervals covering the gage length of the model after the displacement is applied. These intervals can be seen in the Appendix B as ANSYS screenshots.

Also "Expected Avg. Stress" shown in the following tables are the average stress values of

tensile tests at 0.4 and 0.5 mm of displacement within the gage length.

Table 6.4: FE Results of Fully Characterized Parts

Energy Density (J/mm^2)	Elongation Entered (mm)	Expected Avg. Stress (MPa)	Found Stress Interval (MPa)
0.025	0.4	14.238	11.422-13.370
	0.5	17.389	14.277-16.713
0.029	0.4	14.045	13.039-14.925
	0.5	17.169	16.299-18.656
0.030	0.4	13.906	12.361-14.147
	0.5	17.047	15.452-17.684
0.033	0.4	14.213	13.174-15.080
	0.5	17.323	16.468-18.850
0.037	0.4	13.980	13.129-15.024
	0.5	17.206	16.411-18.780

The results showed that, the model is working correctly and 80 % of analyses are found within the interval. Only the parts having energy density of 0.025 J/mm^2 remained below the desired value. This is probably because some of its mechanical properties are out of the range.

6.4 Prediction of Undetermined Results

Parts having energy density values below 0.025 J/mm^2 are so weak that they fail even before mounting the specimen on the test machine. Therefore the trendlines fitted to the other results are conditionally extrapolated in order to predict the undetermined results.

Extrapolation is carried out by adding a predicted result for the lowest energy density value (0.016 J/mm^2) as a real data point to the graphics. Then a new trendline is fitted through those data points and the mid data points are calculated from the equation of that trendline. In order to check the uniqueness of the predicted results several combinations of the minimum values are added to graphics and different trendlines are fitted. Mid data points found by those trenlines are used as inputs to ANSYS and results are compared.

In tensile and torsion tests values like, modulus of elasticity in Z direction (E_z), shear modulus in ZP plane (G_{zp}, where P is either X or Y) and Poisson's ratio in ZP direction (v_{zp}, where P is either X or Y) could not be found for low energy density values. Since the Poisson's ratio value has almost a linear trendline, the equation of the line is used directly without making any modifications and values are determined from that equation (Table 6.5)

Equation of the trendline:

$$v_{zp} = -192.272(ED)^2 + 10.292\,(ED) + 0.230 \tag{6.5}$$

Table 6.5: Poisson's Ratio values found from the trendline

ED (J/mm^2)	0.016	0.019	0.02	0.024
v_{zp}	0.345	0.356	0.359	0.366

Then a 2 step study is performed for determination of the modulus of elasticity in Z direction and shear modulus in ZP plane.

In the first step, the restrictions are specified primarily. Due to the experiences, modulus of elasticity in Z direction has to be lower than modulus of elasticity in plane direction ($E_z <$ E_p). On the other hand each value has to be lower than or equal to the previous value having higher energy density. Therefore for the lowest energy density part, restrictions are found as: $E_z < 970$ MPa and $G_{pz} < 30$ MPa.

Then modulus of elasticity in Z direction is entered from 400 to 900 MPa with an increment of 50 MPa while at the same time shear modulus is entered from 10 to 25 MPa with an increment of 5 MPa for each modulus of elasticity value. Simulation is run for the lowest energy density part in these combinations and the stress distribution is observed.

For the lowest energy density part, a displacement of 0.4mm caused a stress distribution with an average value of 8.7 MPa. Therefore combinations of modulus of elasticity and shear modulus giving a maximum stress value more than 8.7 MPa are accepted as trial data points. Determined data points for initial guesses can be seen in Table 6.6.

In the second step of the study, trial data points found in the first step of the study are added

Table 6.6: Determined data points for initial guess (for ED = 0.016 J/mm^2)

E_z (MPa)	450	750	800	850	900
G_{pz}(MPa)	15	20	20	20	20
Max Stress (MPa)	8.758	8.752	8.757	8.761	8.764

to the graphic as real test results and the trendline is extrapolated. Using the equation of that trendline missing properties of the second, the third and the forth energy density value parts are predicted. Simulations are run for each combination and results covering the average stress value of the real tests are found. A trendline is accepted when all tests came valid. Similar to the first step 0.4mm of displacement is applied in the simulations. Results are given in Tables 6.7 to 6.11.

Table 6.7: Comparison for E_z = 450 MPa and G_{pz} = 15 MPa (Out of interval for ED = 0.019 J/mm^2. Tests interrupted.)

Energy Density (J/mm^2)	0.016	0.019	0.020	0.024
Exp. Avg. Stres (MPa)	8.700	11.585	12.115	13.566
Ansys Min (MPa)	7.618	9.007		
Ansys Max (MPa)	8.74	10.506		

Table 6.8: Comparison for E_z = 750 MPa and G_{pz} = 20 MPa

Energy Density (J/mm^2)	0.016	0.019	0.020	0.024
Exp. Avg. Stres (MPa)	8.700	11.585	12.115	13.566
Ansys Min (MPa)	7.635	10.57	11.04	12.748
Ansys Max (MPa)	8.74	12.108	12.647	14.602

Table 6.9: Comparison for E_z = 800 MPa and G_{pz} = 20 MPa

Energy Density (J/mm^2)	0.016	0.019	0.020	0.024
Exp. Avg. Stres (MPa)	8.700	11.585	12.115	13.566
Ansys Min (MPa)	7.64	10.576	11.046	12.75
Ansys Max (MPa)	8.745	12.114	12.653	14.604

Table 6.10: Comparison for E_z = 850 MPa and G_{pz} = 20 MPa

Energy Density (J/mm^2)	0.016	0.019	0.020	0.024
Exp. Avg. Stres (MPa)	8.700	11.585	12.115	13.566
Ansys Min (MPa)	7.643	10.582	11.051	12.752
Ansys Max (MPa)	8.749	12.121	12.658	14.606

Table 6.11: Comparison for E_z = 900 MPa and G_{pz} = 20 MPa (Non uniform stress distribution observed for ED = 0.019 and 0.020 J/mm^2)

Energy Density (J/mm^2)	0.016	0.019	0.020	0.024
Exp. Avg. Stres (MPa)	8.700	11.585	12.115	13.566
Ansys Min (MPa)	7.647	9.007	11.055	12.754
Ansys Max (MPa)	8.752	12.126	12.663	14.657

From Table 6.7 to Table 6.11, results of trials for different trendlines are given. As shown in the tables, all valid shear modulus values are 20 MPa while modulus of elasticity values in Z direction is 750, 800 and 850 MPa. According to this information modulus of elasticity value in Z direction has vary within the interval of 700 MPa and 900 MPa. On the other hand shear modulus in has to vary within the interval of 15 and 25 MPa. Hence mean values of each interval which verify all the energy density values (Ez = 800 MPa and Gpz = 20 MPa) are taken as the master guess points and trendlines are extrapolated due to this combination (Figure 6.15, Figure 6.16).
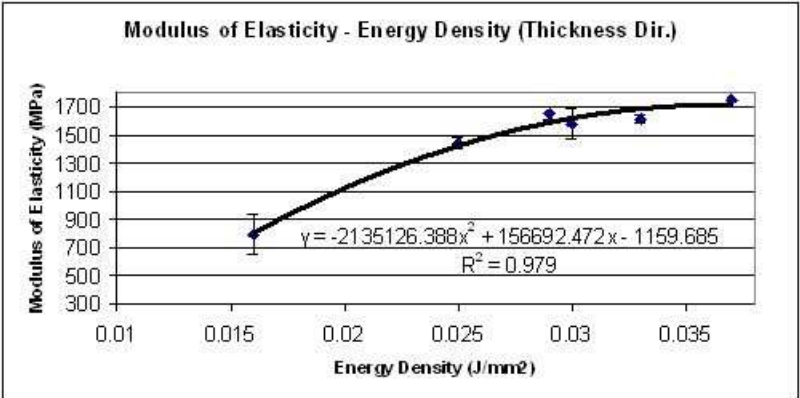

Figure 6.15: Extrapolated Modulus of Elasticity Trendline
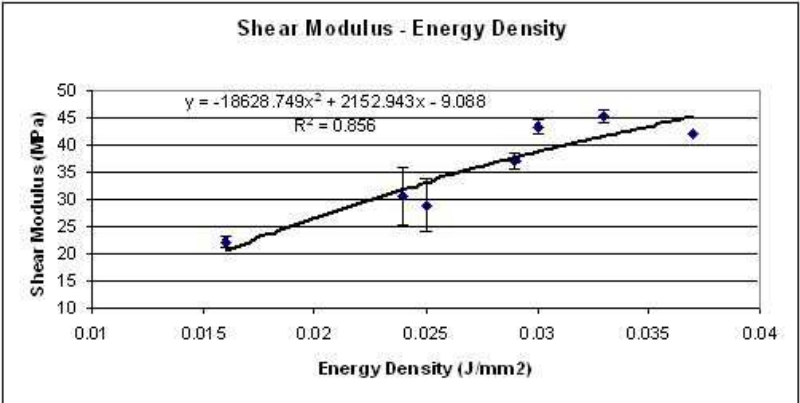
Figure 6.16: Extrapolated Shear Modulus Trendline

Eventually by using the equations below undetermined elastic properties of parts produced

via SLS are found. Total compliance matrices of those energy density sets are given in table 6.12.

$$E_z = -2135126.388(ED)^2 + 156692.472\,(ED) - 1159.685 \qquad (6.6)$$

$$G_{pz} = -18628.749(ED)^2 + 2152.943\,(ED) - 9.088 \qquad (6.7)$$

Table 6.12: Elastic properties of parts having low energy density values (Pink values are the initial guess points while yellow values are determined due to the equations of the trendlines extrapolated.)

	R1	R2	R3	R4
	0.016	0.019	0.02	0.024
E_x (MPa)	997.725	1362.250	1421.350	1641.840
E_y (MPa)	997.725	1362.250	1421.350	1641.840
E_z (MPa)	800.802	1046.691	1120.114	1371.102
ν_{xy}	0.268	0.355	0.365	0.370
ν_{yz}	0.430	0.464	0.455	0.439
ν_{xz}	0.430	0.464	0.455	0.439
G_{xy} (MPa)	393.301	502.824	520.489	599.299
G_{yz} (MPa)	20.590	25.093	26.519	31.852
G_{xz} (MPa)	20.590	25.093	26.519	31.852

After the determination of the values it is seen that the parts having energy density value of 0.025 J/mm2 which remained out of range in the first analyses, has modulus of elasticity in X and Y direction over the trendline and has shear modulus value below the trendline. Therefore these values found from tests are recalculated with the corresponding equations of the trendlines (Table 6.13).

Results found due to extrapolated trendlines are given in table 6.14.

Table 6.13: Modified elastic properties for R5 parts

Energy Density (J/mm^2)	0.025	0.025
Ex	1712.817	1634.088
Ey	1712.817	1634.088
Ez	1443.300	1443.300
ν_{xy}	0.368	0.368
ν_{yz}	0.440	0.440
ν_{xz}	0.440	0.440
G$_{xy}$	626.213	626.213
G$_{yz}$	28.798	33.093
G$_{xz}$	28.798	33.093

Table 6.14: Finite Element Results of specimens with predicted elastic properties

Energy Density (J/mm2)	Elongation Entered (mm)	Expected Avg. Stress (MPa)	Found Stress Interval (MPa)
0.016	0.4 mm	8.700	7.64-8.745
	0.5 mm	10.481	9.55-10.931
0.019	0.4 mm	11.585	10.576-12.114
	0.5 mm	14.133	13.22-15.143
0.02	0.4 mm	12.115	11.046-12.653
	0.5 mm	14.766	13.808-15.817
0.024	0.4 mm	13.566	12.75-14.604
	0.5 mm	16.514	15.938-18.255
0.025	0.4 mm	14.238	12.629-14.466
	0.5 mm	17.389	15.786-18.082

6.5 Modeling of Graded Porous Structures

Graded porous specimens are modeled by considering distinct grades that are perfectly bonded together. Each grade is assigned elastic properties determined in tests and analyses.

Same 2D model of the tensile specimen is extruded in the thickness of the grade. Then it is copied and offset in thickness direction 3, 5 or 7 times (Figure 6.17).

- Preprocessor -> Modeling -> Copy -> Volumes
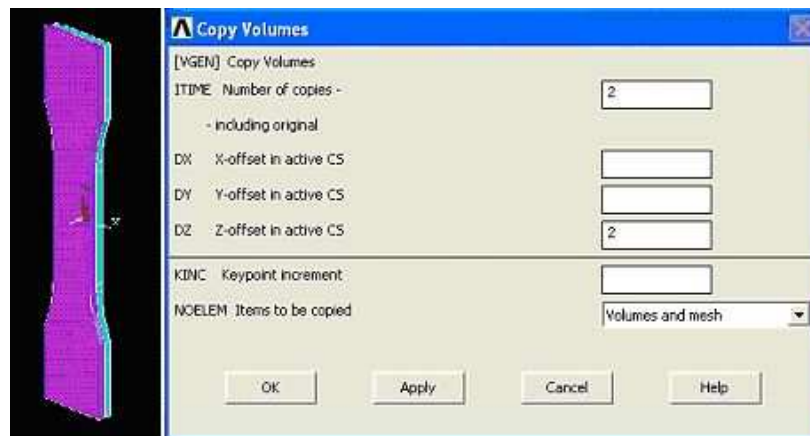
Figure 6.17: Modeling of graded porous specimens

After that volumes are glued together. Hence we generate the tensile test specimen with distinct grades perfectly bonded to each other.

- Preprocessor -> Modeling -> Operate -> Booleans -> Glue -> Volumes

Define each grade's elastic properties separately from the material models section. Use Material menu to add new model (Figure 6.18).

- Preprocessor -> Material Props -> Material Models
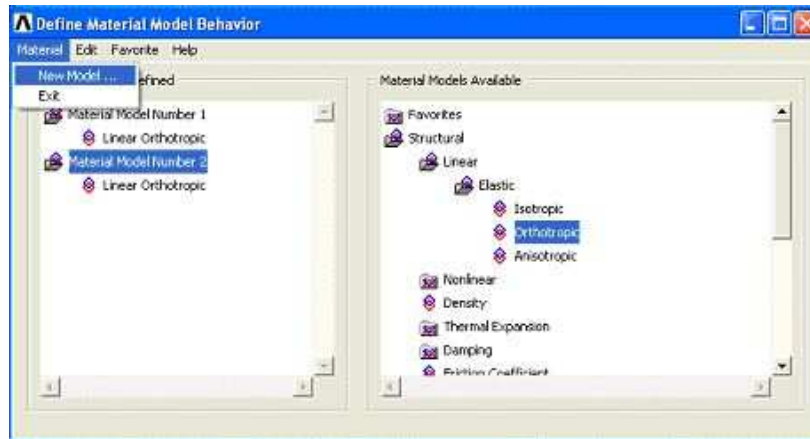
Figure 6.18: Adding different material models to the analyses

These elastic models are assigned to the grades in the meshing section. In meshing attributes menu, select "Picked Volumes" and choose the volume to be assigned. Then define the material number from the following screen in figure 6.19.

- Preprocessor -> Meshing -> Mesh Attributes -> Picked Volumes -> Material Number
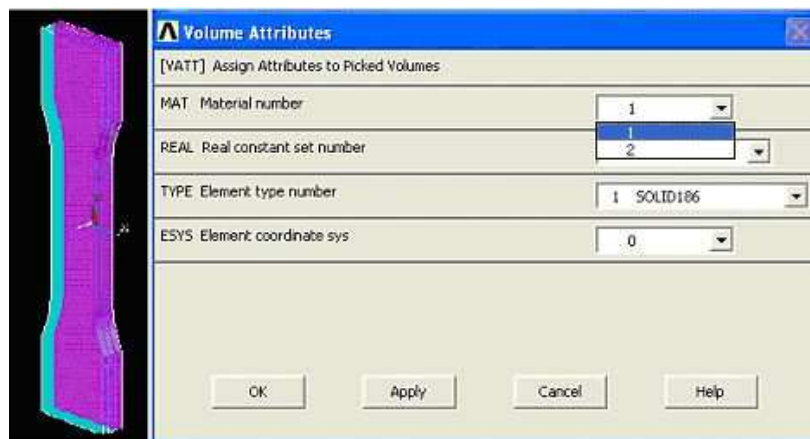
Figure 6.19: Modeling of graded porous specimens

Unlike uniform porous model, finer mesh options applied to graded porous models. In order to have precise results, models are divided into smaller finite elements. Tetrahedral mesh elements with a smart size of 1 (which is the finest mesh) is applied to the graded model

(Figure 6.20)

- Preprocessor -> Meshing -> Mesh Tool
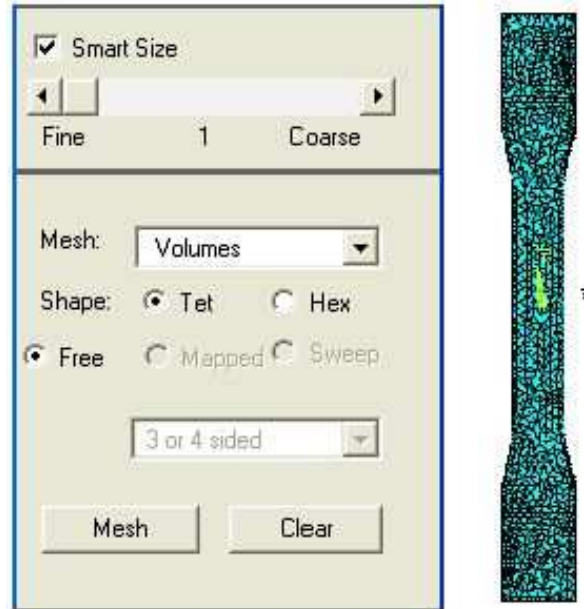
Figure 6.20: Smart size 1 Tetrahedral Free Meshing

Since each grade has distinct elastic properties, they elongate separately. However they are perfectly bonded together, they tend to bend on each other. While the loading boundary conditions are being applied, zero displacement in X and Z directions are applied differently compared to uniform model. 0.4 mm and 0.5 mm loads are applied to Type I and Type II specimens having 3, 5 or 7 grades. All simulations satisfy the applied displacement values around the gage area for both weak and strong sides. Results are given in the Appendix C.

6.6 Analyses of Porous Graded Specimens

Similar to uniform porous models, 0.4 mm and 0.5 mm of displacement is applied to the graded models. In order to simulate the gage length elongation, these displacement values had to be multiplied with 2.3 (115/50, where 115 is the grip to grip distance while 50 is the gage length). Therefore, 0.92 mm of displacement was applied for 0.4 mm and 1.15 mm of

displacement was applied for 0.5 mm for uniform porous specimens. Then tensile tests values are compared with the stress interval found within the gage length of the model. Results are given in table 6.15.

Table 6.15: Comparison of tensile tests with simulations for graded specimens. (W) designates the "weak side", (S) designates "strong side". All stress values are in "MPa", all displacement values are in "mm".

		Exp. Stress (W)	Found Stress Interval (W)	Exp. Stress (S)	**Found Stress Interval (S)**
TI3G	0.4mm	11.238	6.657-9.003	16.036	11.349-13.349
	0.5mm	14.426	8.322-11.254	19.027	14.187-17.119
TI5G	0.4mm	16.940	4.908-7.679	15.947	10.449-13.220
	0.5mm	20.050	6.135-9.599	19.071	13.062-16.525
TI7G	0.4mm	16.505	6.333-9.791	15.090	9.791-13.248
	0.5mm	19.445	7.916-12.238	17.945	12.238-16.560
TII3G	0.4mm	16.105	9.840-12.377	15.664	12.377-14.914
	0.5mm	19.107	12.266-15.407	18.786	15.407-18.587
TII5G	0.4mm	16.407	8.250-11.220	15.408	11.220-14.189
	0.5mm	19.434	10.312-14.024	18.648	14.024-17.737
TII7G	0.4mm	15.140	10.513-14.218	14.517	10.513-14.218
	0.5mm	18.210	13.142-17.773	17.640	13.142-17.773

According to the simulations, almost none of the stress intervals covered the expected stress values. Results can be further improved be refining the mesh around the gage length of the model. However, increasing the finite element number inside the model increases the solution time which requires a faster work station. But most of the time results can not be improved as much as expected stress values. Therefore performing more tensile tests is suggested to minimize the experimental errors.

CHAPTER 7

DISCUSSION

In this thesis mechanical characterization of porous polyamide parts produced via selective laser sintering rapid prototyping method is sought. Several mechanical tests are performed in order to determine the variation of elastic properties of the plastic polyamide material (nylon 12 based PA2200) due to the variation of the process parameters of the EOSINT P380 SLS machine. Since the parts do not exhibit isotropic behavior tests are repeated for different directions. Also fracture toughness variation over the process parameters is examined. Finally a 3D model is created in ANSYS finite element program and tensile tests of uniform porous and graded porous parts are simulated.

The process parameters are the results given in İlkgün's thesis [2] where the upper and lower values of individual process parameters of the SLS machine are determined. These parameters, laser power, hatching distance and laser scanning speed, can be varied within a range in order to build functional parts provided that the limits are not exceeded. Energy density is the combination of those parameters among which it is directly proportional to laser power and inversely proportional to laser scanning speed and hatching distance. If energy density value is lower than a certain limit parts curl and layers do not bond well, on the other hand; if it is higher than a certain limit parts burn and degrade. By considering this information 9 energy density values are achieved.

Since parts are built layer by layer and sintered, they exhibit a certain degree of porosity which is inversely proportional to the energy density value. Therefore, it is expected that the parts get strengthen with the increase of the energy density.

Furthermore layer by layer production causes orthotropic behavior of the parts built. Accord-

ing to the results in literature, orientation of layers in the production chamber leads negligible difference in average values of the mechanical properties. Thus,the whole part is assumed to be transversely isotropic. This is a special case of orthotropic materials which is represented by 5 independent elastic constants.

Uniform porous tensile test specimens are produced in both thickness and length directions according to the ASTM D638 standard. Parts built in thickness direction are used to obtain the elastic properties such as modulus of elasticity in X and Y directions and Poisson's ratio of the XY plane; while parts built in length direction are used to obtain modulus of elasticity in Z direction and Poisson's ratios of the ZX or ZY planes. Other properties are determined by the equalities valid for orthotropic materials. Tensile tests are performed with a Zwick Z020 tensile test machine. 5 different tests are performed for each energy density set to check the repeatability.

Uniform Porous torsion test specimens are produced to determine the final independent elastic constant which is shear modulus in ZX or ZY plane. Tests are performed with a SM 21 torsion test machine. Similarly dependent properties are calculated with the valid formulation. 3 different tests are performed for each energy density set to check the repeatability.

Finally, uniform porous compact tension fracture toughness specimens are produced according to ASTM D5045. Several iterations are performed in order to determine the best thickness which ensures plane strain condition. A clevis adapting the compact tension specimens to the Zwick tensile testing machine is produced and 3 different tests are performed for each energy density set to check the repeatability.

After the characterization of uniform porous specimens, graded porous tensile test specimens having distinct grades are built. Two types of specimens are produced with 3, 5 and 7 grades. Energy density values of distinct grades varied from 0.016 J/mm^2 to 0.030 J/mm^2 for Type I specimens while they are varied from 0.019 J/mm^2 to 0.033 J/mm^2 for Type II specimens. Effects of different energy density intervals are sought as well as effect of number of grades.

After all tests, results are evaluated and irrelevant ones are eliminated by using the Chauvenet's Criterion. This criterion rejects experimental data if the deviation of the result from the mean is less than a certain limit.

In tensile tests, for specimens built in length direction and torsion tests, no valid data is ob-

tained for specimens having energy density values lower than 0.025 J/mm^2. This is due to the fact that parts are so weak that they fail even before mounting them on the test set up.

As an additional work, availability of filling the material with resin is sought. This study is conducted with uniform porous specimens and Type I graded specimens. Tensile tests are performed and results are compared to those obtained for the specimens not filled with resin; and possible gains on mechanical properties are investigated.

After mechanical tests are conducted, a 3D model is created with ANSYS. Fully characterized parts are used to check the validity of the model. 0.4 and 0.5 mm of displacement is applied to the model and stress variation on the gage area is compared that obtained from the tensile tests. Then, the model is used to predict the undetermined results. Initial guess points are added to the undetermined property's results and the trendline is extrapolated several times. The results acquired from the trendlines are tested and the valid interval which give the desired values are found. Eventually all sets are fully characterized.

The study is concluded with the analyses of 3D graded porous specimens. Either 0.4 mm or 0.5 mm of displacement is applied to the model for all the graded specimens.

At the beginning the objectives of this thesis are stated as mechanical characterization of uniform porous specimens; mechanical characterization of graded porous specimens and modeling of the specimens with a finite element program. At the end of the study it can be said that all the objectives stated for this thesis are successfully met.

CHAPTER 8

CONCLUSIONS

Results given in previous chapters show that mechanical properties of parts are highly dependent on process parameters. Mechanical properties increase with energy density, having a maximum around default value and then decrease; since they burn and degrade due to the excessive applied energy. This trend is clearly seen in tensile tests for parts built in the thickness direction.

Following conclusions are drawn in this study:

- Since porosity is varied directly by changing the energy density value, it affects density of the parts. Therefore, mechanichal properties can be varied by changing the energy density value.

- No necking is observed during tensile tests. Specimens break just after the linear portion which is similar to the behavior of brittle materials such as glass. Thus, rupture strength values are nearly the same as ultimate tensile strength values.

- For low density parts, contouring increases the strength of the specimen; therefore all specimens are produced without contours.

- For tensile test specimens built in thickness direction, modulus of elasticity varies between 997.7 MPa to 1714.5 MPa, ultimate tensile strength and rupture strength vary between 20 MPa to 44 MPa and Poisson's ratio vary between 0.27 and 0.37. However there seems to be a numerically increasing trend for Poisson's ratio; only weakest parts have the value 0.27. Other sets have values around 0.36.

- Some extra parts are produced having energy density values different from previously

determined ones; but still within the pre-determined energy density interval. The results achieved from those parts are almost on the same trend which confirms the tests to be valid. On the other hand, modulus of elasticity and ultimate tensile strength values determined for default parts are very close to those given by the manufacturer. This also confirms the validity.

- For tensile test specimens built in length direction, elastic properties for energy density values lower than 0.025 J/mm^2 could not be found. The parts are weak since the layers are placed perpendicular to the load direction. Modulus of elasticity varies between 1440 MPa to 1750 MPa, ultimate tensile strength and rupture strength vary between 23 MPa to 39 MPa and Poisson's ratio varies between 0.34 and 0.37. Although, it is expected to get much lower values for specimens built in length direction compared to the specimens built in thickness direction; for high energy density values results are nearly the same for both tensile tests. But, trends decrease sharply and for low energy density values difference increases.

- For torsion tests, parts expected to fail between the planes but they shattered like glass for high energy density values. Also shear properties for energy density values lower than 0.024 J/mm^2 could not be determined since the parts are weak. Shear modulus varies between 29 MPa and 45 MPa.

- For fracture toughness tests, several iterations are made to produce the clevis for attaching the specimen. It is showed that for high energy density values thicker specimens are necessary to ensure plane strain condition. On the other hand, specimens are so hard that the pre-crack which has to be initiated with a razor blade could not be opened with razor blades. Therefore, it is created during the production and just a small part is sharpened before the tests. Mode I fracture toughness of the specimens varies between 2 MPa $\sqrt{m}$ and 4.3 MPa $\sqrt{m}$. In tests it is observed that some specimens did not fail completely after the test has stopped while some parts break suddenly just after the maximum load achieved.

- For graded porous specimens, two types of specimens are produced with 3, 5 and 7 grades and tested. Type I specimens had distinct grades varied between 0.016 J/mm^2 and 0.03 J/mm^2 where 0.016 J/mm^2 is the weakest energy density value and Type II specimens had distinct grades varied between 0.019 J/mm^2 and 0.033 J/mm^2 where

0.033 J/mm^2 is the strongest energy density value. The results are compared by considering the types and by considering the number of grades. Accordingly, number of grades doesn't have a significant effect on the strength. For both types, increasing the grade number increased strength less than 1 MPa. On the other hand, Type II parts having the strongest grade possess approximately 13% more strength than Type I parts having the weakest grade. For Type I - 7 grade parts, the weakest grade failed before the whole structure therefore larger difference is observed between UTS and rupture strength.

- Resin filled composite specimens are produced and tensile tests are performed. Specimens having energy densities of 0.016 J/mm^2, 0.019 J/mm^2, 0.020 J/mm^2, gained considerable amount of strength compared to the not filled parts while stronger parts have similar strength values. This shows that resin is filled more to the higher porous specimens as expected. On the other hand, around 10% of strength gain is observed for the resin filled Type I graded specimens.

- 3D finite element model is created by using the ANSYS finite element analysis program. Tensile tests of specimens built in thickness direction are modeled by applying displacements of 0.4 - 0.5 mm. The results are compared to the ones acquired in real tests. In the first part of the study, fully characterized parts are simulated to check the validity of the model; then in the second part, model is used to predict the undetermined values. An initial guess point is added to the data set and the trendline found is extrapolated. Other results are calculated from the equation of the trendline. In order to check the uniqueness of the values several iterations are conducted and the best value is chosen.

- Eventually, following equations are obtained from the trendlines fitted through data points. These equations can be used to predict the mechanical properties of plastic polyamide parts produced via selective laser sintering method. In equations "ED" is in "J/mm^2" and "E" and "G" is in "MPa".

  –

$$E_x = E_y = -2916740.240(ED)^2 + 181329.545\,(ED) - 1076.188$$

  –

$$E_z = -2135126.388(ED)^2 + 156692.472\,(ED) - 1159.685$$

93

–

$$v_{xy} = -441.279(ED)^2 + 26.439\,(ED) - 0.012$$

–

$$v_{zp} = -192.272(ED)^2 + 10.292\,(ED) + 0.230$$

–

$$\frac{v_{zp}}{E_z} = \frac{v_{pz}}{E_p} \Rightarrow \text{p} = \text{isotropy} - \text{plane (XorY)}$$

–

$$G_{xy} = \frac{2(1 + v_p)}{E_p} \Rightarrow \text{p} = \text{isotropy} - \text{plane (XorY)}$$

–

$$G_{xz} = G_{yz} = -18628.749(ED)^2 + 2152.943\,(ED) - 9.088$$

Numerical results and screenshots of ANSYS analyses are provided in the Appendices B, C and D.

REFERENCES

[1] Pham, D.T., Gault, R.S., "A Comparison on Rapid Prototyping Methods", International Journal of Machine Tools and Manufacture 38 (1998) 1257-1287.

[2] Ilkgun, O., "Effects of Production Parameters on Porosity and Hole Properties in Laser Sintering Rapid Prototyping Process". M.S. thesis. Middle East Technical University, Ankara, Turkey, 2005.

[3] Webb., P.A., "A review o f rapid prototyping (RP) techniques in the medical and biomedical sector", Journal of Medical Engineering & Technology, Volume 24, Number 4, 2000, pp. 149-153.

[4] Lohfeld, S., Barron, V., Mchugh, P.E., "Biomodels of Bone: A Review", Annals of Biomedical Engineering, Vol. 33, No. 10, 2005, pp. 1295-1311.

[5] Kruth, J.P., Leu, M.C., Nakagawa, T., "Progress in Additive Manufacturing and Rapid Prototyping", Annals of the CIRP Vol. 47/2, 1998, pp. 525-540.

[6] Fang, Z., Starly, B., Sun, W, "Computer-aided Characterization for Effective Mechanical Properties of Porous Tissue Scaffolds", Computer-Aided Design, Vol. 37, 2005, pp. 65-72.

[7] Shishkovsky, I., "Stress - strain analysis of porous scaffolds made from titanium alloys synthesized via SLS method", Applied Surface Science, Accepted Manuscript, 2008.

[8] Low, K. H., Leong, K. F., Chua, C. K., Du, Z. H., Cheah, C.M., "Characterization of SLS Parts for Drug Delivery Devices", Rapid Prototyping Journal, Vol. 7, 2001, pp. 262-267.

[9] Gibson, I., Shi, D., "Material Properties and Fabrication Parameters in Selective Laser Sintering Process", Rapid Prototyping Journal, Vol. 3, 1997, pp. 129-136.

[10] Picture showing a part produced via SLA, (14.05.09), Available at: http://computer.howstuffworks.com/stereolith3.htm

[11] Picture showing parts produced via FDM, (14.05.09), Available at: http://www.cs.cmu.edu/ rapidproto/students.98/susans/project2/pros.html

[12] Picture showing a part produced via 3DP, (14.05.09), Available at: http://www.psfk.com/2009/01/shapeways-3d-printing-marketplace.html

[13] Hopkinson, N., Majewski, C.E., Zarringhalam, H., "Quantifying the degree of particle melt in Selective Laser Sintering", CIRP Annals - Manufacturing Technology, Vol. 58, 2009, pp. 197-200.

[14] Pham, D.T., Dimov, S., Lacan, F., "Selective laser sintering: applications and technological capabilities", Proc Instn Mech Engrs, Vol. 213 Part B, 1999, pp. 435-449.

[15] Salmoriaa, G.V., Leitea, J.L., Ahrensa, C.H., Lagob, A., Piresc, A.T.N., "Rapid manufacturing of PA/HDPE blend specimens by selective laser sintering: Microstructural characterization", Polymer Testing, Vol. 26, 2007, pp. 361-368.

[16] Rochusa, P., Plesseriaa, J.-Y., Van Elsenb, M., Kruthb, J.-P., Carrusc, R., Dormalc, T., "New applications of rapid prototyping and rapid manufacturing (RP/RM) technologies for space instrumentation", Acta Astronautica (61), 2007, pp. 352 - 359.

[17] Kolosov, S., Vansteenkiste, G., Boudeau, N., Gelin, J.C., Boillat, E., "Homogeneity aspects in selective laser sintering (SLS)", Journal of Materials Processing Technology, Vol. 177, 2006, pp. 348-351.

[18] Song, J.L., Li, Y.T., Deng, Q.L., Hu, D.J., "Rapid prototyping manufacturing of silica sand patterns based on selective laser sintering", Journal of Materials Processing Technology, 2007, pp. 614-618.

[19] Raghunath, N., Pandey, P.M., "Improving accuracy through shrinkage modelling by using Taguchi method in selective laser sintering", International Journal of Machine Tools & Manufacture, Vol. 47, 2007, pp. 985-995.

[20] Kieback, B., Neubrand, A., Riedel, H., "Processing techniques for functionally graded materials", Materials Science and Engineering, A362, 2003, pp. 81-105.

[21] Information about FGMs, (16.12.09), Available at: http://www.oeaw.ac.at/esi/english/research/materials/comp/fgms.html

[22] Information about FGMs, (16.12.09), Available at: http://www.azom.com/Details.asp?ArticleID=1592

[23] Berry, E., Brown, J. M., Connell, M., Craven, C. M., Efford, N. D., Radjenovic, A., Smith, M. A., "Preliminary experience with medical applications of rapid prototyping by selective laser sintering", Medical Engineering Physics, Vol. 19, No. 1, 1997, pp. 90-96.

[24] Tan, K. H., Chua, C. K., Leong, K. F., Cheah, C. M., Gui, W. S., Tan, W. S., Wiria, F. E., "Selective laser sintering of biocompatible polymers for applications in tissue engineering", Bio-Medical Materials and Engineering, Vol. 15, 2005, pp. 113-124.

[25] Williams, J. M., Adewunmi, A., Schek, R. M., Flanagan, C. L., Krebsbach, P.H., Feinberg, S. E., Hollister, S. J., Das, S., "Bone tissue engineering using polycaprolactone scaffolds fabricated via selective laser sintering", Biomaterials, Vol. 26, 2005, pp. 4817-4827.

[26] ASTM Standard D638-03: Standard Test Method for Tensile Properties of Plastics, Annual Book of ASTM Standards, ASTM International, West Conshohocken, PA, 2003.

[27] Caulfield, B., McHugh, P.E., Lohfeld, S., "Dependence of mechanical properties of polyamide components on build parameters in the SLS process", Journal of Materials Processing Technology, Vol. 182, 2007, pp. 477-488.

[28] Perry, C.C., "Strain-Gage reinforcement effects on orthotropic materials", Experimental Techniques, 1986, pp. 20-24.

[29] Knoppers, G.E., Dijkstra, J., van Vliet, W.P., "The Design of Graded Material Objects", Additive Manufacturing International Conference Proceedings, 2006.

[30] Watari, F., Yokoyama, A., Omori, M., Hirai, T., Kondoa, H., Uo, M., Kawasaki, T., "Biocompatibility of materials and development to functionally graded implant for biomedical application", Composites Science and Technology, Vol. 64, 2004, pp. 893-908.

[31] Shishkovski, I., "Synthesis of functional gradient parts via RP methods", Rapid Prototyping Journal, Vol. 7, No 4, 2001, pp. 207-211.

[32] Leong, K. F., Chua, C. K., Gui, W. S., Verani, "Building porous biopolymeric microstructures for controlled drug delivery devices using selective laser sintering", International Journal of Advanced Manufacturing Technology, Vol. 31, 2006, pp. 483-489.

[33] Chung, H., Das, S., "Functionally graded Nylon-11/silica nanocomposites produced by selective laser sintering", Materials Science and Engineering, Vol. A 487, 2008, pp. 251-257.

[34] Chung, H., Das, S., "Processing and properties of glass bead particulate-filled functionally graded Nylon-11 composites produced by selective laser sintering", Materials Science and Engineering, Vol. A 437, 2006, pp. 226-234.

[35] Jande, Y.A.C., "Manufacturing and Characterization of Uniformly Porous and Graded Porous Polymeric Structures via Selective Laser Sintering". M.S. thesis. Middle East Technical University, Ankara, Turkey, 2009.

[36] Jones, R.M., "Mechanics of Composite Materials", 2nd ed., Taylor & Francis, 1999.

[37] Information about Transverse Isotropy, (16.12.09), Available at: http://www.efunda.com/formulae/solid-mechanics/mat-mechanics/

[38] Information about TDG DAQ, (05.01.09), Available at: http://www.metutech.metu.edu.tr/sirketler/product-view.php?cid=300

[39] Ajovalasit, A., Zuccarello, B., "Local reinforcement effect of a strain gauge installation on low modulus materials", J. Strain Analysis, Vol. 40 No. 7, 2005, pp. 643-653.

[40] Information about TML Strain Gauges, (05.10.08), Available at: http://www.tml.jp/e/product/strain-gauge/list/gf-list.html

[41] Information about Tensile Test, (12.08.09), Available at: http://www.instron.us/wa/applications/test-types/tension/default.aspx

[42] ASTM Standard E143-02: Standard Test Method for Shear Modulus at Room Temperature, Annual Book of ASTM Standards, ASTM International, West Conshohocken, PA, 2002.

[43] ASTM Standard D5045-99: Standard Test Method for Plane-Strain Fracture Toughness and Strain Energy Release Rate for Plastic Materials, Annual Book of ASTM Standards, ASTM International, West Conshohocken, PA, 1999.

[44] Slide Show for Chauvenet's Criterion, (06.07.2008), Available at: http://atlas.cc.itu.edu.tr/ erdem/olcme/olcme-03.pdf

[45] Holman, J.P., "Experimental Methods for Engineers", 5th ed., McGraw Hill, 1989.

[46] Dally, J.W., Riley, W.F., "Experimental Stress Analysis", 3rd ed., McGraw Hill, 1991.

[47] ANSYS 11 help files.

[48] Polyamide PA2200 Material Data Sheet, (15.09.09), Available at: http://www.eos.info/en/products/plastic-laser-sintering/materials.html

Appendix A

MATERIAL PROPERTIES OF PA2200 [48]

Material Properties:

Average grain size	Laser diffraction	60	µm
Bulk density	DIN 53466	0,435 - 0,445	g/cm³
Density of laser-sintered part	EOS-Method	0,9 - 0,95	g/cm³

Mechanical Properties*:

Tensile Modulus	DIN EN ISO 527	1700 ± 150	N/mm²
Tensile strength	DIN EN ISO 527	45 ± 3	N/mm²
Elongation at break	DIN EN ISO 527	20 ± 5	%
Flexural Modulus	DIN EN ISO 178	1240 ± 130	N/mm²
Charpy - Impact strength	DIN EN ISO 179	53 ± 3,8	kJ/m²
Charpy - Notched impact strength	DIN EN ISO 179	4,8 ± 0,3	kJ/m²
Izod – Impact Strength	DIN EN ISO 180	32,8 ± 3,4	kJ/m²
Izod – Notched Impact Strength	DIN EN ISO 180	4,4 ± 0,4	kJ/m²
Ball indentation hardness	DIN EN ISO 2039	77,6 ± 2	
Shore D - hardness	DIN 53505	75 ± 2	

Thermal Properties:

Melting point	DIN 53736	172 - 180	°C
Vicat softening temperature B/50	DIN EN ISO 306	163	°C
Vicat softening temperature A/50	DIN EN ISO 306	181	°C

Appendix B

ANSYS SIMULATIONS OF UNIFORMLY POROUS PARTS

**Contour Plots in following figures designates stress intervals**
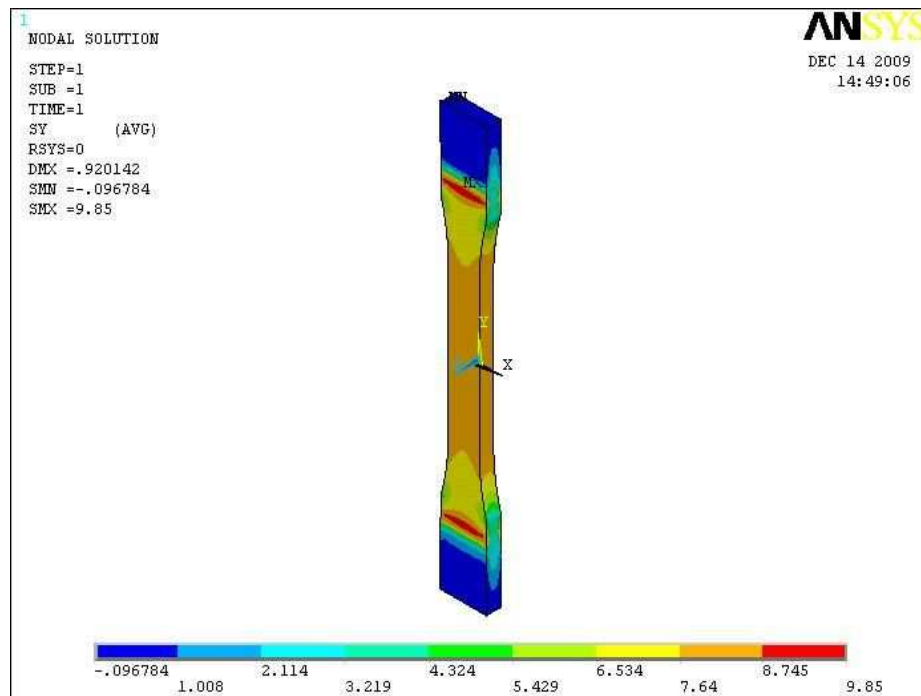
Figure B.1: R1 - 0.4 mm of displacement applied
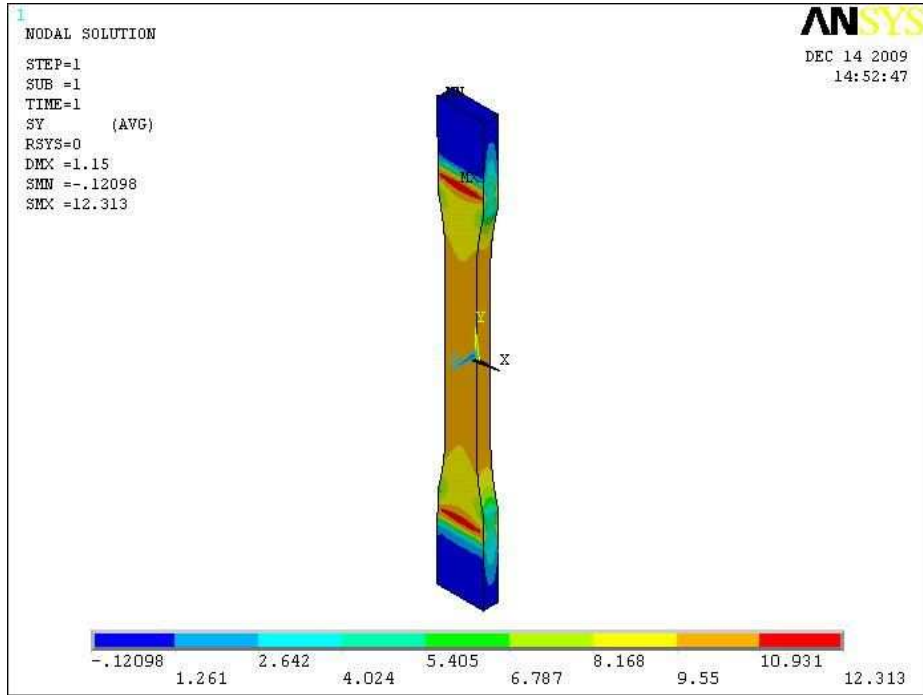
Figure B.2: R1 - 0.5 mm of displacement applied
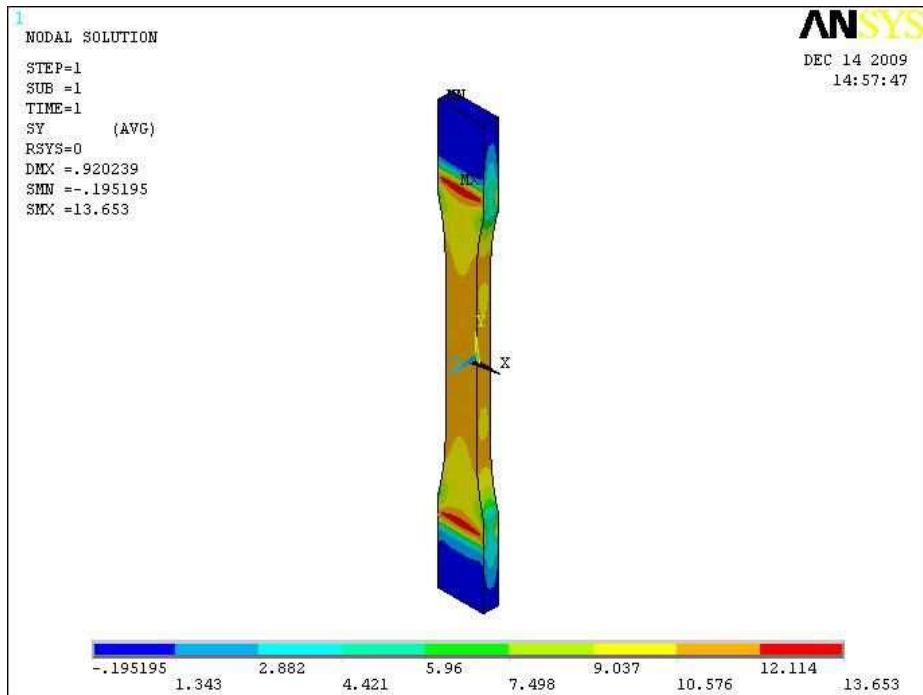
Figure B.3: R2 - 0.4 mm of displacement applied

102
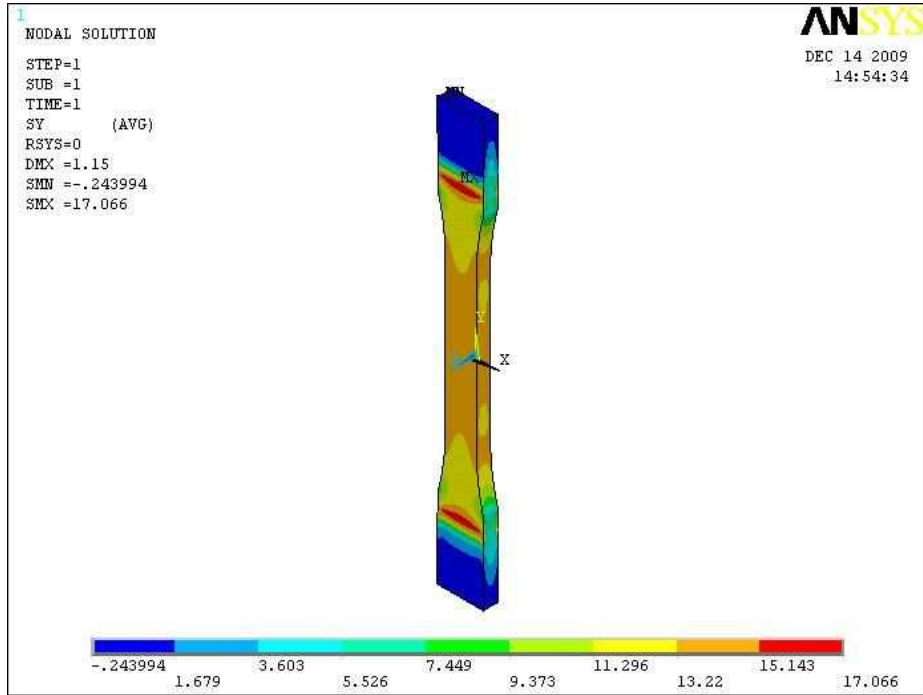
Figure B.4: R2 - 0.5 mm of displacement applied
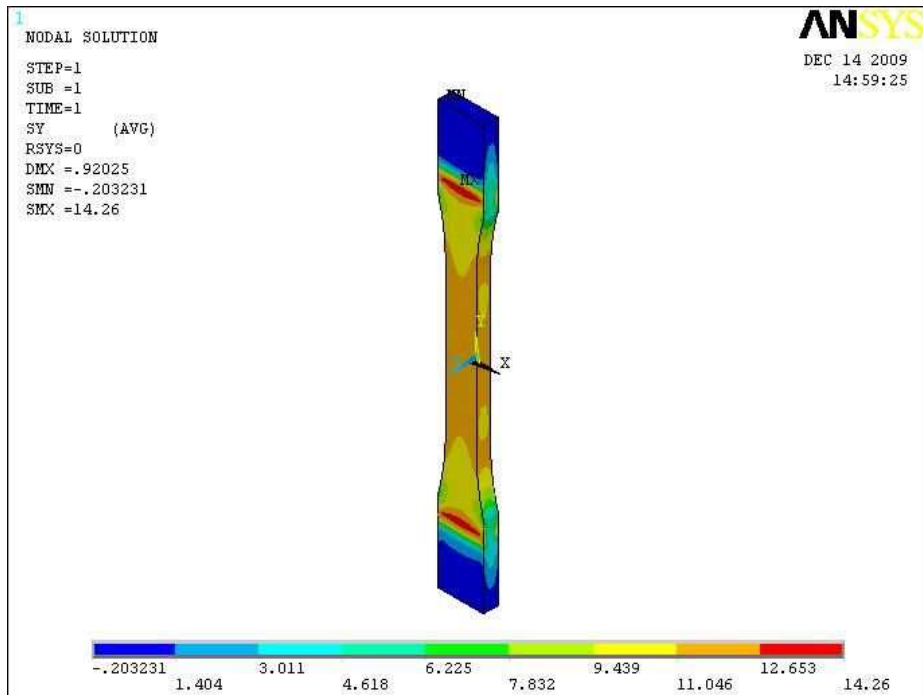
Figure B.5: R3 - 0.4 mm of displacement applied
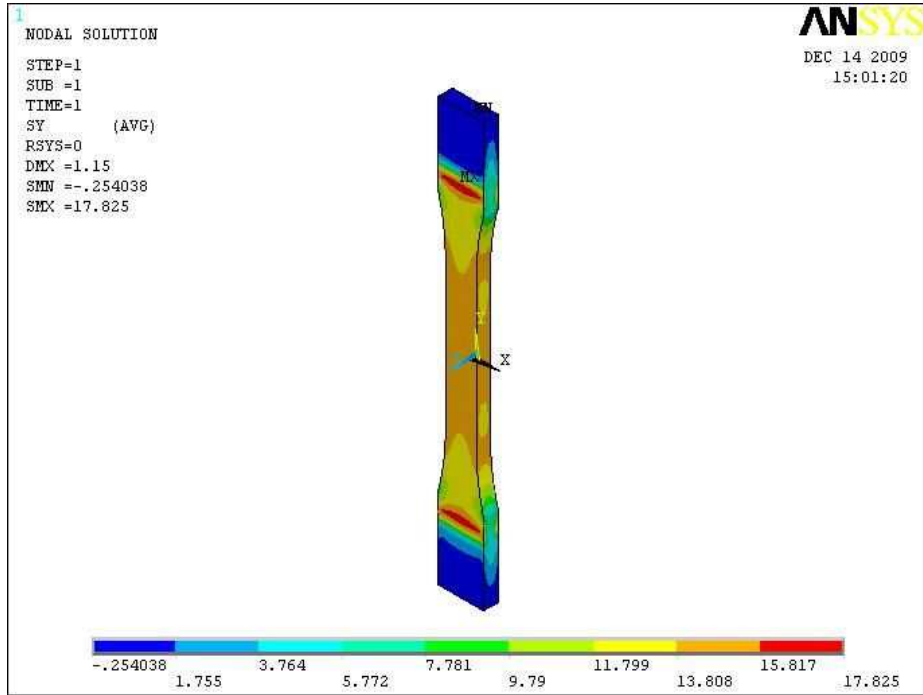
Figure B.6: R3 - 0.5 mm of displacement applied
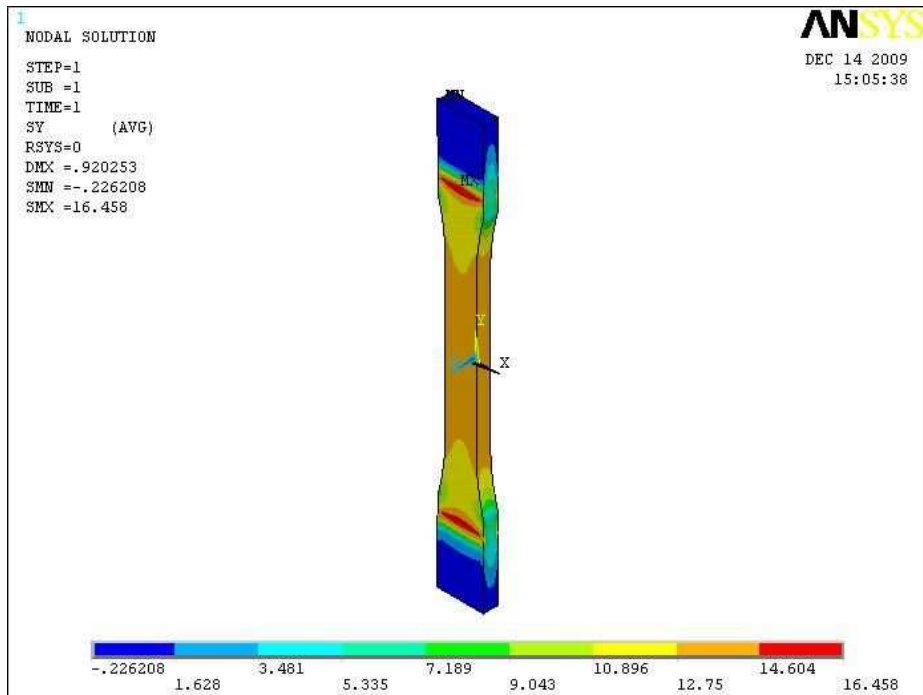
Figure B.7: R4 - 0.4 mm of displacement applied
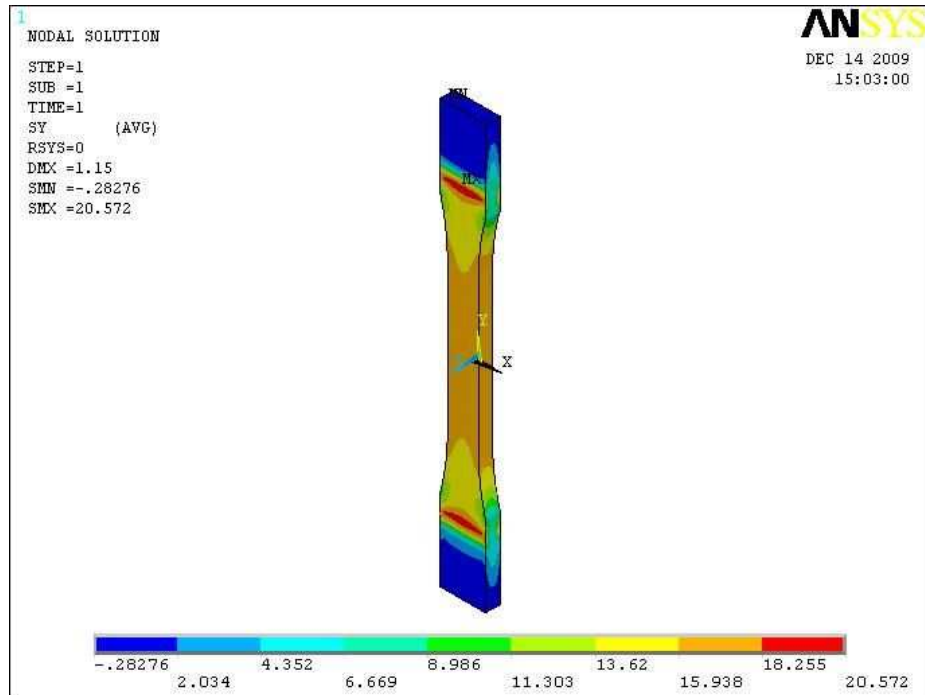
Figure B.8: R4 - 0.5 mm of displacement applied
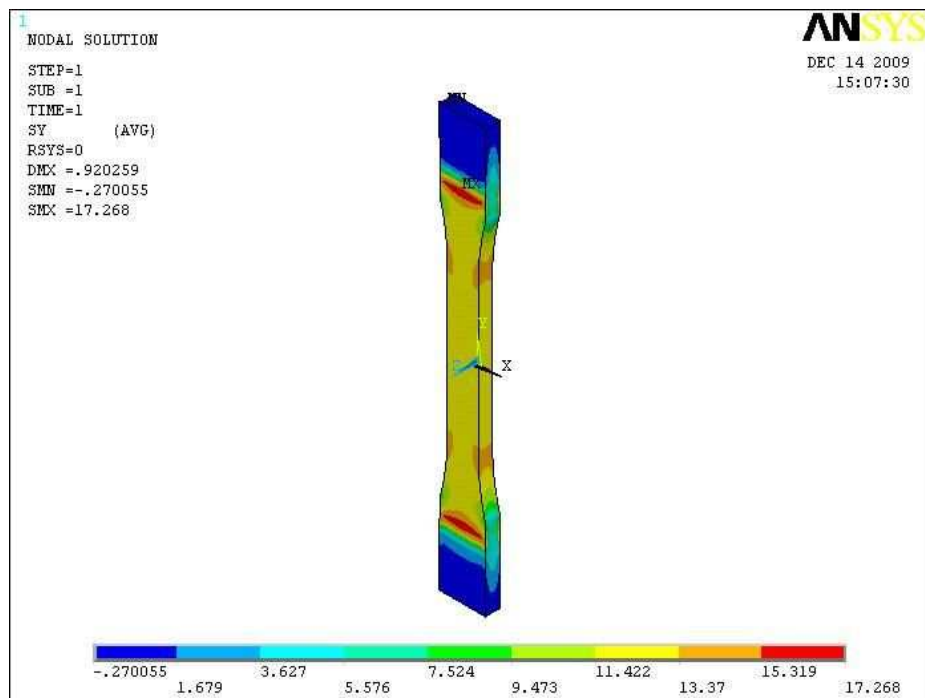
Figure B.9: R5 - 0.4 mm of displacement applied, (not modified, see section 6.4)
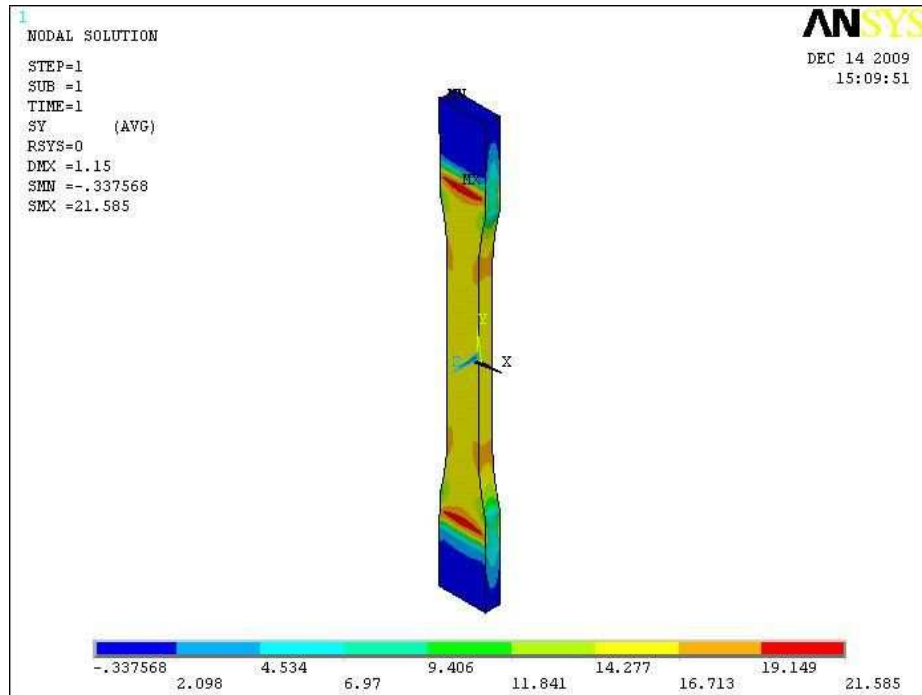
Figure B.10: R5 - 0.5 mm of displacement applied, (not modified, see section 6.4)
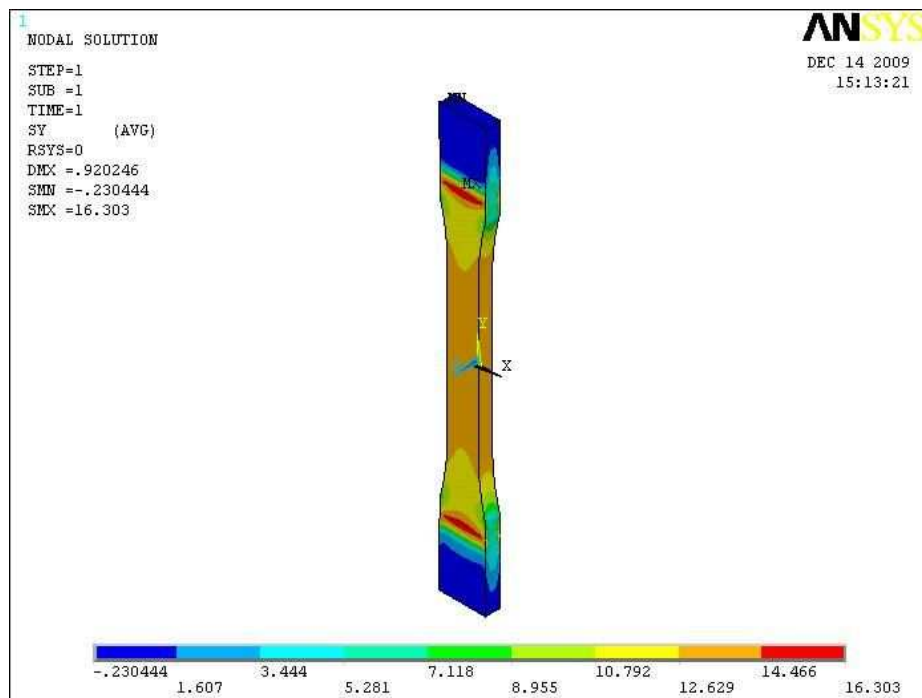
Figure B.11: R5 - 0.4 mm of displacement applied, (modified, see section 6.4)
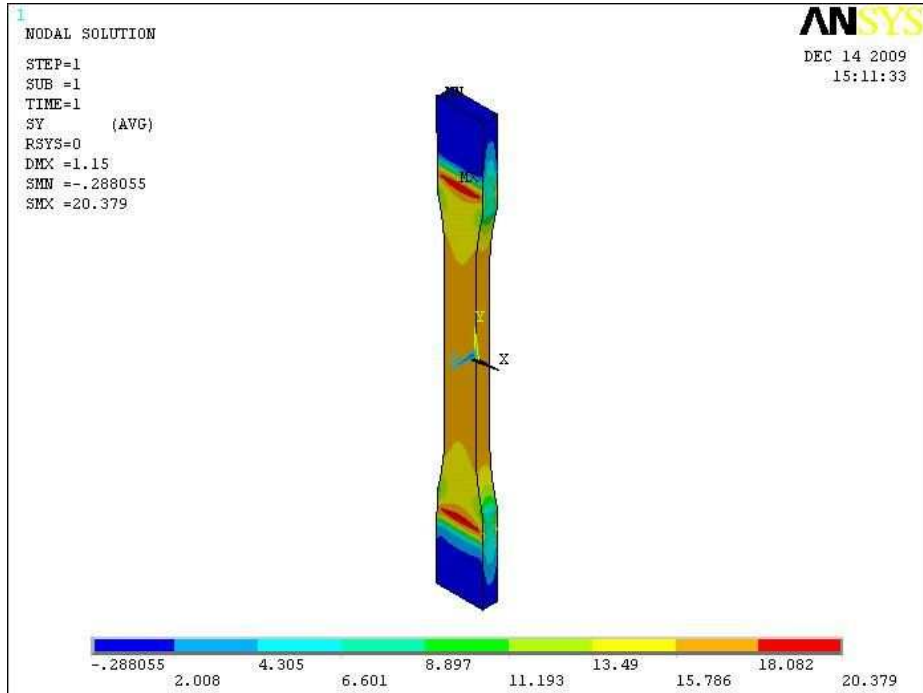
Figure B.12: R5 - 0.5 mm of displacement applied, (modified, see section 6.4)
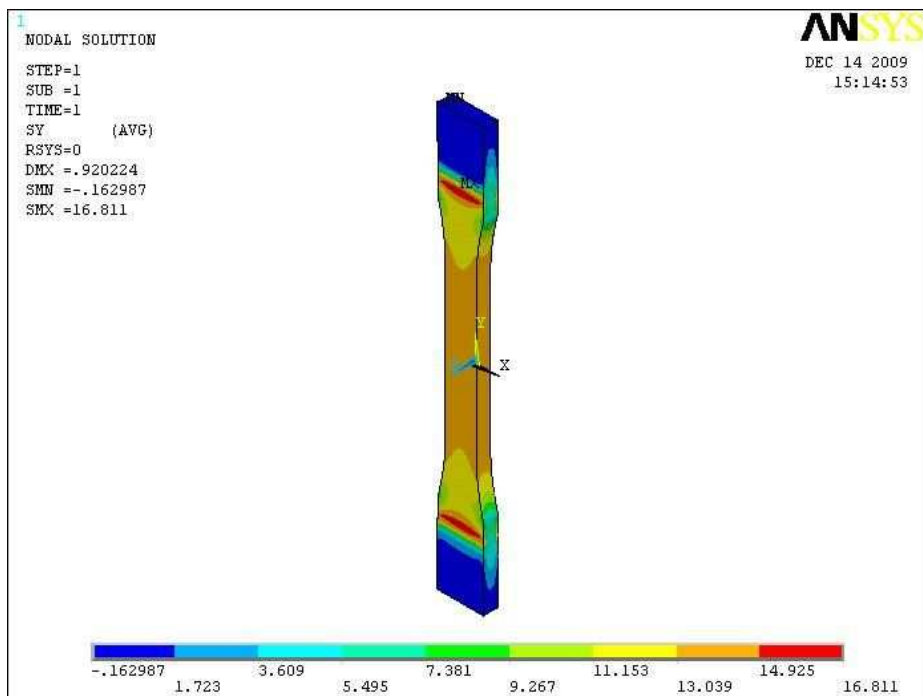
Figure B.13: R6 - 0.4 mm of displacement applied
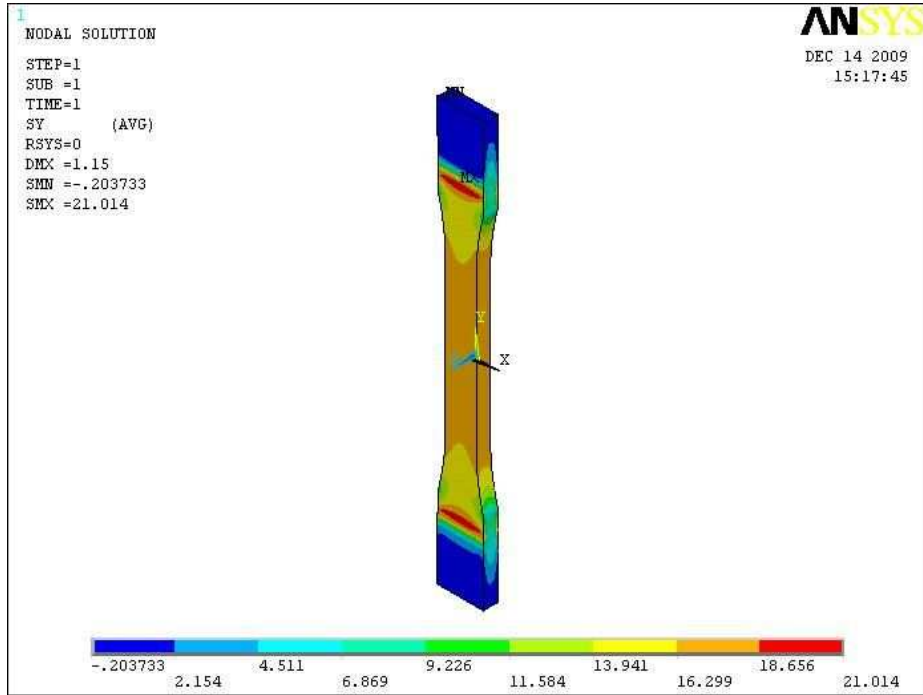
Figure B.14: R6 - 0.5 mm of displacement applied
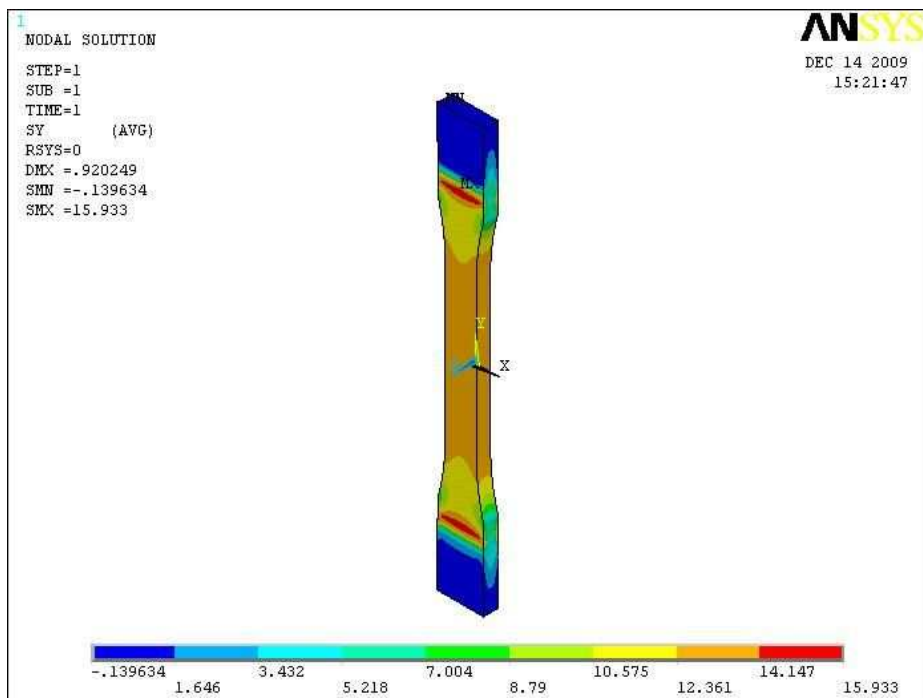
Figure B.15: R7 - 0.4 mm of displacement applied
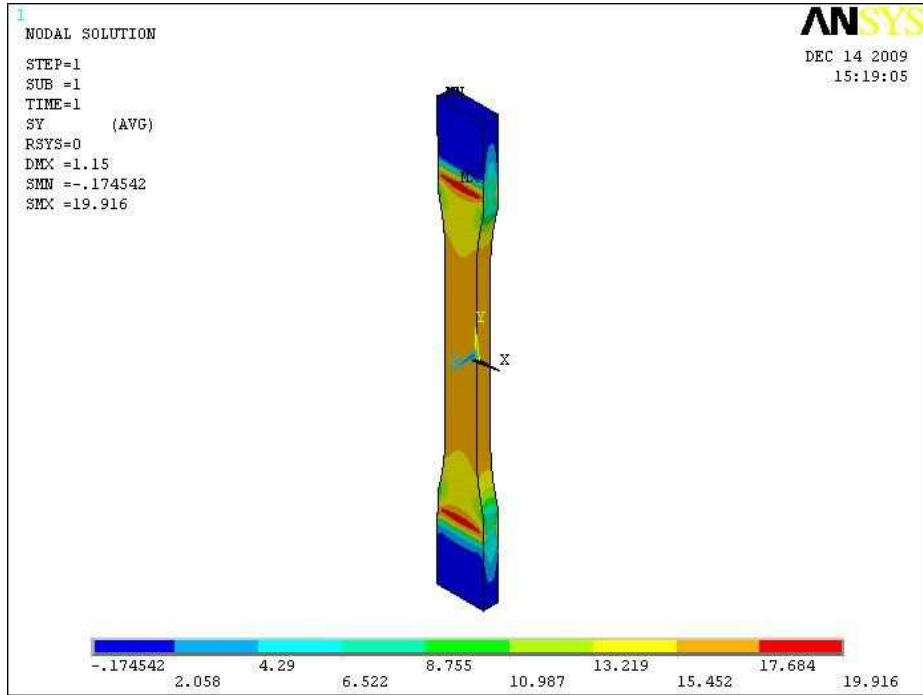
Figure B.16: R7 - 0.5 mm of displacement applied
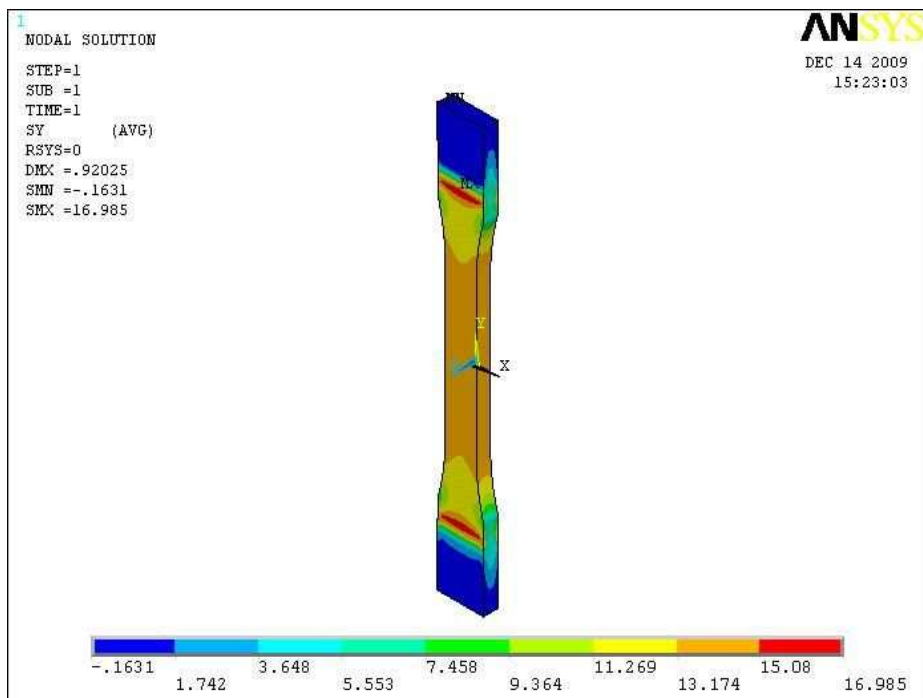
Figure B.17: R8 - 0.4 mm of displacement applied
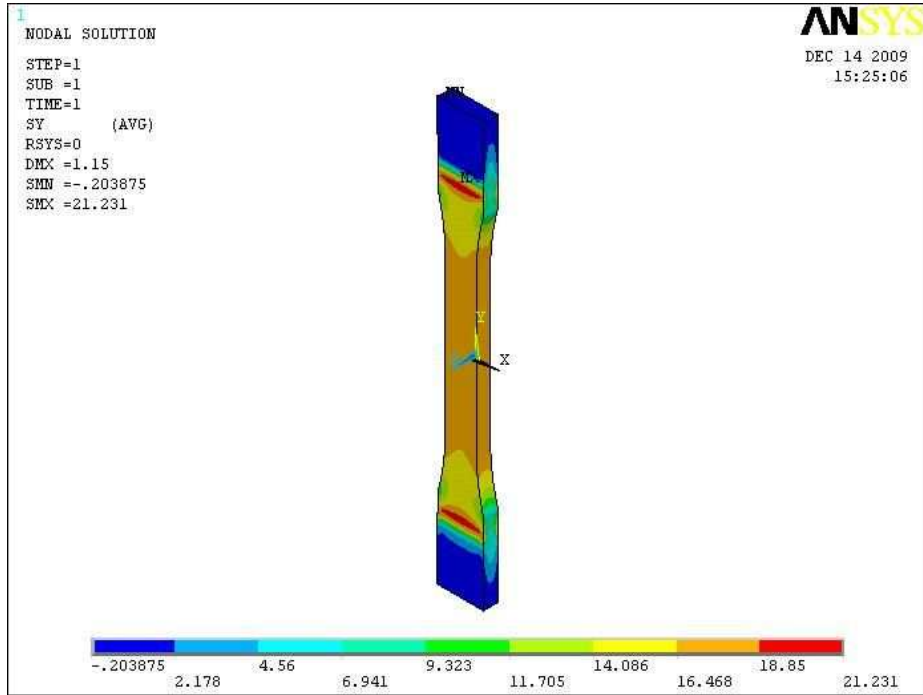
Figure B.18: R8 - 0.5 mm of displacement applied
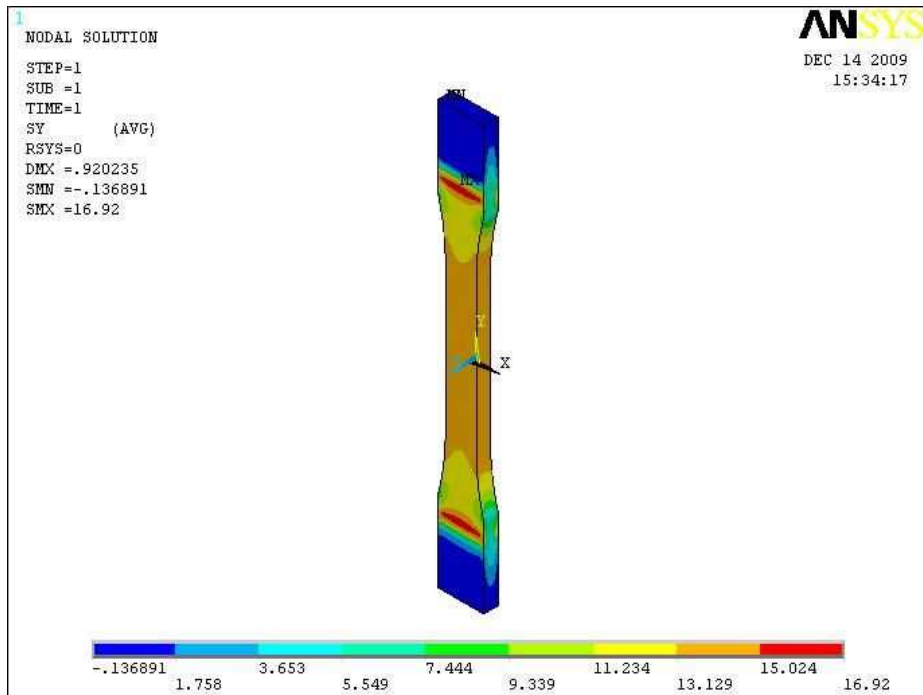
Figure B.19: R9 - 0.4 mm of displacement applied
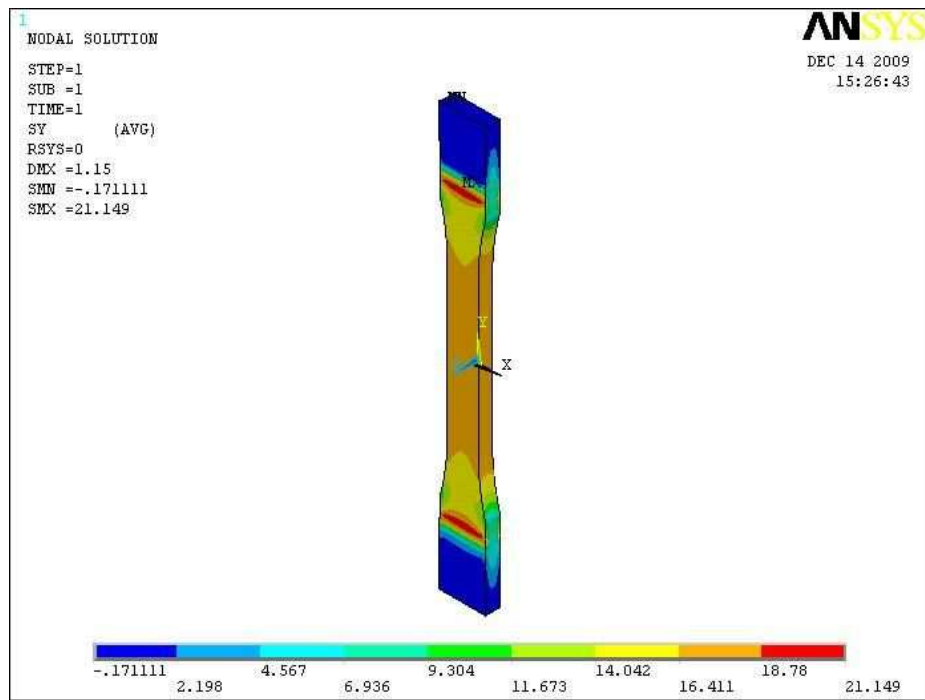
Figure B.20: R9 - 0.5 mm of displacement applied

Appendix C

ANSYS SIMULATIONS OF GRADED POROUS PARTS

Contour Plots in following figures designates stress intervals
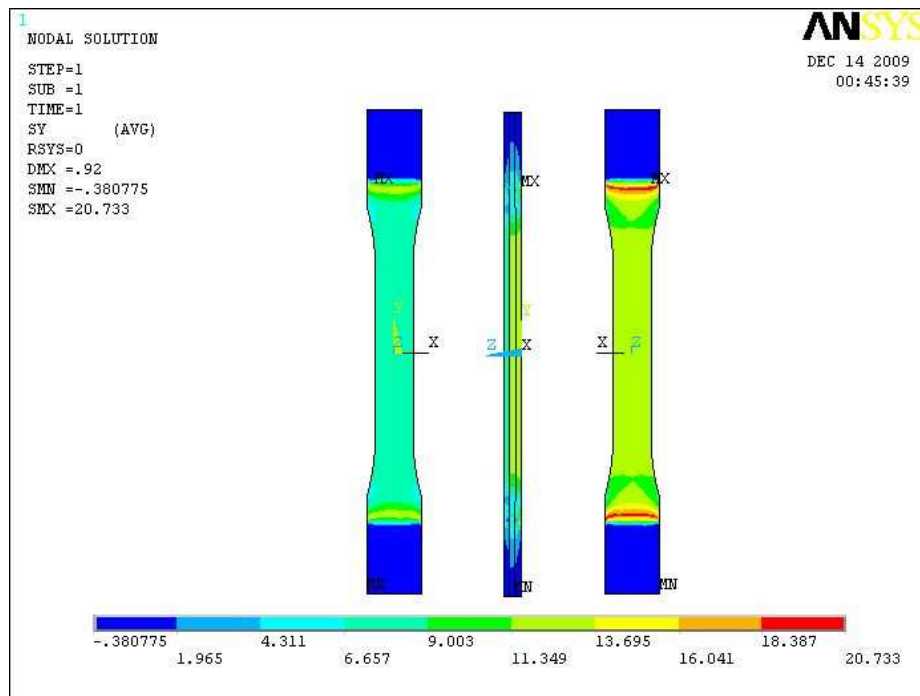

Figure C.1: TI3G - 0.4 mm of displacement applied
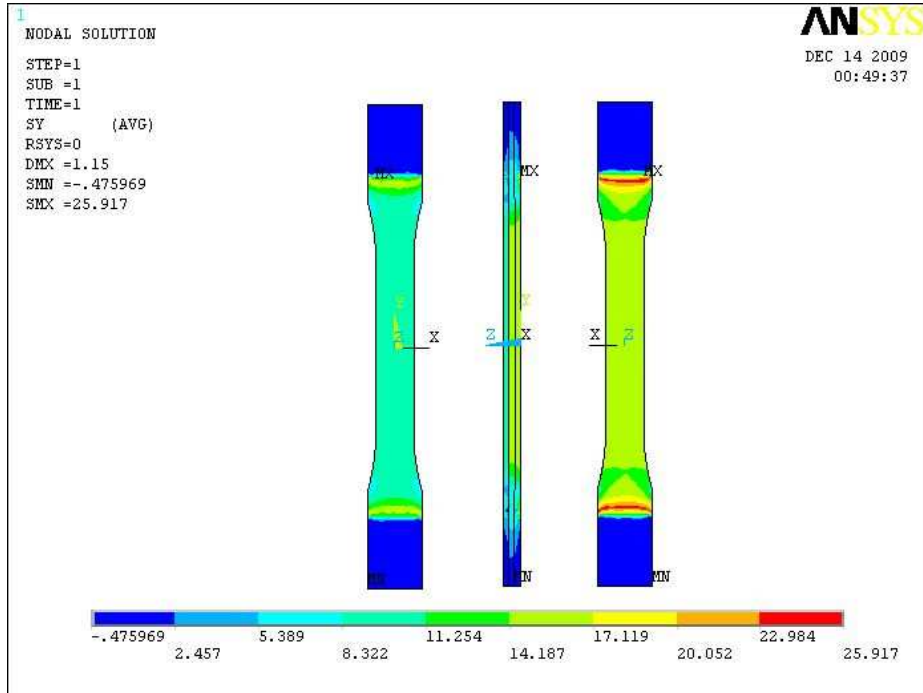
Figure C.2: TI3G - 0.5 mm of displacement applied
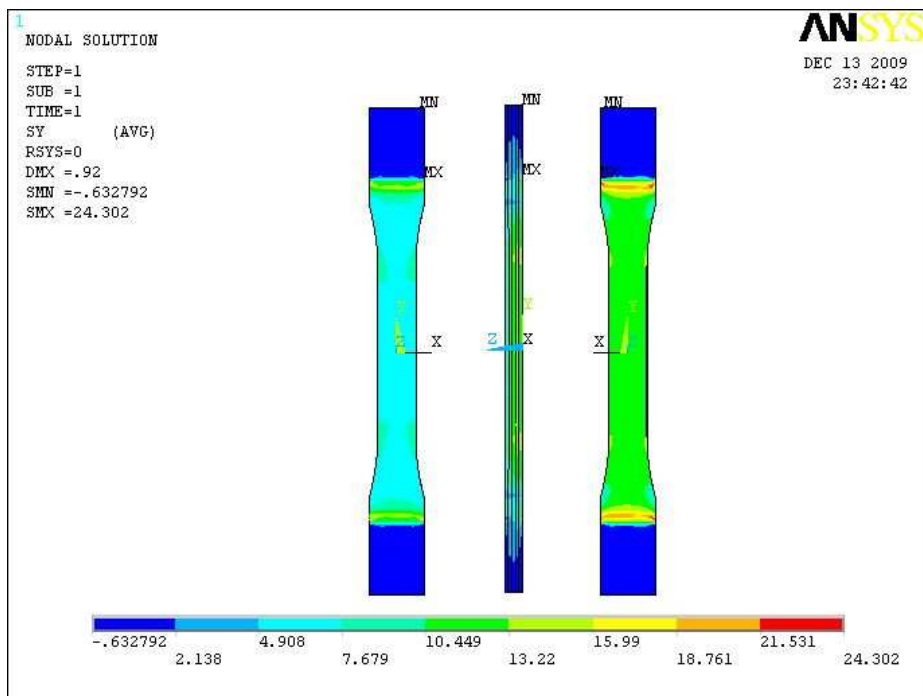
Figure C.3: TI5G - 0.4 mm of displacement applied
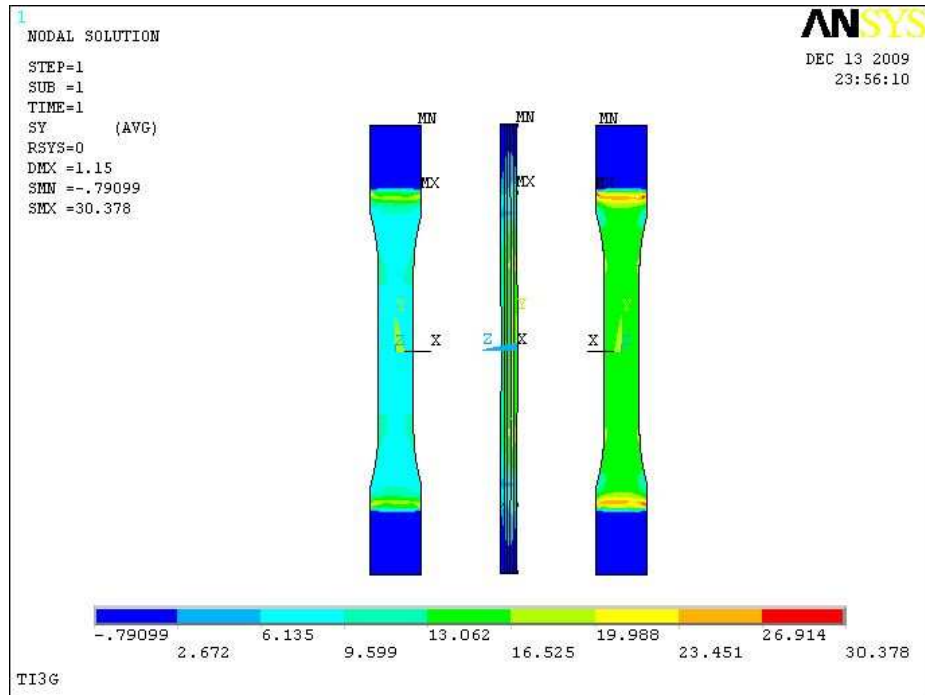
Figure C.4: TI5G - 0.5 mm of displacement applied
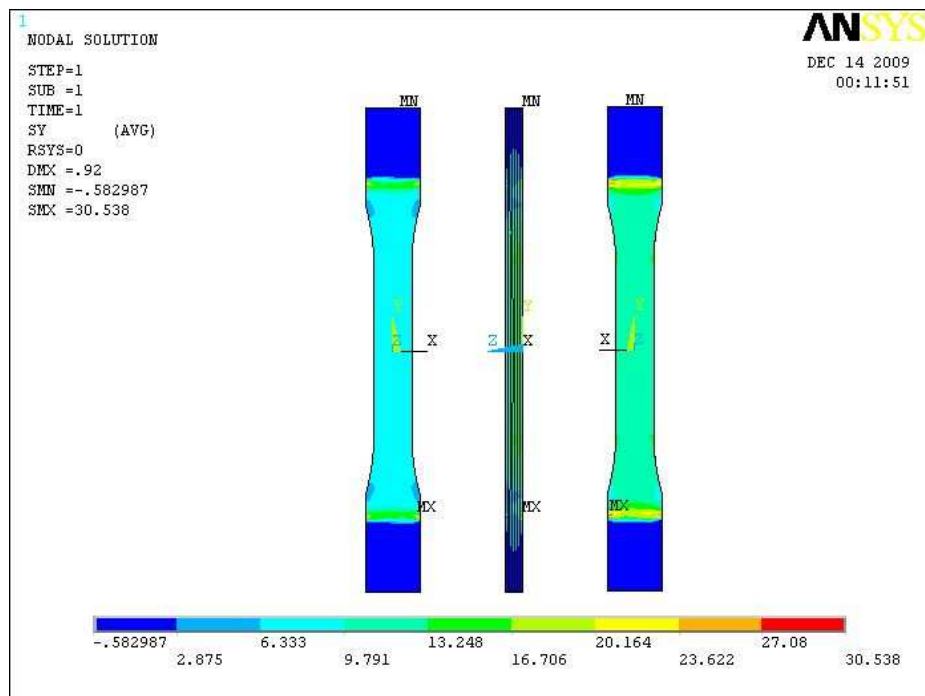
Figure C.5: TI7G - 0.4 mm of displacement applied

114
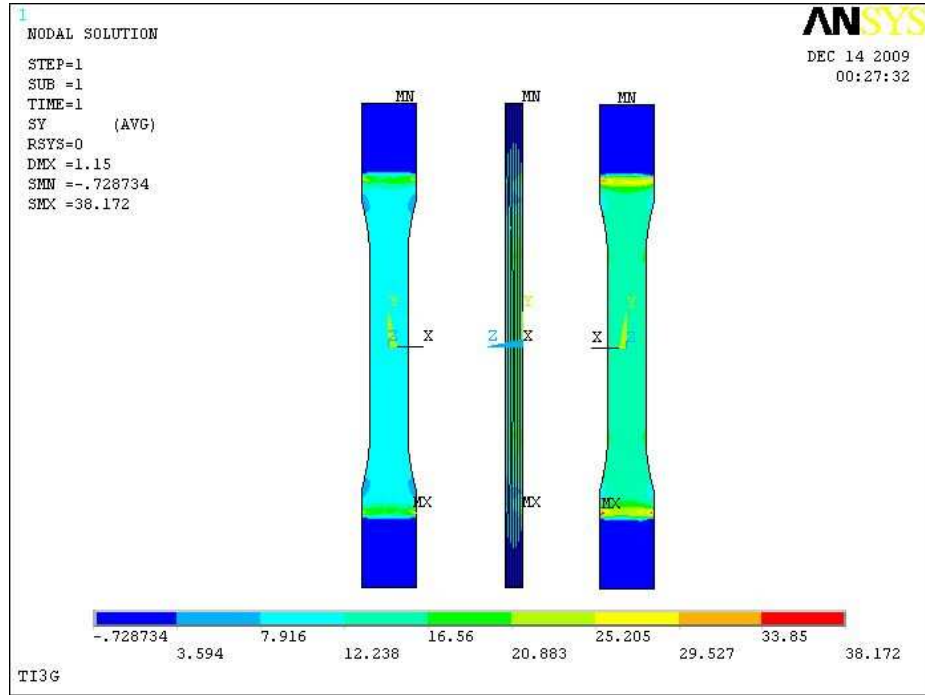
Figure C.6: TI7G - 0.5 mm of displacement applied
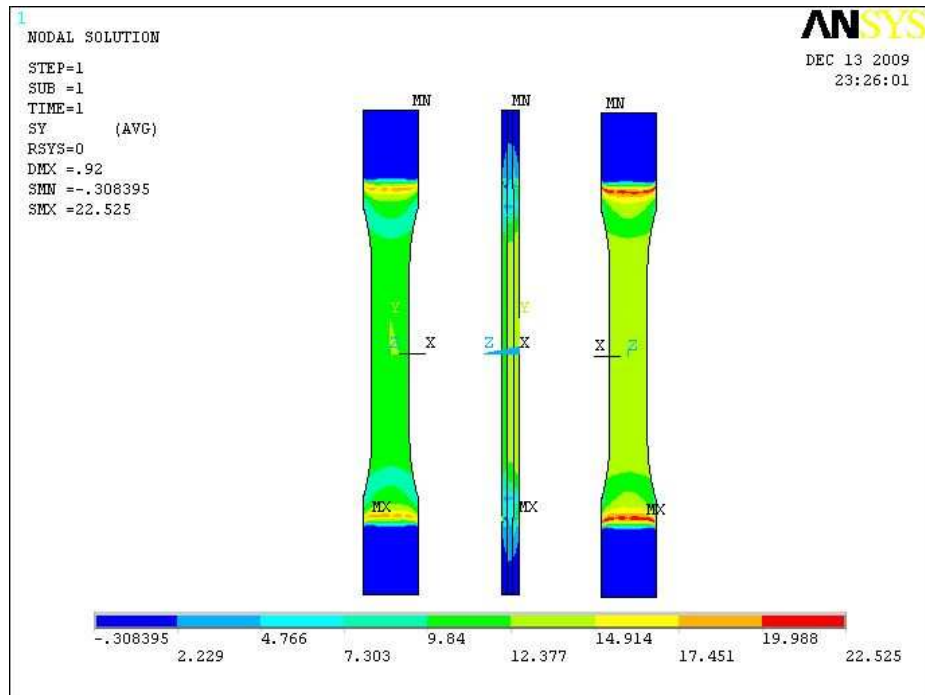
Figure C.7: TII3G - 0.4 mm of displacement applied
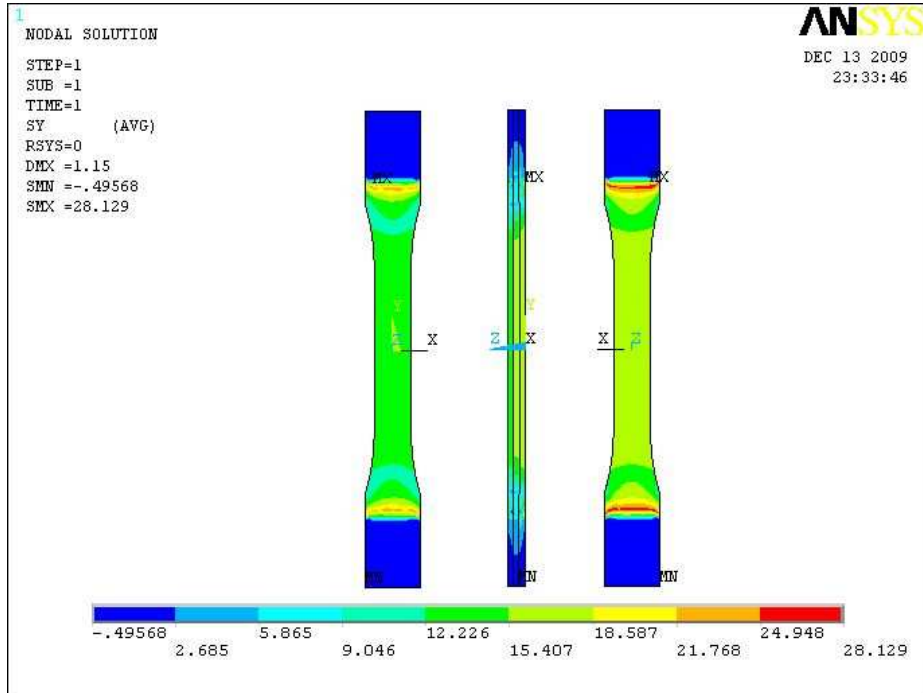
Figure C.8: TII3G - 0.5 mm of displacement applied
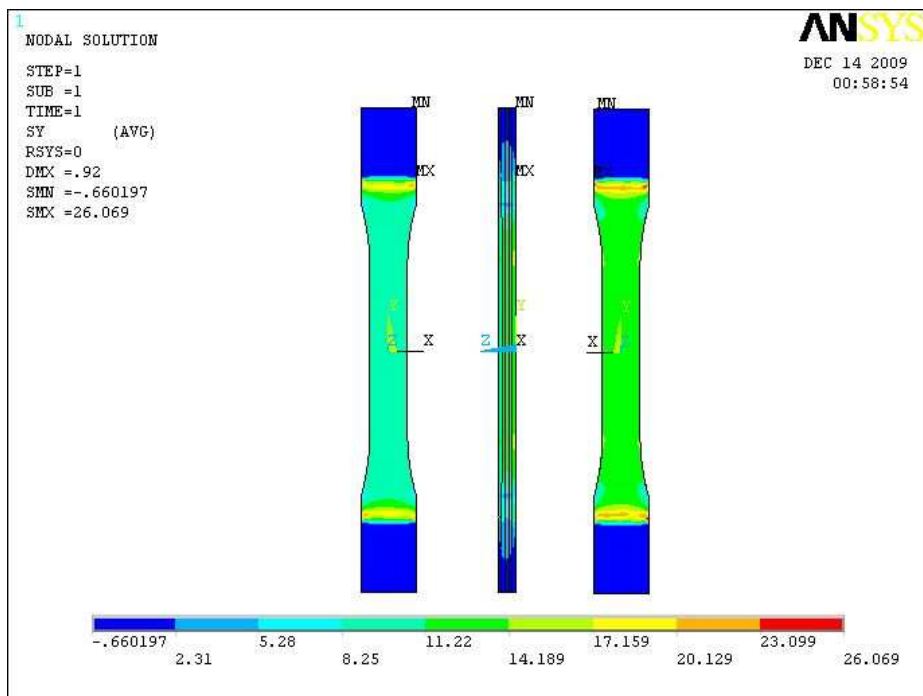
Figure C.9: TII5G - 0.4 mm of displacement applied
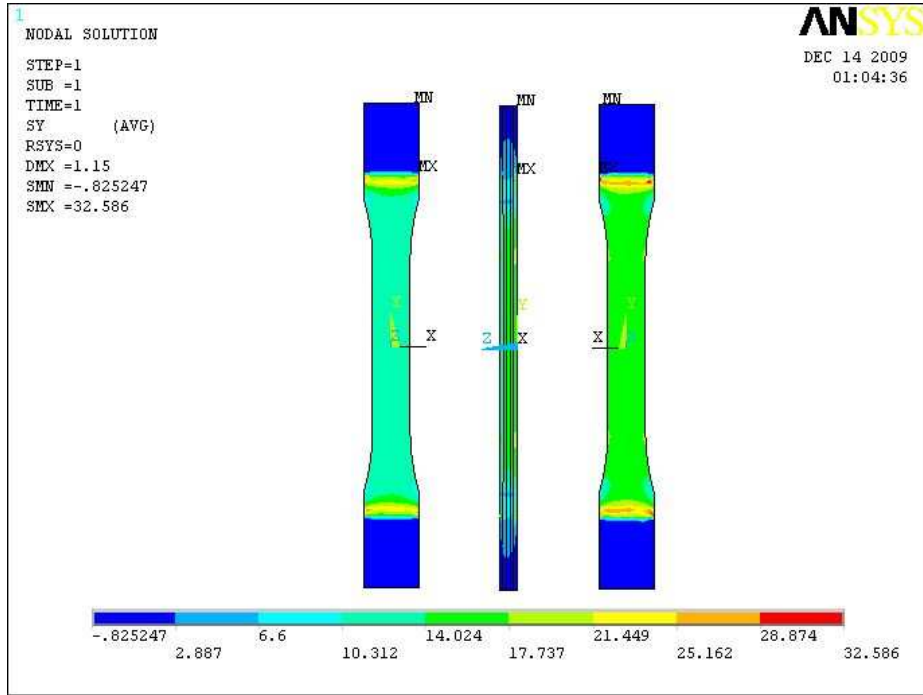
Figure C.10: TII5G - 0.5 mm of displacement applied
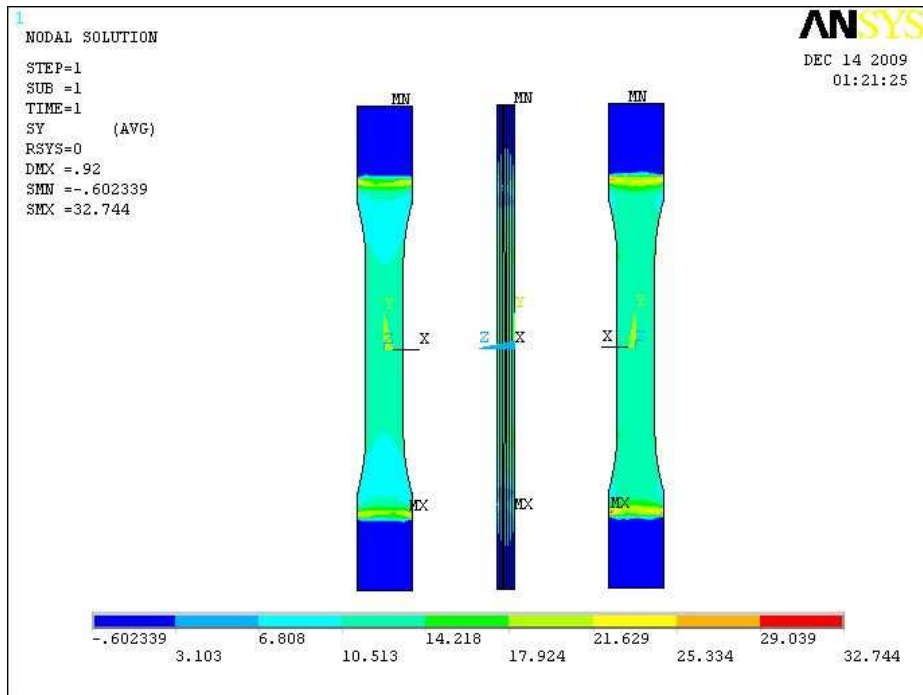
Figure C.11: TII7G - 0.4 mm of displacement applied
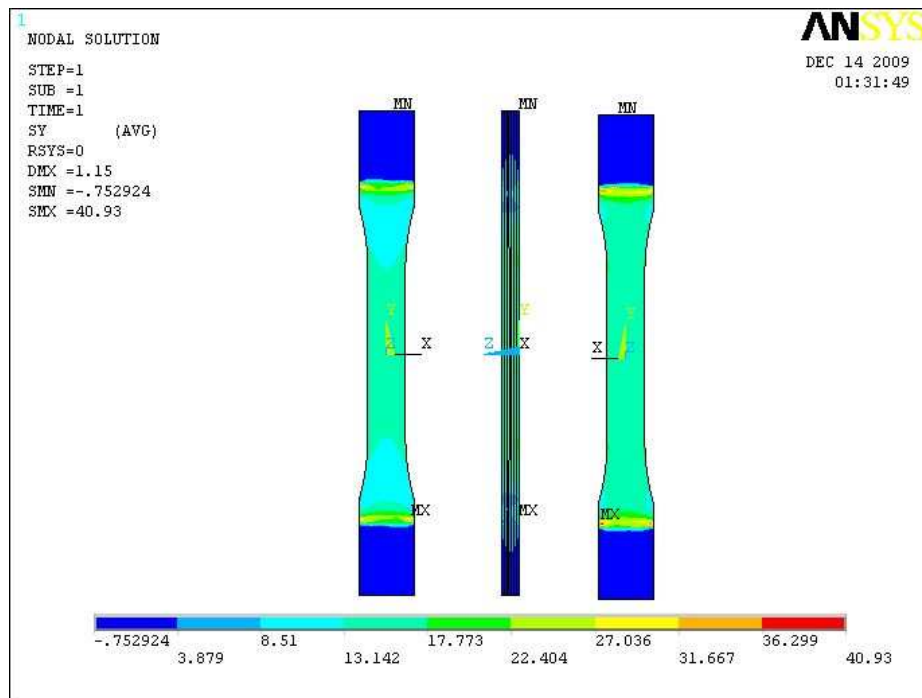
Figure C.12: TII7G - 0.5 mm of displacement applied

Appendix D

COMPLIANCE MATRICES OF PARTS PRODUCED VIA SLS

Table D.1: Complete compliance matrices of parts produced via SLS over the varying energy density values

	R1	R2	R3	R4	R5
ED (J/mm^2)	0.016	0.019	0.02	0.024	0.025
E$_x$(MPa)	997.725	1362.250	1421.350	1641.840	1634.088
E$_y$(MPa)	997.725	1362.250	1421.350	1641.840	1634.088
E$_z$(MPa)	800.802	1046.691	1120.114	1371.102	1443.300
ν_{xy}	0.268	0.355	0.365	0.370	0.368
ν_{yz}	0.430	0.464	0.455	0.439	0.440
ν_{xz}	0.430	0.464	0.455	0.439	0.440
G$_{xy}$(MPa)	393.301	502.824	520.489	599.299	626.213
G$_{yz}$(MPa)	20.590	25.093	26.519	31.852	33.093
G$_{xz}$(MPa)	20.590	25.093	26.519	31.852	33.093
	R6	R7	R8	R9	
ED (J/mm^2)	0.029	0.03	0.033	0.037	
E$_x$(MPa)	1686.950	1608.100	1714.480	1701.860	
E$_y$(MPa)	1686.950	1608.100	1714.480	1701.860	
E$_z$(MPa)	1653.000	1579.200	1613.833	1751.833	
ν_{xy}	0.353	0.385	0.384	0.369	
ν_{yz}	0.364	0.372	0.395	0.335	
ν_{xz}	0.364	0.372	0.395	0.335	
G$_{xy}$(MPa)	623.334	580.437	619.304	621.661	
G$_{yz}$(MPa)	36.987	43.249	45.187	42.017	
G$_{xz}$(MPa)	36.987	43.249	45.187	42.017	

**Colored cells in table designates values predicted (pink), extrapolated trendline (yellow),

modified (orange) (see section 6.4)**